COMPUTATIONAL STUDIES ON ORGANOCATALYSIS

Chunhui Liu

Dipòsit Legal: T.192-2014

UNIVERSITAT ROVIRA I VIRGILI
COMPUTATIONAL STUDIES ON ORGANOCATALYSIS
Chunhui Liu
Dipòsit Legal: T.192-2014

UNIVERSITAT ROVIRA I VIRGILI
COMPUTATIONAL STUDIES ON ORGANOCATALYSIS
Chunhui Liu
Dipòsit Legal: T.192-2014

Chunhui Liu

Computational Studies on Organocatalysis

DOCTORAL THESIS

Supervised by Prof. Feliu Maseras

UNIVERSITAT ROVIRA I VIRGILI

TARRAGONA

2013

UNIVERSITAT ROVIRA I VIRGILI
COMPUTATIONAL STUDIES ON ORGANOCATALYSIS
Chunhui Liu
Dipòsit Legal: T.192-2014

Institute of Chemical Research of Catalonia (ICIQ)
Avgda. Països Catalans 16,
43007 Tarragona (Spain)
Tel. (+34) 977 920 200

Prof Feliu Maseras, group leader at the Institute of Chemical Research of Catalonia (ICIQ), and research supervisor for Chunhui Liu.

I STATE that the present study, entitled "Computational Studies on Organocatalysis" presented by Chunhui Liu for the award of the degree of doctor, has been carried out under my supervision at the Institute of Chemical Research of Catalonia (ICIQ), and that it fulfils all the requirements to be eligible for the Doctorate Award.

Tarragona, September 2013

Doctoral Thesis Supervisor

Prof. Feliu Maseras

UNIVERSITAT ROVIRA I VIRGILI
COMPUTATIONAL STUDIES ON ORGANOCATALYSIS
Chunhui Liu
Dipòsit Legal: T.192-2014

Acknowledgements

This thesis is an important event in my life - a challenging and exciting one. I am really grateful to a number of people for their assistance and supporting for the fulfillment of this thesis.

First of all I am extremely grateful to Prof. Feliu Maseras, who offered me an opportunity to study at ICIQ (Institute of Chemical Research of Catalonia) by providing me with a scholarship and a hospitable working environment. It has always been a pleasure to discuss with him about the academic issues. His advice helped me a lot in grasping some good ideas during all my research.

I would like to thank Prof. Fahmi Himo for his hospitality in his group in Stockholm during the summer of 2012. This is a good opportunity to learn new knowledges and new research fields. I believe it is useful for my research in future.

I would like to thank Núria Vendrell for the large help after I came to Spain. If no her, my life would become worse. Also thank Martin Gumbau for helping me with a lot of technical problems.

I would like to thank Maria Besora Bonet and Ataualpa Braga for teaching me a lot of things in the first stages of my research project, especially Maria Besora; she has always been there for me, to help with all the difficulties that arose. I am most grateful for her comments and suggestions during the phase of the development and the writing of this thesis. I also thank Charles Goehry, Chamil Sameera, Carina Backtorp, Steven Donald, Torstein Fjermestad, Abel Locati, Jesús Jover, Laura Mateus, Maxime Mercy, Elena Herrero, Ainara Nova, Víctor Fernández Álvarez, Prof. Carles Bo, Cristina Pubill, Pere Miró, Mickael Gicquel, Simon Pierrefixe, Alex Hamilton, Fernando Gómez, Xavier Sanz López, Dolores Melgar Freire, Nuno Bandeira, Prof. Núria López, Jaime Gómez, Mónica Garcia, Crisa Vargas, Luca Bellarosa, Gerard Novell, Neyvis Almora Barrios, Guillem Revilla López, Max García Melchor, Sergey Pogodin, Giuliano Carchini, Rodrigo García Muelas and Miquel A. Garcia Ratés with lots of help and support from them. I would like to extend my particular thanks to Charles Goehry for introducing me a lot of programs and Abel Locati for the correction of my thesis writing.

I am also grateful to my Chinese friends in ICIQ, and in Tarragona with a lot of help when I'm in trouble and sharing my joy when I am happy.

Lastly, I am indebted to my husband, my parents, my sister and brother, for their love, constant support and patience for all these years. Especially, my husband Peilin Han, I am deeply grateful for his love, moral support, encouragement and patience for finishing my PHD.

Thanks to all people who have helped me in last four years, here too much to put them all, but thank you so much!!!

UNIVERSITAT ROVIRA I VIRGILI
COMPUTATIONAL STUDIES ON ORGANOCATALYSIS
Chunhui Liu
Dipòsit Legal: T.192-2014

The work of this thesis has been possible thanks to financial support from the "Ministerio de Ciencia e Innovación" and the Institute of Chemical Research of Catalonia (ICIQ). The work has been carried out within the framework of the project "Diseño de Catalizadores para una Química Sostenible: Una Aproximación Integrada" (CONSOLIDER CS2006-0003) belonging to the program CONSOLIDER-INGENIO 2010 of the "Ministerio de Ciencia e Innovación".

UNIVERSITAT ROVIRA I VIRGILI
COMPUTATIONAL STUDIES ON ORGANOCATALYSIS
Chunhui Liu
Dipòsit Legal: T.192-2014

Contents

Contents

Contents

Chapter1

Introduction

1.1 Organocatalysis

For a long time, homogeneous catalysis was almost synonymous with transition metal catalysis,[1] with a small niche reserved to biocatalysis.[2] Things have changed very much in recent years. Since about the year 2000, the organocatalysis has grown rapidly to become one of the most important fields in organic chemistry.[3] In organocatalysis, the catalyst is a small organic molecule, often with chiral properties. Homogenous catalysis is now definitely extended with this third subject.

One of the main reasons for the success of organocatalysis is that it overcomes some of the limitations of transition metal catalysis and biocatalysis, thus becoming an ideal complement. Most transition metal catalysts are rather expensive. A number of them also have stability concerns, in particular with water (or moisture) and oxygen. Many metals are moreover poisonous, leading to the need for caution to handle toxic waste and expensive purification due to the strict requirements for pharmaceutical products.[4] Enzymes (biocatalysts) are not stable under many synthetic conditions and are difficult or expensive to obtain in large quantities.[5] They might also have a narrow substrate range and may be difficult to tune to the desired product. Compared with transition metal catalysts and enzymes, the advantages of organocatalysts include their lack of sensitivity to moisture and oxygen, their ready availability, low cost, and low toxicity, which confers a huge direct benefit in the production of pharmaceutical intermediates. Because of these advantages, organocatalysis has become a wide range of research area over the last decade.[6] It is now generally accepted that organocatalysis is one of the main branches of enantioselective synthesis, and a useful tool in the catalysis toolbox. Since 2000, the organocatalysis field has grown exponentially from a handful of publications in 2001 to more than 1200 in 2011,

and in parallel, the number of citations have also increased up to 40000 last year. The labels "golden age"[7] and "golden rush"[8] have been applied to organocatalysis, and many researchers from academia and the chemical industry have entered this field. Most research efforts have focused on the development of new reactivities and asymmetric methodologies.

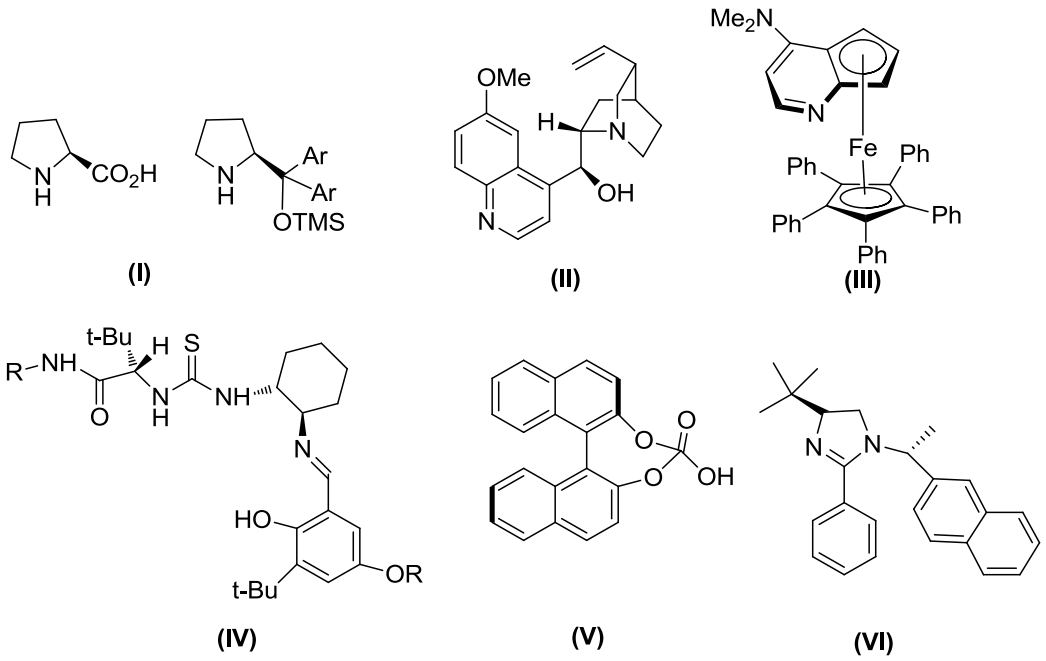

(I) **(II)** **(III)**

(IV) **(V)** **(VI)**

Scheme 1.1 Selected typical chiral catalysts used in organic catalysis.

A selection of typical organocatalysts is shown in **Scheme 1.1**. Proline is a chiral amino acid, which as such or in the form of a derivative **(I)**, catalyzes aldol and related C-C bond formation reactions.[9] Cinchona alkaloids such as quinine **(II)**, which has been abundantly used as a chiral base[10] or as a chiral nucleophilic catalyst,[11] have served as the basis for many highly enantioselective phase-transfer catalysts. The planar chiral DMAP derivative **(III)**[12] is extremely selective in several nucleophilic catalysis. Although contains a ferrocene moiety, it is often regarded an organocatalyst because its "active site" is the pyridine nitrogen atom. Chiral thiourea derivatives **(IV)**[13] have enabled excellent enantioselectivity. Phosphoric acid derivatives **(V)**[14] have been used for the activation of the substrate *via* hydrogen bonds, and imidazole derivatives **(VI)**[15] have also been applied to highly enantioselective reactions.

Organocatalysis has developed greatly, but there are still uncertainties regarding mechanistic details. The full understanding of these mechanisms would be surely beneficial for process improvement. Computations studies help to mechanistic understanding, but their application in organocatalysis has been so far to a certain extent limited.[16] This thesis is devoted to the mechanistic study of three organocatalytic reactions. General knowledge on each of the reactions is described briefly in the rest of this section.

1.1.1 Lewis-acid catalysis for Friedel-Crafts reactions

The Friedel-Crafts (FC) reaction is one of the oldest organic transformations to employ Lewis acid as promoters. The reaction was discovered in 1877 when Charles Friedel and James Mason Crafts isolated amyl-benzene after the treatment of amyl chloride with $AlCl_3$ in benzene (**Scheme 1.2**).[17] Now these reactions have become important both in fundamental research and industrial application, and one of the most powerful C-C bond forming reactions in organic synthesis.[18] There are two main types of Friedel–Crafts reactions: alkylation reactions and acylation reactions, both preceded by electrophilic aromatic substitution. They become very useful tools for the synthesis of numerous aromatic compounds. Over the intervening years, many Lewis acids including BF_3, $BeCl_2$, $TiCl_4$, $SbCl_5$ or $SnCl_4$ have been described as catalysts for the FC reaction.[19] Furthermore, strong Brønsted-acids including sulfuric acid, hydrofluoric acid or super acids such as $HF{\bullet}SbF_5$ and $HSO_3F{\bullet}SbF_5$ have also been shown to accelerate this transformation.[20] With the need for more environmentally and economically benign processes, the development of FC reactions using only catalytic amounts of a metal or acid catalyst would be highly desirable.

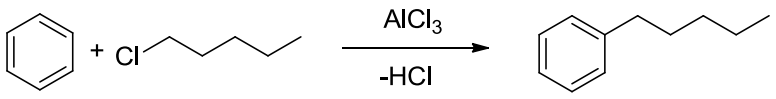

Scheme 1.2 $AlCl_3$-mediated reaction between armyl chloride and benzene as developed by Friedel and Crafts.[17]

Water is one of the simplest molecules with Brønsted–acid capabilities. The coordination of water molecules to the carbonyl function in Diels–Alder reactions[21] and Claisen rearrangements,[22] resulted in the enhancement of the reaction rate. The multiple role of water in organocatalytic reactions has been recently discussed.[23] However, as far as we know, the direct involvement of a water molecule in the chiral metal-containing Brønsted–acid catalysis has been rarely reported so far.[24] In this line, Carmona and co-workers disclosed the use of the water adduct of the chiral iridium fragment (η^5–C_5Me_5) Ir {(*R*)–Prophos} (Prophos = propane–1,2–diylbis(diphenylphosphane) (labeled as **1**) as the chiral Brønsted–acid catalyst (**Scheme 1.3**) for the Friedel–Crafts (FC) reaction between ethyl 3,3,3-trifluoromethylpyruvate and indole at low temperature. We are interested in the mechanism of this reaction, and we will try to evaluate the catalytic roles of the metal complex and water molecule in this reaction.

It can be argued that the presence of a transition metal atom invalidates the consideration of this process as organocatalysis. However it must be mentioned that the transition metal does not bind directly with the substrate, but acts exclusively as support for the water molecule. The metal complex plays indeed a critical role both a reaction facilitator and as source of chirality, but in none of these roles the presence of a transition metal atom is critical, as would be the case in conventional transition metal catalysis.

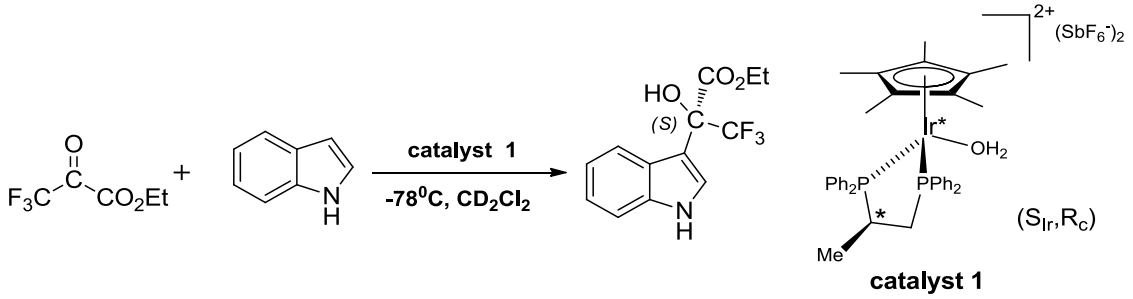

Scheme 1.3 Catalytic Friedel–Crafts reaction (experimental data from Prof. Daniel Carmona group).

1.1.2 Proline catalysis

L-proline and its derivatives are perhaps the organocatalyst that has been most successfully applied until now. The natural L-form is usually used, but proline is available in both enantiomeric forms. This induces an asset when compared to enzymatic catalysis.[25] Compared with other amino acids, proline is the only natural amino acid showing the genuine secondary amine functionality. Thus, the nitrogen atom of proline has a higher pKa value than other amino acids and features an enhanced nucleophilicity. In all, proline can be used as a nucleophile with carbonyl compounds or a Michael acceptor to form either an iminium ion or an enamine. In these reactions, the carboxylic function of the amino acid acts as a Brønsted acid, indicating that the proline is a bifunctional catalyst. In this thesis, we will study the intramolecular aldol reaction using L-proline derivative as catalyst.

1.1.2.1 Development of the intramolecular aldol reaction catalyzed by proline derivatives

Proline was first investigated as a small molecule catalyst in the Hajos-Parrish-Eder-Sauer-Wiechert reaction (**Scheme 1.4**). In 1970, L-proline-catalyzed intramolecular aldol cyclizations were studied in the synthesis of optically pure starting materials for the **CD** rings of steroids (**Scheme 1.5**).[26] Later, Hajos and Parrish isolated the hydrindane dione **3** in an early proline-catalyzed intramolecular aldol cyclization.[27] Although they got encouraging results, the field did not expand until the 1990's, when a large interest in proline as a catalyst was rekindled. In particular, in 1997 Barbas and co-workers[28] investigated this reaction again for the synthesis of the Wieland-Miescher ketone (**5**) (**Scheme 1.6**). This problem is not fully solved yet, and has been recently treated by the group Bonjoch,[29] who has reported a highly efficient enantioselective synthesis of Wieland-Miescher ketone using N-Ts-(S_a)-Binam-L-prolinamide as the organocatalysts under solvent-free conditions and benzoic acid, see **Scheme 1.7**.

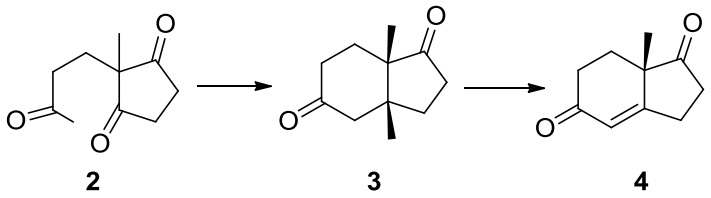

Scheme 1.4 L-proline catalyzed Hajos-Parrish-Eder-Sauer-Wiechert reaction.

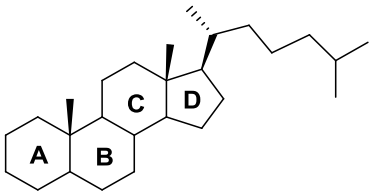

Scheme 1.5 Steroid.

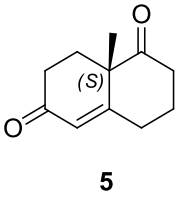

Scheme 1.6 Wieland-Miescher ketone.

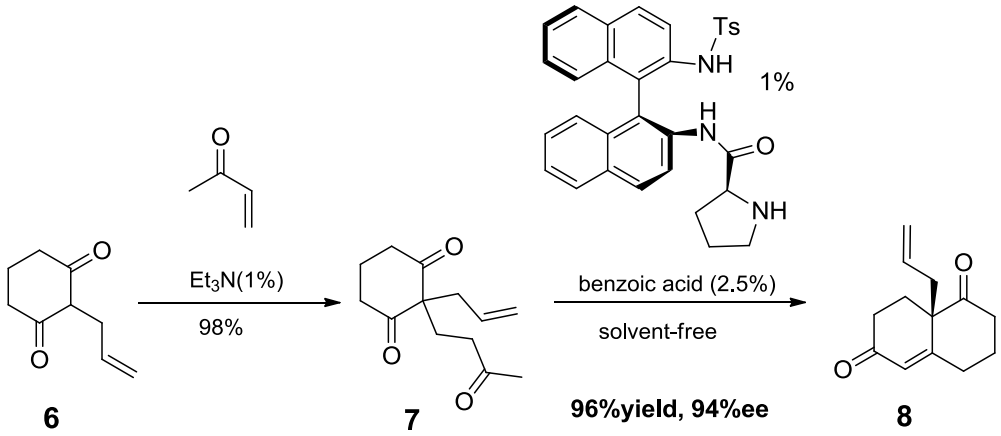

Scheme 1.7 Synthesis of the Wieland-Miescher ketone through a Robinson annulation step.[29b]

1.1.2.2 Enamine mechanism

The mechanism of intramolecular aldol reaction catalyzed by proline has been computationally studied by Houk,[30] who proposed in collaboration with experimental groups, what can be labeled as **Houk-List** model, or enamine mechanism.[31] The original study of this process by Houk is summarized in **Scheme 1.8**.[30] All energies are referred to that of the transition state of the favored mechanism D. Mechanism E, corresponding to the uncatalyzed reaction is 10.7 kcal/mol above mechanism D, thus confirming the catalytic role of proline. The first mechanism in the Scheme (Mechanism A) is the nucleophilic attack of exocyclic enol ether to a carbinolamine in order to displace the catalyst, originally proposed by Hajos and Parrish.[27] This mechanism A should proceed through a carbinolamine intermediate that it is actually higher than the transition state for the uncatalyzed reaction (12.7 *vs* 10.7 kcal.mol^{-1}), and must be thus discarded. The second mechanism in the Scheme (Mechanism B) is a variation of the first also suggested by Hajos and Parrish.[27] It involves simultaneous proton transfer and nucleophilic attack by an enaminium, assisted by the carboxylate. The corresponding transition state has an energy of 29.0 kcal.mol^{-1} and mechanism B must be also discarded. The third mechanism in the Scheme (Mechanism C) had been suggested by Agami,[32] and involves a second molecule of proline in the proton transfer process from the carboxylic acid. This mechanism can be discarded from the experimental data. List and coworkers reported the evidence of the absence of nonlinear effects in these reactions, indicative of a one-proline mechanism.[31b] From a computational point of view, mechanism C would be disfavored by the entropic penalties associated with the involvement of an extra molecule of proline. The fourth (Mechanism D) is the favored one. It involves an enamine intermediate with concerted C-C bond formation and proton transfer from the carboxylic acid group to the carbonyl acceptor and is the energetically favored. A key species in this mechanism is the enamine intermediate, which is formed directly from the iminium intermediate.

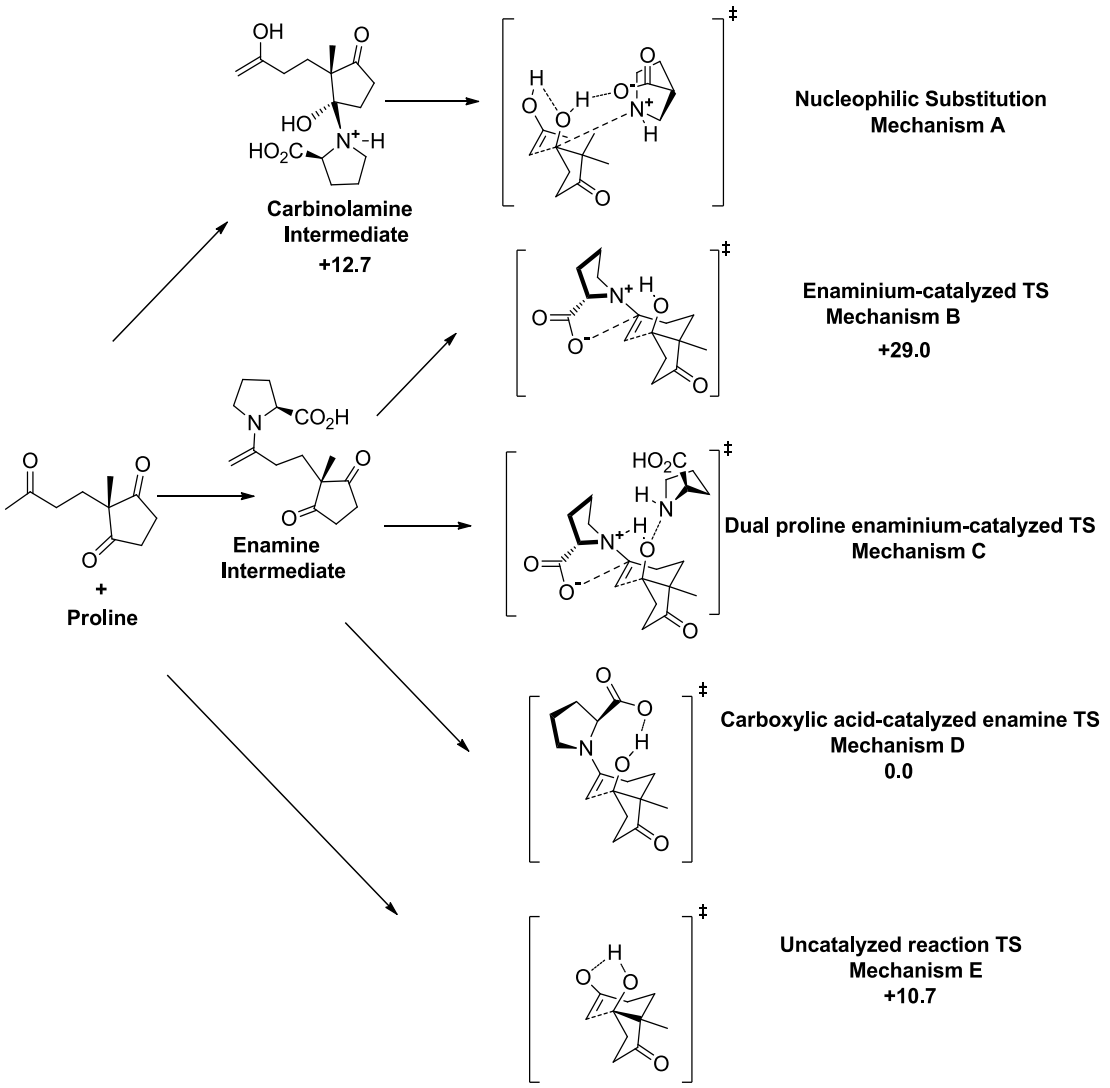

Scheme 1.8 The four mechanisms analyzed by Houk for the Hajos-Parrish reaction together with the uncatalyzed reaction. Relative energies (E + ZPE, kcal.mol^{-1}; ZPE=zero-point energy) in solvent are in kcal.mol^{-1}. Reproduced from reference [30].

1.1.2.3 Oxazolidinone mechanism

An alternative to the enamine mechanism has been proposed for the intermolecular aldol reaction that was originally reported by List, Lerner and Barbas.[33] This alternative to the **Houk-List**[30b, 31b, 34, 35] model has been proposed by Seebach and Eschenmoser.[36] Both mechanisms are presented in **Scheme 1.9**. The **Houk-List** mechanism represented in the inner circle goes through enamine **d**, while the **Seebach-Eschenmoser** alternative follows

the outer circle and goes through a bicyclic oxazolidinone **g**. There is still no unanimity on the scientific community about which is the operative mechanism. Seebach proposal was based on the existence of NMR detections of oxazolidinones reported by the groups of List[31a] and Blackmond group.[37] More recently, Gschwind[38] detected and characterized enamine intermediates in proline-catalyzed aldol reactions for the first time experimentally and showed the direct formation of enamine carboxylic acids from oxazolidinones in dimethylsulfoxide solvent. The presence of oxazolidinone intermediates is also by NMR, IR and other kinetic measurements.[36, 31a, 37a, 39] However, the fact that oxazolidinone can be formed in the media does not mean that the reaction has to go through it. In a more recent report, List and co-workers presented an elegant structural characterization of a series of proline enamines, engendering considerable impetus in favor of the enamine mechanism in proline catalysis.[35] Based on these experimental results, the Sunoj group[40] computed the mechanistic possibilities involving the enamine and oxazolidinone pathways for the proline catalyzed self-aldol reaction of propanal, see **Scheme 1.9**. They found out that the **Houk-List** model is more effective toward rationalizing the experimentally observed enantio- and diastereoselectivities than the Seebach-Eschenmoser. It seems clear that the enamine mechanism is operating in at least some case, but there is still not sufficient evidence to discard the oxazolidinone mechanism for all cases.

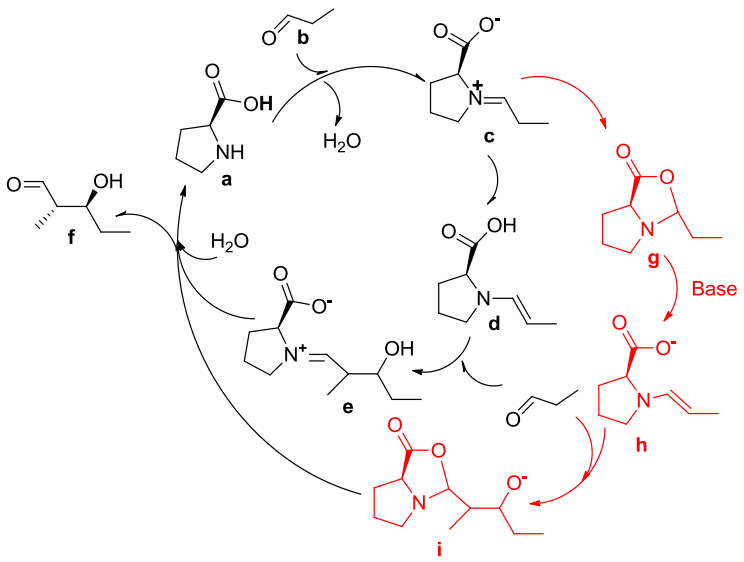

Scheme 1.9 Mechanistic possibilities involving the enamine (**Houk-List** model, black colour) and oxazolidinone (**Seebach-Eschenmoser** model, red colour) pathways. Reproduced from reference [40a].

This mechanism dichotomy is however not relevant for the work reported in this thesis. We will deal with an intramolecular aldol reaction that takes place without base additives in this step. As the **Seebach-Eschenmoser** mechanism needs a base to be operative, we will discard it in our studies, and we will concentrate on the **Houk-List** mechanism. Thus, we will consider a mechanism that goes consecutively through carbinolamine, iminium and enamine intermediates.

1.1.3 Chiral phosphoric acid catalysis

BINOL-derived phosphoric acid esters have become powerful chiral Brønsted acid catalysts in many enantioselective reactions. They constitute a series of strong, sterically tunable acids, and have found a wealth of applications. One of the best examples of this type of process is the asymmetric Mannich reactions investigated by Akiyama and coworkers (**Scheme 1.10**).[41] The proven catalytic effectiveness of HBF_4 in the Mannich reaction, led these authors to try phosphoric acid esters of BINOL fragments with nitrophenyl substituents, because of their low pKa (~1.3), cyclic structure, and the availability of the chiral source. The results were successful both in terms of yield and selectivity. About the same time, Terada and co-workers reported[42] a similar catalyst based on the phosphoric acid esters of BINOL fragments with phenyl substituents. Their optimized catalyst provides the high enantioselectivity and yield for the direct Mannich reaction of N-Boc imines, eliminating the hydrogen bond required by Akiyama´s catalyst, and providing a more practical, easily cleavable protected amine without prior nucleophile formation (**Scheme 1.11**). After Akiyama and Terada´s results, chiral phosphoric acids have become popular catalysts for many reactions, including: enamine addition,[43] transfer hydrogenation[44] Friedel–Crafts,[45] Strecker-type,[46] and Aza-Diels-Alder reactions,[47] as well as the reduction of imines[48] and enamides,[49] and allylboration of aldehydes.[50] It is a rapidly growing area of green catalysts.

In 2010, Rueping and Lin[51] reported the synthesis of *trans*-fused furanobenzopyrans (labeled as **10** in **Scheme 1.12**) through inverse-electron-demand (IED) [4+2] cycloaddition of *o*-hydroxybenzaldimines with 2,3-dihydro-2H-furan (DHF) catalyzed by chiral N-triflylphosphoramide. In the same year, Fochi and co-workers reported the synthesis of *cis*-fused furanobenzopyrans (labeled as **9** in **Scheme 1.12**) obtained through

an analogous reaction, but catalyzed in this case by chiral phosphoric acid.[52] The same reactants and slightly different catalysts produced different diastereomers of the product. We are interested in the origin of this different behavior, so we will analyze the topic in this doctoral thesis.

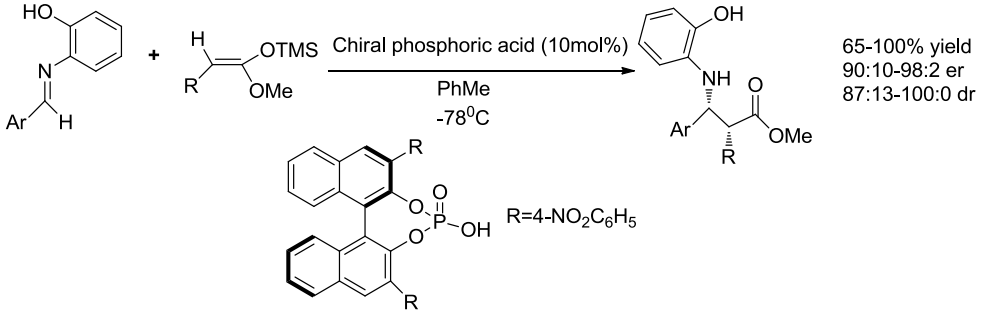

Scheme 1.10 Akiyama´s asymmetric Mannich reaction.[41]

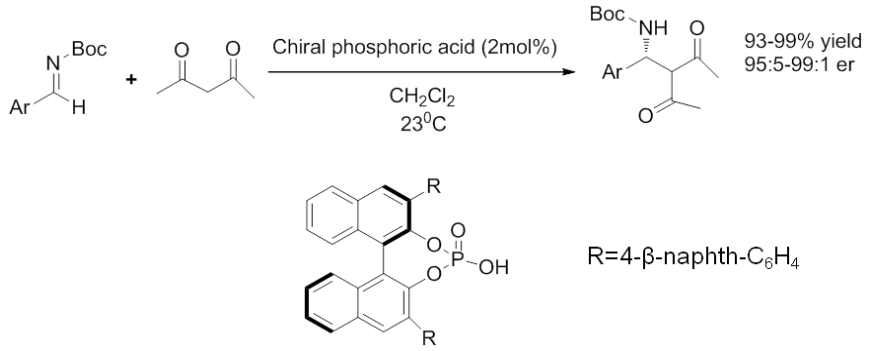

Scheme 1.11 Terada´s enantioselective Mannich reaction.[42]

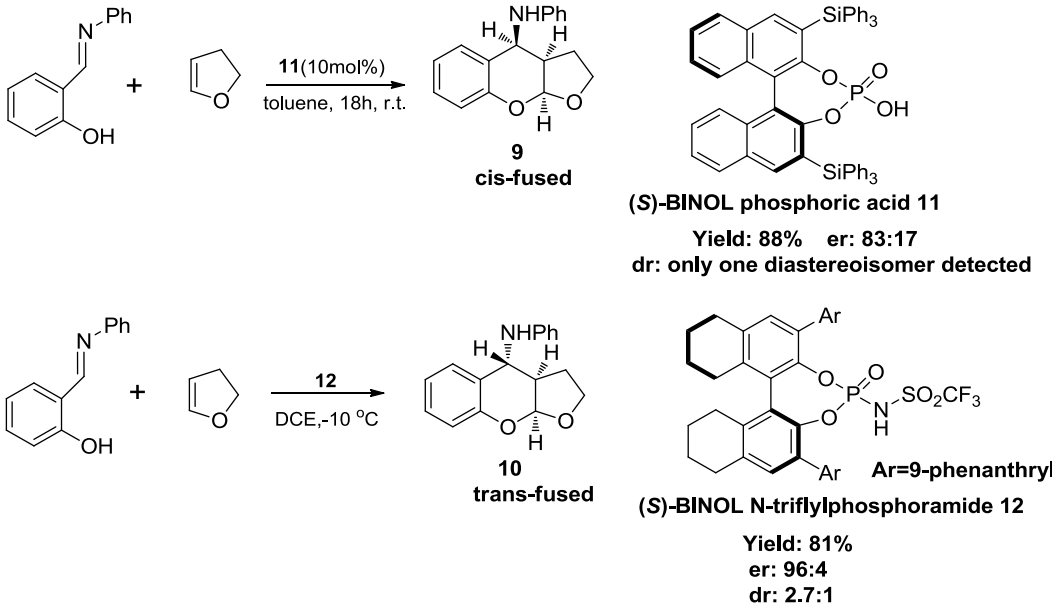

Scheme 1.12 Reaction of *o*-hydroxybenzaldimines with 2,3-dihydro-2H-furan(DHF) catalyzed by (*S*)-BINOL-derived phosphoric acid and N-triflylphosphoramide.[51,52]

1.2 Computational methods for organocatalysis

In the course of this thesis, we have used mostly standard methods. The particular details for each system are given in each chapter. In this section, we present a brief summary of the DFT and DFT/MM methods we have used to compute the energy, followed by discussions on specific technical approaches applied in different chapters that have been highlighted because they may be less well known or to dispel possible confusions.

1.2.1 Energy evaluation with DFT and DFT/MM methods

All computational analysis starts from the calculation of the energy, and for this we have used in most cases density functional theory (DFT). Density functional theory (DFT) is a computational method that derives the properties of the molecule based on its electron distribution. Modern formulations of DFT are based on the Hohenberg–Kohn theorem. In the last two decades, DFT has become the most widely used quantum chemical method[53,54] in chemistry and physics. No exact functional of general application has been so far found, and because of this, research activity continues in functional development. DFT lacks the strong hierarchy of expected quality of results that is present on Hartree-Fock based methods. A classification can nevertheless be made based on the criteria of Perdew *et al.*, who categorized their development into five rung functionals, as called "Jacob's ladder".[55] The five rungs of this ladder are:

(1) Local density approximation (LDA). The basic approximation is the local density approximation (LDA) which considers that the energy depends only on the density, but not on its gradient or higher order derivatives. This LDA approximation was first proposed by Dirac in 1930.[56] The local spin-density approximation (LSDA) included the electron spin dependence in the description,[57] and was designed for systems with unpaired electrons. These functional are good for solid state physics, but limited in the reproduction of chemical properties.

(2) Generalized gradient approximation (GGA). In these functionals, the density functional depends on the density and on the density gradient. The approximation is more complex than that of the LDA functionals. Functionals following the GGA formalism

typically improve the results obtained with LDA functionals, in particular in the calculation of chemical properties. Their performance is however limited in a number of cases, for example when accurate descriptions of Van der Waals interactions are needed.[58] They bring no significant improvement for calculations in the solid state.[59] Among the numerous functionals following the GGA formalism, BP86,[60,61] and BLYP are widely used.[60, 62]

(3) Meta-GGA approximation. In this approach the energy dependence is extended to include the second derivative of the density, that is, the Laplacian, as well as the kinetic energy density. Example of meta-GGA functionals are as TPSS[63] and M06-L.[64]

(4) Hybrid approximation. This is a very popular class of functionals, which combines the exchange-correlation term of the GGA, or meta-GGA, approximation with a part of the Hartree-Fock exchange. Hybrid GGA functionals have been widely used because they bring a significant improvement over the GGA functionals in a number of cases. The most popular hybrid functional is B3LYP. Truhlar and coworkers have developed a suite of hybrid meta-GGA density functionals including M06, M06HF, M062X, M05, and M052X.[65] Hybrid Meta-GGA functionals are now increasingly used in chemical modeling, because some of them appear to describe accurately molecular systems containing weak interactions (such as van der Waals interactions).

(5) Non local functionals. The energy dependence can be extended beyond the terms described above. There is work on the development of these functionals, but none of them has reached so far a widespread use.

A significant methodological development that has gained widespread application in recent years but stays out of this classification is the introduction of dispersion corrections. In addition to mixing the HF-exchange into a given density functional, the extended hybrid functionals developed by Grimme and co-workers include a fraction of the MP2 correlation energy calculated with hybrid DFT orbitals.[66] In the revisions of Gaussian09 used during this thesis, the only Grimme functional available for geometry optimizations is B97D.[67]

Different functionals have been used throughout this thesis. In particular, we have applied the hybrid GGA functional B3LYP, and the hybrid Meta-GGA functionals M06, M062x and B97D.

Quantum Mechanics (QM) methods grow computationally demanding as the system size increases. A solution to the problem of computational cost for large systems is the use of different descriptions for different regions of the system. The combination of QM (Quantum Mechanics) and MM (Molecular Mechanics) in QM/MM methods is particularly interesting. In an ideal case, it allows the investigation of large and complicated systems at a reasonable cost while still yielding the necessary accuracy. The idea is to apply a quantum molecular method to the most important part (chemically relevant, or difficult to describe) of the molecule, and a molecular mechanics method to the rest of the system. In this thesis the ONIOM method,[68] a subtractive QM/MM scheme, has been used.

1.2.2 Specific approaches used in this work

1.2.2.1 Evaluation of isomer population and enantiomeric excess

According to statistical thermodynamics, in an equilibrium situation involving low interconversion barriers, the fraction of total molecules in a given isomeric form can be obtained from the Boltzmann distribution outlined in Eq. (1.1):

$$p_i = \frac{n_i}{\sum_j n_j} = \frac{e^{-G_i/(RT)}}{\sum_j e^{-G_j/(RT)}} = \frac{Q_i}{Q} \quad (1.1)$$

In Eq. (1.1), the left hand side p_i is the fraction of total molecules in isomeric form i, G_i is the energy of isomer i, n_i, n_j are numbers of molecules in a given isomeric form, R is the ideal gas constant, equal to 8.314 J.mol^{-1}.K^{-1} and T is the temperature in K. Q is the partition function.

Simple mathematical manipulations allow to simplify the formula above moving from absolute, in principle large, G_i values to relative ones ΔG_i. , where the energy is referred to that of the most stable isomer, as shown in Eq. (1.2),

$$e^{-G_i/RT} = e^{-(\Delta G_i + G_{ref})/(RT)} = Ce^{-\Delta G_i/(RT)}$$

$$p_i = \frac{e^{-\Delta G_i/(RT)}}{\sum_j e^{-\Delta G_j/(RT)}} = \frac{Q_{i(relat)}}{Q_{(relat)}} \qquad (1.2)$$

An analogous reasoning can be applied to the relationship between transition state energies and reaction selectivity. In this case, there is kinetic control, and we have to make the reasonable assumption that the relative population of two different products is related to the population of the transition states leading to them. This approach, which is exact for simple mechanisms with parallel paths to each of the two products differing only in the key transition state, yields Eq. (1.3),

$$er = \frac{S}{R} = \frac{\Sigma_i e^{-\Delta G_{Si}/(RT)}}{\Sigma_i e^{-\Delta G_{Ri}/(RT)}}$$

$$ee = \frac{S-R}{S+R} = \frac{er-1}{er+1} * 100 \qquad (1.3)$$

In this case *S* is the major enantiomer, and *R* is the minor one, and the extended summations account for the possibility than more of one pathway leads to each of the enantiomers. ΔG_{Si}, ΔG_{Ri} are relative transition state energies. All have to be referred to the same origin of energies, which can be the reactant, or the lowest energy transition state.

1.2.2.2 Calculation of the free energy in solution

In this thesis, the free energy in solution is calculated in most cases through Eq. (1.4):

$$G_{(sol)} = G_{(gas)} - E_{(gas)} + E_{(sol)} \qquad (1.4)$$

$G_{(sol)}$ is the free energy in solution, $E_{(sol)}$ is the potential energy in solution, $G_{(gas)}$ is the free energy in gas phase, $E_{(gas)}$ is the potential energy in gas phase. This procedure was followed because the direct evaluation of frequencies in solution was not available in the early part of the thesis. The entropic contributions had to be thus calculated in gas phase,

and it was assumed that they would be the same in solution. In some of the most recent calculations, we have applied the formally more elegant approach of computing directly the free energy corrections in solution. These cases are indicated in the text.

1.2.2.3 Basis set superposition error (BSSE)

When the atoms of interacting molecules (or of the different parts of the same molecule) approach one another, their basis functions overlap. If the basis set is not perfectly balanced, electrons may move from the more "base-poor" part to the more "base-rich" region, in a computational artifact that will wrongly overstabilize the system. This is the basis set superposition error (BSSE). In the dimer, basis functions on one monomer compensate for the basis set incompleteness on the other monomer. Through the BSSE effect, the dimer will be lowered in energy and the strength of the bond overestimated.

One of the most popular methods to reduce BSSE is the counterpoise (CP) correction,[69] which is briefly described here. In mathematical terms, the uncorrected interaction energy (including BSSE) between two fragments A, B, is described in Eq. (1.5):

$$\Delta E_{\text{int}}(AB) = E_{ab}^{AB}(AB) - E_{a}^{A}(A) - E_{b}^{B}(B) \quad (1.5)$$

Where the subscripts denote the basis used, the superscripts denote the geometry, and the symbol in parentheses denotes the chemical system considered. Thus, $E_{ab}^{AB}(AB)$ represents the energy of the bimolecular complex AB evaluated in the full basis set ab, computed at the geometry of the full system. Likewise, fragments A and B are each evaluated at their own geometries in their own basis sets.

It would be in principle better to compute all systems with the full basis set ab, as shown in Eq. (1.6).

$$\Delta E_{\text{int}}^{CP}(AB) = E_{ab}^{AB}(AB) - E_{ab}^{A}(A) - E_{ab}^{B}(B) \quad (1.6)$$

The relationship between both expressions can be decomposed in two parts, one corresponding to each fragment:

$$\begin{aligned} E_{BSSE}(A) &= E_{ab}^{A}(A) - E_{a}^{A}(A) \\ E_{BSSE}(B) &= E_{ab}^{B}(B) - E_{b}^{B}(B) \end{aligned} \quad (1.7)$$

$E_{ab}^{A}(A)$ monomer A in the dimer basis ab, $E_{a}^{A}(A)$ monomer A in its monomer basis a, $E_{ab}^{B}(B)$ monomer B in the dimer basis ab, $E_{b}^{B}(B)$ monomer B in its monomer basis b.

The CP correction is the defined in Eq.(1.8):

$$\Delta E_{CP} = E_{ab}^{A}(A) + E_{ab}^{B}(B) - E_{a}^{A}(A) - E_{b}^{B}(B) \quad (1.8)$$

1.3 Objectives

Organocatalysis is an increasingly important field in chemistry, its contributions to the field of asymmetric synthesis being particularly important. Further developments in the field will be substantially helped by an improved mechanistic understanding, and we consider that computational chemistry can assist in bringing this improved understanding. This thesis has the following objectives:

- Evaluate the performance of DFT and DFT/MM methods for the reproduction of experimental enantiomeric excess values in organocatalytic processes. These methods have proved its value in the field of transition metal catalysis, and it is important to see how they work in organocatalytic systems and identify the possible pitfalls.

- Analyze the mechanism of the Friedel–Crafts (FC) reaction between ethyl 3,3,3-trifluoromethylpyruvate and indole catalyzed by water plus the iridium complex (η^5–C_5Me_5) Ir {(*R*)–Prophos} (Prophos = propane–1,2–diylbis(diphenylphosphane) reported by Carmona and co-workers. Is it an organocatalytic process or is the iridium center interacting with the substrates? How is enantioselectivity transmitted from the diphosphane ligand to the reaction center?

- Study the intramolecular aldol reaction leading to Wieland-Miescher ketones catalyzed by N-Ts-(S_a)-binam-L-prolinamide in the presence of carboxylic acids reported by Bonjoch and co-workers. What is the difference between proline and prolinamide as catalysts? What is the role of the carboxylic acid co-catalyst? What is the origin of enantioselectivity?

- Clarify the mechanism for the [4+2] cyclization reaction between *o*-hydroxybenzaldimine and 2,3-dihydro-2H-furan leading to furanobenzopyrans catalyzed by phosphoric acid derivatives. What are the key interactions ruling the selectivity? Why do seemingly similar

catalysts such as a (*S*)-BINOL-derived phosphoric acid ester and an N-triflylphosphoramide derivative of a (*S*)-BINOL ester produce different selectivities?

- Provide qualitative explanations for the origin of selectivity in each of the systems studied, and see how they fit the generally established views on chiral reactions.

1.4 References

[1]. Metal catalysis: (a) Asymmetric Catalysis in Organic Synthesis, Ed.: Noyori R., Wiley, New York, **1994**; (b) Comprehensive Asymmetric Catalysis, Eds.: Jacobsen E. N., Pfaltz A., Yamamoto H., Springer, Berlin, **1999**; (c) Catalytic Asymmetric Synthesis, 2nd ed, Eds.: Ojima I., Wiley-VCH, New York, **2000**; (d) Transition Metals for Organic Synthesis, 2nd ed, Eds.: Beller M., Bolm C., Wiley-VCH, Weinheim, **2004**.

[2]. Biocatalysis: (a) Biocatalysts for Fine Chemicals Synthesis, Ed.: Roberts S. M., Wiley-VCH, New York, **1999**; (b) Enzyme Catalysis in Organic Synthesis, 2nd ed, Eds.: Drauz K., Waldmann H., Wiley-VCH, Weinheim, **2002**; (c) Biocatalysis, Eds.: Bommarius A. S., Riebel B. R., Wiley-VCH, Weinheim, **2004**.

[3]. (a) Dalko P. I., Moisan L., *Angew. Chem*, **2001**, 113, 3840; *Angew. Chem. Int. Ed*, **2001**, 40, 3726; (b) List B., *Synlett*, **2001**, 1675; (c) List B., *Tetrahedron*, **2002**, 58, 2481; (d) Dalko P. I., Moisan L., *Angew. Chem*, **2004**, 116, 5248; *Angew. Chem. Int. Ed*, **2004**, 43, 5138; (e) Berkessel A., GrOger H., Asymmetric Organocatalysis, Wiley-VCH, Weinheim, **2005**; (f) Seayad J., List B., *Org. Biomol. Chem*, **2005**, 3, 719; (g) Lelais G., MacMillan D. W. C., *Aldrichimica. Acta*, **2006**, 39, 79; (h) Enders D., Grondal C., Hüttl M. R. M., *Angew. Chem. Int. Ed*, **2007**, 46, 1570; (i) Enders D., Wang C., Liebich J. X., *Chem. Eur. J*, **2009**, 15, 11058; (j) Grondal C., Jeanty M., Enders D., *Nature Chemistry*, **2010**, 2, 167; (k) Grossmann A., Enders D., *Angew. Chem*, **2012**, 124, 320; *Angew. Chem. Int. Ed*, **2012**, 51, 314.

[4]. (a) Schreiner P. R., *Chem. Soc. Rev*, **2003**, 32, 289; (b) Dalko P. I., Moisan L., *Angew. Chem. Int. Ed*, **2001**, 40, 3726.

[5]. (a) Schoemaker H. E., Mink D., Wubbolts M. G., *Science*, **2003**, 299, 1694; (b) Broerse J. E. W., Visser B., Assessing the Potential in Biotechnology: Building on Farmers' Knowledge, Eds: Bunders J., Haverkort B., Hiemstra W., Macmillian Education Ltd, London and Bashingstoke, **1996**.

[6]. For some general reviews on organocatalysis. (a) Bertelsen S., Jørgensen K. A., *Chem. Soc. Rev.*, **2009**, 38, 2178; (b) Palomo C., Oiarbide M., López R., *Chem. Soc. Rev*, **2009**, 38, 2178; (c) MacMillan D. W. C., *Nature*, **2008,** 455, 304; (d) Melchiorre P., Marigo M., Carlone A., Bartoli G., *Angew. Chem. Int. Ed*, **2008**, 47, 6138; (e) Dondoni A., Massi A., *Angew. Chem. Int. Ed*, **2008**, 47, 4638.

[7]. Dalko P. I., Moisan L., *Angew. Chem. Int. Ed*, **2004**, 43, 5138.

[8]. Melchiorre P., Marigo M., Carlone A., Bartoli G., *Angew. Chem. Int. Ed*, **2008**, 47, 6138.

[9]. For proline derivatives: (a) Priem G., Anson M. S., Macdonald S. J. F., Pelotier B., Campbell I. B., *Tetrahedron Lett*, **2002**, 43, 6001; (b) Priem G., Pelotier B., Campbell I. B., Macdonald S. J. F., Anson M. S., *Synlett*, **2003**, 5, 679; (c) Priem G., Pelotier B., Macdonald S. J. F., Anson M. S., Campbell I. B., *J. Org. Chem*, **2003**, 68, 3844; (d) Shaw S. A., Aleman P., Vedejs E., *J. Am. Chem. Soc*, **2003**, 125, 13368; (e) Rabalakos C., Wulff W. D., *J. Am. Chem. Soc*, **2008**, 130, 13524.; (f) Tang Z., Jiang F., Yu L. T., Cui X., Gong L. Z., Mi A. Q., Jiang Y. Z., Wu Y. D., *J. Am. Chem. Soc*, **2003**, 125, 5262; (g) Hartikka A., Arvidsson P. I., *Eur. J. Org. Chem*, **2005**, 20, 4287; (h) Mase N., Nakai Y., Ohara N., Yoda H., Takabe K., Tanaka F., Barbas C. F. III., *J. Am. Chem. Soc*, **2006**, 128, 734; (i) Zhu Q., Lu Y., *Org. Lett*, **2008**, 10, 4803.

[10]. (a) Wynberg H., Staring E. G. J., *J. Am. Chem. Soc*, **1982**, 104, 166; (b) Wynberg H., Staring E. G. J., *J. Am. Chem. Soc*, **1985**, 50, 1977.

[11]. Bolm C., Gerlach A., Dinter C. L., *J. Am. Chem. Soc*, **2000**, 122, 8793.

[12]. (a) Ruble J. C., Tweddell J., Fu G. C., *J. Org. Chem*, **1998**, 63, 2794; (b) Tao B. T., Ruble J. C., Hoic D. A., Fu G. C., *J. Am. Chem. Soc*, **1999**, 121, 5091; (c) Fu G. C., *Acc. Chem. Res*, **2000**, 33, 412.; (d) Murugan, R., Scriven, E. F. V., *Aldrichimica Acta*, **2003**, 36, 21.

[13]. (a) Sigman M. S., Jacobsen E. N., *J. Am. Chem. Soc*, **1998**, 120, 4901; (b) Reisman S. E., Doyle A. G., Jacobsen E. N., *J. Am. Chem. Soc*, **2008**, 130, 7198; (c) Sohtome Y., Tanatani A., Hashimoto Y., Nagasawa K., *Tetrahedron Lett*, **2004**, 45, 5589; (d) Dove A. P., Pratt R. C., Lohmeijer B. G. G., Waymouth R. M., Hedrick J. L., *J. Am. Chem. Soc*, **2005**, 127, 13798.

[14]. (a) Akiyama T., *Chem. Rev*, **2007**, 107, 5744; (b) Terada M., *Chem. Commun*, **2008**, 4097; (c) Terada M., *Synthesis*, **2010**, 1929; (d) Terada M., *Bull. Chem. Soc. Jpn*, **2010**, 83, 101; (e) Terada M., *Curr. Org. Chem*, **2011**, 15, 2227; (f) Terada M., Kanomata K., *Synlett*, **2011**, 1255.

[15]. (a) Corey E. J., Grogan M. J., *Org. Lett*, **1999**, 1, 157; (b) Xu J. Y., Guan Y., Yang S., Ng Y., Peh G., Tan C. H., *Chem. Asian. J*, **2006**, 1, 724.

[16]. (a) Bahmanyar S., Houk K. N., *J. Am. Chem. Soc*, **2001**, 123, 12911; (b) Rankin K. N., Gauld J. W., Boyd R. J., *J. Phys. Chem. A*, **2002**, 106, 5155; (c) Arno M., Domingo L. R., *Theor. Chem. Acc*, **2002**, 108, 232; (d) Hoang L., Bahmanyar S., Houk K. N., List B., *J. Am. Chem. Soc*, **2003**, 125, 16; (e) List B., Hoang L., Martin H. J., *Proc. Natl. Acad. Sci*, **2004**, 101, 5839; (f) Jung Y., Marcus R. A., *J. Am. Chem. Soc*, **2007**, 129, 5492; (g) Houk K. N., Cheong P. H. Y., *Nature*, **2008**, 455, 309; (h) Fjermestad T., Pericás M. A., Maseras F., *Chem. Eur. J*, **2011**, 17, 10050.

[17]. (a) Friedel C., Crafts J. M., Hebd C. R., *Séances Acad. Sci*, **1877**, 84, 1392; (b) Friedel C., Crafts J. M., Hebd C. R., *Séances Acad. Sci*, **1877**, 84, 1450.

[18]. (a) Friedel-Crafts and Related Reactions, Ed.: Olah G. A., Wiley, New York, **1963**; (b) Friedel-Crafts Chemistry, Ed.: Olah G. A., Wiley, New York, **1973**.

[19]. (a) Reddy B. V. S., Chaya D. N., Yadav J. S., Chatterjee D., Kunwa A. C., *Tetrahedron. Letts*, **2011**, 52, 2961; (b) Ghosh A. K., Martyr C. D., Xu C. X., *Org. Lett*, **2012**, 14, 2002; (c) Mukaiyama T., Suzuki K., Han J. S., Kobayashi S., *Chem. Lett*, **1992**, 3, 435; (d) Yang F., Ji K. G., Ali S., Liang Y. M., *J. Org. Chem*, **2011**, 76, 8329.

[20]. Kiasat A. R., Karimi-Cheshmeali M., Soleymani R., Rajabzadeh H., *E-J. Chem*, **2012**, 9, 1875.

[21]. (a) Blake J. F., Jorgensen W. L., *J. Am. Chem. Soc*, **1991**, 113, 7430; (b) Blake J. F., Lim D., Jorgensen W. L., *J. Org. Chem*, **1994**, 59, 803.

[22]. Severance D. L., Jorgensen W. L., *J. Am. Chem. Soc*, **1992**, 114, 10966.

[23]. Gruttadauria M., Giacalone F., Noto R., *Adv. Synth. Catal*, **2009**, 351, 33.

[24]. Sodeoka M., Hamashima Y., *Chem. Commun*, **2009**, 5787.

[25]. Sukumaran J., Hanefeld U., *Chem. Soc. Rev*, **2005**, 34, 530.

[26]. Eder U., Sauer G., Wiechert R., *Angew. Chem. Int. Ed*, **1971**, 10, 496.

[27]. Hajos Z. G., Parrish D. R., *J. Org. Chem*, **1974**, 39, 1615.

[28]. Zhong G., Hoffmann T., Lerner R. A., Danishefsky S., Barbas C. F. III., *J. Am. Chem. Soc*, **1997**, 119, 8131.

[29]. (a) Bradshaw B., Etxebarria-Jardia G., Bonjoch J., Guillena G., Nájera C., Viózquez S. F., *Adv. Synth. Catal*, **2009**, 351, 2482; (b) Bradshaw B., Etxebarria-Jardıa G., Bonjoch J., *J. Am. Chem. Soc*, **2010**, 132, 5966.

[30]. (a) Fernando R. C., Houk K. N., *Angew. Chem. Int. Ed*, **2004**, 43, 5766; (b) Cheong P. H.-Y., Legault C. Y., Um J M., Çelebi-Ölçüm N., Houk K. N., *Chem. Rev*, **2011**, 111, 5042.

[31]. (a) List B., Hoang L., Martin H. J., *Proc. Natl. Acad. Sci*, USA **2004**, 101, 5839; (b). Hoang L., Bahmanyar S., Houk K. N., List B., *J. Am. Chem. Soc*, **2003**, 125, 16.

[32]. (a) Agami C., *Bull. Soc. Chim. Fr*, **1988**, 3, 499-507; (b) Puchot C., Samuel O., Dunach E., Zhao S., Agami C., Kagan H. B., *J. Am. Chem. Soc*, **1986**, 108, 2353.

[33]. List B., Lerner R. A., Barbas C. F. III., *J. Am. Chem. Soc*, **2000**, 122, 2395.

[34]. Bahmanyar S., Houk K. N., Martin H. J., List B., *J. Am. Chem. Soc*, **2003**, 125, 2475.

[35]. Bock D. A., Lehmann C. W., List B., *Proc. Natl. Acad. Sci*, U. S. A., **2010**, 107, 20636.

[36]. Seebach D., Beck A. K., Badine D. M., Limbach M., Limbach M., Eschenmoser A., Treasurywala A. M., Hobi R., Prikoszovich W., Linder B., *Helv. Chim. Acta*, **2007**, 90, 425.

[37]. (a) Iwamura H., Mathew S. P., Blackmond D. G., *J. Am. Chem. Soc*, **2004**, 126, 11770; (b) Iwamura H., Wells D. H., Jr., Mathew S. P., Klussmann M., Armstrong A., Blackmond D. G.,

J. Am. Chem. Soc, **2004**, 126, 16312; (c) Mathew S. P., Iwamura H., Blackmond D. G., *Angew. Chem*, **2004**, 116, 3379; *Angew. Chem. Int. Ed*, **2004**, 43, 3317.

[38]. Schmid M. B., Zeitler K., Gschwind R. M., *Angew. Chem. Int. Ed*, **2010**, 49, 4997.

[39]. Kanzian T., Lakhdar S., Mayr H., *Angew. Chem. Int. Ed*, **2010**, 49, 9526.

[40]. (a) Sharma A. K., Sunoj R. B., *Angew. Chem. Int. Ed*, **2010**, 49, 6373; (b) Sharma A. K., Sunoj R. B., *Chem. Commun*, **2011**, 47, 5759.

[41]. Akiyama T., Itoh J., Yokota K., Fuchibe K., *Angew. Chem. Int. Ed*, **2004**, 43, 1566.

[42]. Uraguchi D., Terada M., *J. Am. Chem. Soc*, **2004**, 126, 5356.

[43]. (a) Terada M., Machioka K., Sorimachi K., *Angew. Chem. Int. Ed*, **2006**, 45, 2254; (b) Terada M., Machioka K., Sorimachi K., *J. Am. Chem. Soc*, **2007**, 46, 10336.

[44]. (a) Rueping M., Antonchick A. P., Theissmann T., *Angew. Chem. Int. Ed*, **2006**, 45, 6751; (b) Rueping M., Antonchick A. P., Theissmann T., *Angew. Chem. Int. Ed*, **2006**, 45, 3683; (c) Rueping M., Antonchick A. P., *Angew. Chem. Int. Ed*, **2007**, 46, 4562.

[45]. (a) Sun F. L., Zheng X. J., Gu Q., He Q. L., You S. L., *Eur. J. Org. Chem*, **2010**, 47; (b) Yang L., Zhu Q. M., Guo S. M., Qian B., Xia C. G., Huang H. M., *Chem. Eur. J*, **2010**, 16, 1638; (c) You S. L., Cai Q., Zeng M., *Chem. Soc. Rev*, **2009**, 38, 2190; (d) Sun F. L., Zeng M., Gu Q., You S. L, *Chem. Eur. J*, **2009**, 15, 8709; (e) Sheng F. Y., Gu Q., Zhang A. J., You S. L., *J. Org. Chem*, **2009**, 74, 6899; (f) Liu H., Dagousset G., Masson G., Retailleau P., Zhu J. P., *J. Am. Chem. Soc*, **2009**, 131, 4598; (g) Kang Q., Zheng X. J., You S. L., *Chem. Eur. J*, **2008**, 14, 3539; (h) Jia Y. X., Zhong J., Zhu S. F., Zhang C. M., Zhou Q. L., *Angew. Chem. Int. Ed*, **2007**, 46, 5565; (i) Kang Q., Zhao Z. A., You S. L., *J. Am. Chem. Soc*, **2007**, 129, 1484.

[46]. (a) Rueping M., Sugiono E., Azap C., *Angew. Chem. Int. Ed*, **2006**, 45, 2617; (b) Rueping M., Sugiono E., Moreth S. A., *Adv. Synth. Catal*, **2007**, 349, 759.

[47]. Akiyama T., Morita H., Fuchibe K., *J. Am. Chem. Soc*, **2006**, 128, 13070.

[48]. Rueping M., Sugiono E., Azap C., Theissmann T., Bolte. M., *Org. Lett*, **2005**, 7, 3781.

[49]. Li G. L., Antilla. J. C., *Org. Lett*, **2009**, 11, 1075.

[50]. Jain P., Antilla J. C., *J. Am. Chem. Soc*, **2010**, 132, 11884.

[51]. Rueping M., Lin M. Y., *Chem. Eur. J*, **2010**, 16, 4169.

[52]. Bernardi L., Comes-Franchini M., Fochi M., Leo V., Mazzanti A., Ricci A., *Adv. Synth. Catal*, **2010**, 352, 3399.

[53]. Density-Functional Theory of Atoms and Molecules, Eds: Parr G., Yang W., Oxford University Press, Oxford, **1989**.

[54]. A Chemist's Guide to Density Functional Theory, Eds: Koch W., Holthausen M. C., Wiley-VCH, New York, **2001**.

[55]. Perdew J. P., Ruzsinszky A., Tao J., Staroverov V. N., Scuseria G. E., Csonka G., *J. Chem. Phys*, **2005**, 123, 62201.

[56]. Dirac P. A. M., *Proc. Cambridge Philos. So*, **1930**, 26, 376.

[57]. Slater J. C., *Phys. Rev*, **1951**, 81, 385.

[58]. Tao J. M., Perdew J. P., *J. Chem. Phys*, **2005**, 122, 7.

[59]. Kurth S., Perdew J. P., Blaha, P., *Int. J. Quant. Chem*, **1999**, 75, 889.

[60]. Becke A. D., *Phys. Rev. A*, **1988**, 38, 3098.

[61]. Perdew J. P., *Phys. Rev. B*, **1986**, 33, 8822.

[62]. Lee C. T., Yang W. T., Parr R. G., *Phys. Rev. B*, **1988**, 37, 785.

[63]. Tao J. M., Perdew J. P., Staroverov V. N., Scuseria G. E., *Phys. Rev. Lett*, **2003**, 91, 4.

[64]. Zhao Y., Truhlar D. G., *J. Chem. Phys*, **2006**, 125, 194101.

[65]. Zhao Y., Truhlar D. G., *Theor. Chem. Acc*, **2008**, 120, 215.

[66]. Schwabe T., Grimme S., *Phys. Chem. Chem. Phys*, **2007**, 9, 3397.

[67]. Grimme S., *J. Comp. Chem*, **2006**, 27, 1787.

[68]. (a) Maseras F., Morokuma K., *J. Comput. Chem*, **1995**, 16, 1170. (b) Humbel S., Sieber S., Morokuma K., *J. Chem. Phys*, **1996**, 105, 1959. (c) Matsubara T., Sieber S., Morokuma K., *Int. J. Quant. Chem*, **1996**, 60, 1101. (d) Svensson M., Humbel S., Froese R. D. J., Matsubara T., Sieber S., Morokuma K., *J. Phys. Chem*, **1996**, 100, 19357. (e) Svensson M., Humbel S., Morokuma K., *J. Chem. Phys*, **1996**, 105, 3654. (f) Vreven T., Morokuma K., *J. Comput. Chem*, **2000**, 21, 1419. (g) Vreven T., Byun K. S., Komaromi I., Dapprich S., Montgomery J. A., Jr., Morokuma K., Frisch M. J., *J. Chem. Theory and Comput*, **2006**, 2, 815.

[69]. Boys S. F., Bernardi F., *Mol. Phys*, **1970**, 19, 553.

Chapter1

Chapter 2

Asymmetric Friedel-Crafts hydroxyalkylation of indoles catalyzed by chiral Brønsted-acids

2.1 Experimental background

Chiral Brønsted-acid catalysis is a rapidly growing area of organocatalysis.[1] The H–bond donating ability of the catalysts are usually increased by means of electron–withdrawing substituents.[1a,d,g] Metal containing substituents have been rarely employed to this end. In this respect, Sodeoka and Hamashima reported that chiral cationic Pd aqua complexes catalyze the C-C bond forming reaction between enolates and carbon based electrophiles in a highly enantioselective manner.[2] And Yamamoto *et al*. reported that the coordination of binols to $SnCl_4$ enhances the acidity of the former, rendering active Brønsted-acid catalysts for the enantioselective protonation of silyl enol ethers and biomimetic cyclization of polyprenoids.[3] In this line, Carmona and co-workers disclosed the use of the water adduct of the chiral iridium fragment (η^5–C_5Me_5) Ir {(*R*)–Prophos} (Prophos = propane–1,2–diylbis(diphenylphosphane)[4] (labeled as **1**) as chiral Brønsted–acid catalyst (**Scheme 2.1**) for the Friedel–Crafts (FC) reaction between ethyl 3,3,3-trifluoromethylpyruvate and indole at the low temperature (**Scheme 2.2**).

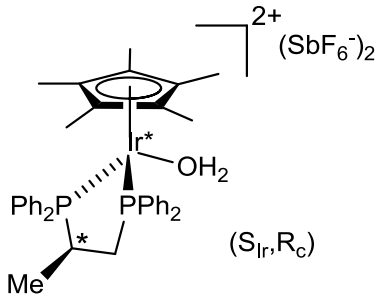

Scheme 2.1 Brønsted-acid catalyst **1**.

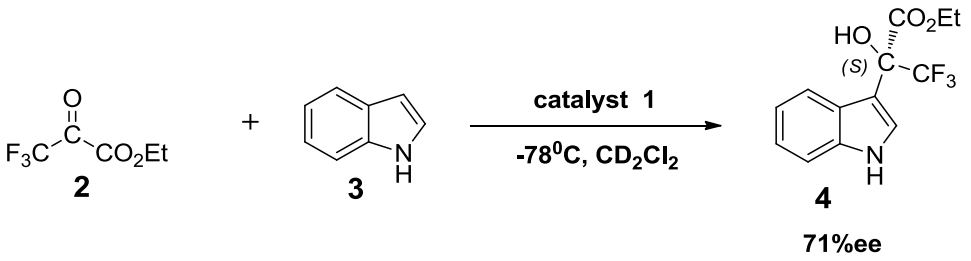

Scheme 2.2 Catalytic Friedel–Crafts reaction (experimental data from Prof. Carmona group) .

Water is one of the simplest molecules with Brønsted–acid capabilities. The coordination of the water molecules to the carbonyl function in Diels–Alder reactions[5] and Claisen rearrangements[6] results in the enhancement of the reaction rate. The manifold role of water in some organocatalytic reactions has been extensively discussed.[7] However, as far as we know, the direct involvement of a water molecule in chiral metal-containing Brønsted–acid catalysis has been rarely reported so far.[2] Therefore, based on Prof. Carmona group experimental results, we carried out a computational study on the mechanism of this reaction (**Scheme 2.2**) and evaluated the catalytic role of the metal complex and water in this reaction.

2.2 Computational details

Density functional theory (DFT) calculations were performed using the **Gaussian 09** suite of programs[8] with the M06 functional.[9] Geometries were fully optimized using the Stuttgart/Dresden ECPs (SDD) basis set[10] for Ir, while the polarized 6-31G(d)[11] basis set was used for all remaining atoms C, O, P, N, F, and H. The natures of the stationary points as minima or transition states were confirmed by frequency calculations at the experimental temperature -78^{0}C. The connectivity between the transition state and the associated minima was confirmed by a combination of intrinsic reaction coordinate (IRC) calculations (in the region near the transition state) and geometry optimization (connecting the final point of the IRC to the local minimum). Solvation effects were introduced through single-point calculations based on the optimized gas phase geometries using SMD model[12] at the M06 level with the SDD basis set for Ir, and 6-31+G (d) basis set for all

remaining atoms. Dichloromethane (dielectric constants of 8.93) was used as solvent. The potential energies in solution were taken directly from the SCRF calculation, and the free energies in solution were obtained from the additional introduction of the gas phase entropy corrections (refer to **1.2.2.2**).

2.3 Free energy profile of the model system

In order to save computing resource, at the beginning we use the model system (**Scheme 2.3**) for a mechanistic study. On the reactant **2-t**, the only change was the replacement of an ethyl group of the pyruvate by a methyl group. This should have a minor electronic effect, but helps the calculation by reducing the conformational complexity. The changes in the catalyst **1-t** were more substantial. The pending phenyl groups of the diphosphine were replaced by hydrogen atoms and the methyl groups of the Cp* ligands were also replaced by hydrogen atoms. This reduced substantially the cost of the calculations.

The computed free energy profile is reported in **Figure 2.1**. Optimized structures are shown in **Figure 2.2**. The methyl 3,3,3-trifluoromethylpyruvate **2-t** approaches initially the catalyst-model **1-t** to form **ADD1-t**, and two hydrogen bonds are formed between hydrogen atoms of the iridium-bound water molecule and the oxygen of the pyruvate carbonyl, with distances of 1.76 Å and 1.89 Å. **ADD1-t** is 3.4 kcal.mol^{-1} above the separate reactants, reasonable because of the entropy loss associated to the bimolecular process. Afterwards, the approach of indole **3** to **ADD1-t** results in barrierless formation of species **ADD2-t**, with a relative free energy of 5.2 kcal.mol^{-1}. In **ADD2-t**, the carbon-carbon bond is already formed (1.57Å), and a hydrogen atom is transferred from the water molecule (O-H, 1.63 Å) to a carbonyl of the pyruvate (O-H, 1.01 Å). There is no barrier associated to the formation of **ADD2-t** from **ADD1-t** plus indole, the process takes place spontaneously in our gas phase geometry optimization. **ADD2-t** is an ion pair between an anionic metal complex and the protonated product. The evolution from **ADD2-t** to the products goes through transition state **TS1-t**. In **TS1-t**, a hydrogen atom is transferred from the indole (C-H 1.29 Å) back to the metal complex (O-H 1.37 Å). **TS1-t** is 7.9 kcal.mol^{-1} above the separate reactants. This is the highest free energy in the whole process and is consistent with the experimental observation of a fast process. **TS1-t** evolves towards **ADD3-t** (**Figure 2.1**), where the Friedel-Crafts product is weakly bound to the

catalyst through hydrogen bonds (1.74 Å and 1.92 Å). **ADD3-t** is 11.8 kcal.mol^{-1} below the separate reactants. Separation of the product **4-t** and regeneration of the **1-t** catalyst is favorable in the free energy scale; the overall exergonicity of the whole process is 12.6 kcal.mol^{-1}.

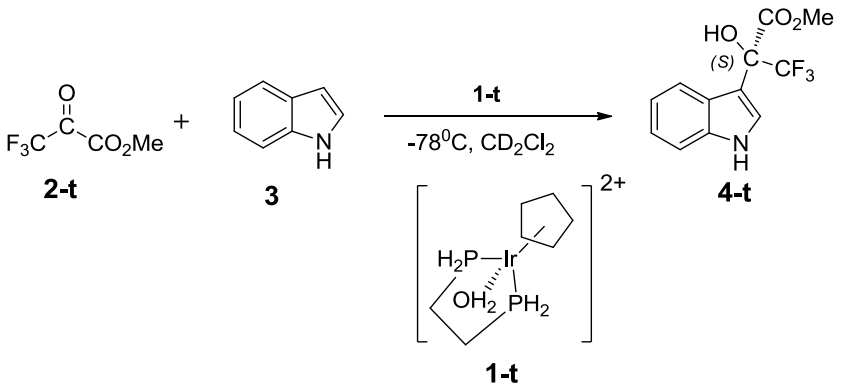

Scheme 2.3 Model system.

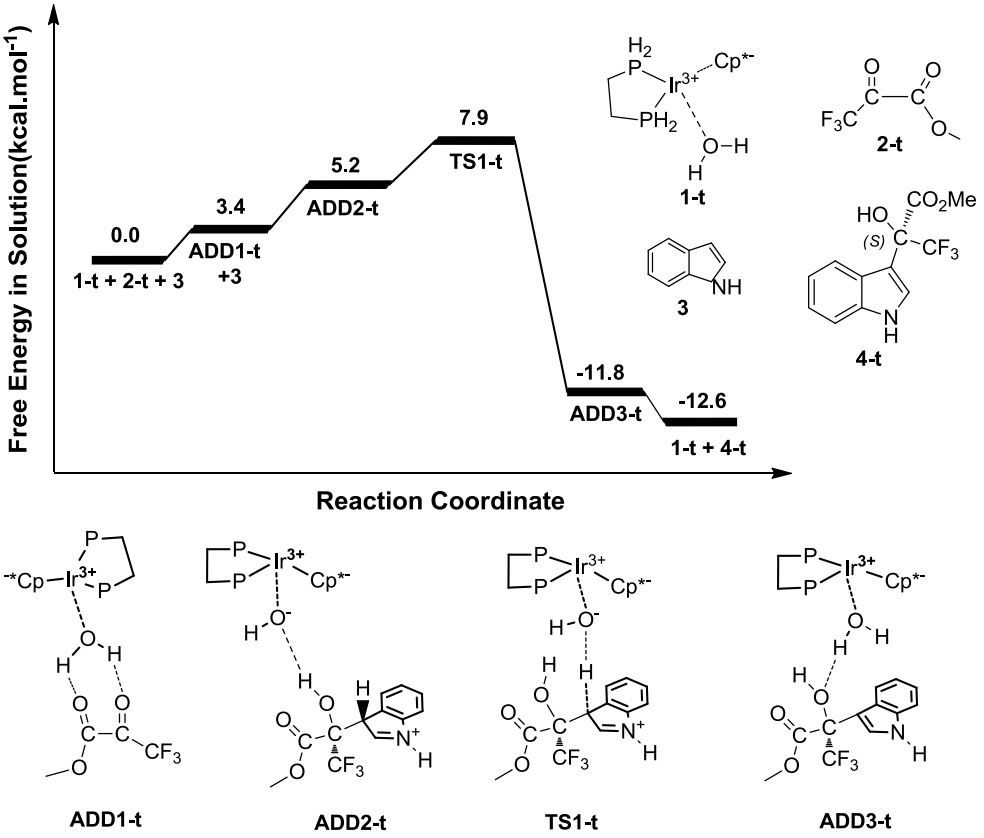

Figure 2.1 Energy profile for the **(*S*)-product** reaction in the model system. Relative free energies in solution are given in kcal.mol^{-1}.

Through the discussion of the model system, the process of this reaction is stepwise. The first step is the formation of a C-C bond together with the transfer of a proton from water molecule to the substrate. The second step is the rate determining one, which is the transfer of a proton from the substrate to the hydroxyl group to regenerate a water molecule. Based on the model system, we studied the pathway of the real system.

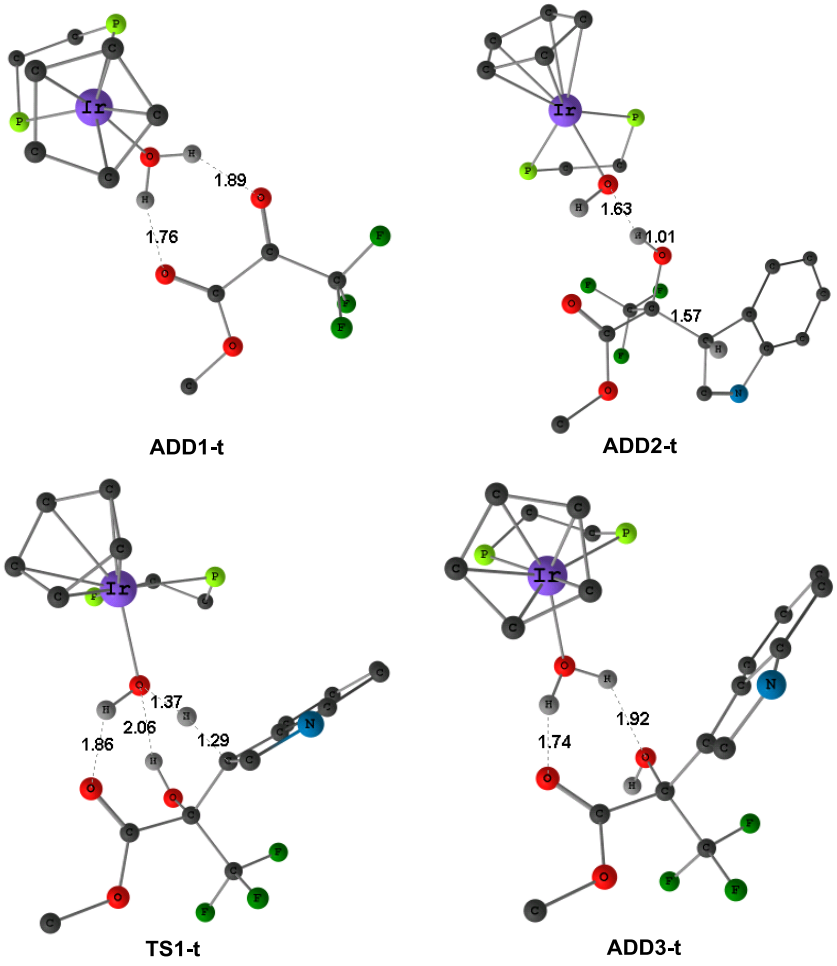

Figure 2.2 M06 optimized structures of adducts **ADD1-t**, **ADD2-t**, **ADD3-t**, and transition state **TS1-t**. Selected distances are given in Å (some H atoms are omitted for clarity).

2.4 Free energy profile of the real system

The free energy profiles for the reaction leading to the **(*S*)-product** and the optimized structures involved in this reaction are shown in **Figure 2.3**. The pathway of the real

system is similar to that of the model system. The chiral Brønsted acid **1** and pyruvate **2** form a hydrogen-bond complex **ADD1**, which is stabilized mainly by two favorable hydrogen bonding interactions (both O...H distances are 1.86Å). In **ADD2**, the carbon-carbon bond is already formed (1.56Å), and a hydrogen atom is transferred from the water molecule to a carbonyl of the pyruvate. There is no barrier associated to the formation of **ADD2** from **ADD1** plus indole. **ADD3** is formed through **STS1-1**. A hydrogen atom is transferred from the indole back to the metal complex in **STS1-1**. Distances for the hydrogen being transferred are C-H 1.29 Å and O-H 1.39 Å. And two "OH….O" hydrogen

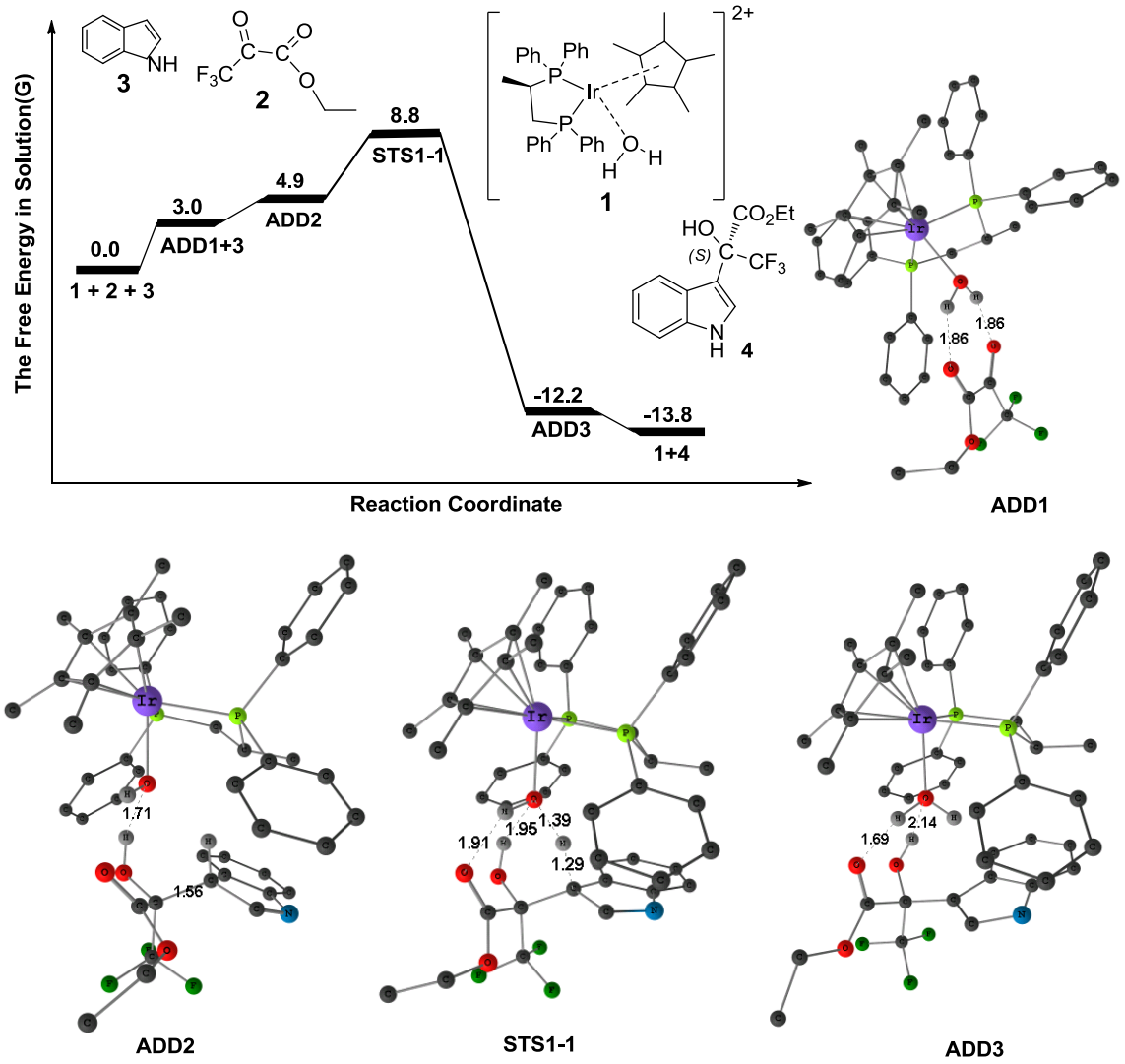

Figure 2.3 Energy profile for the **(*S*)-product** reaction in the real system at -78^{0}C. Selected distances are given in Å; relative free energies in solution are given in kcal.mol^{-1}. (Some H atoms are omitted for clarity).

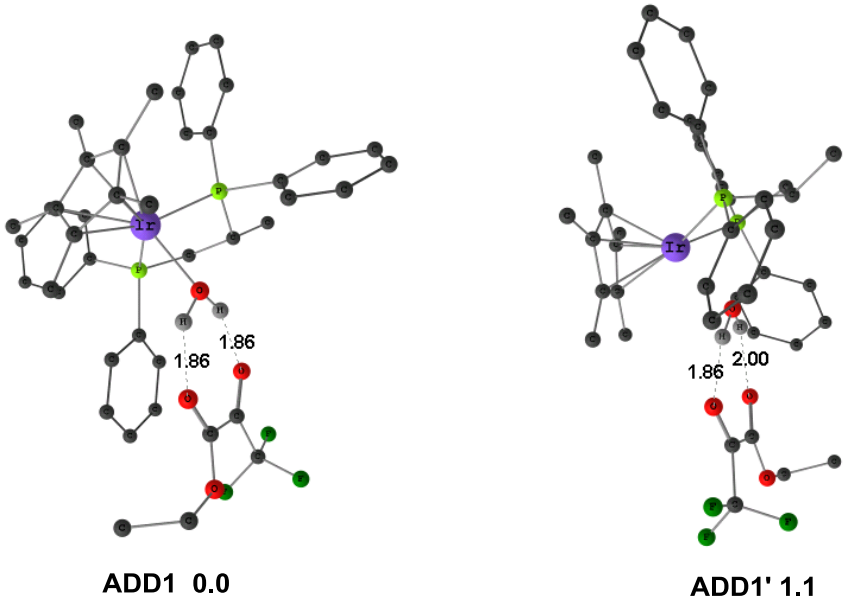

Figure 2.4 M06 optimized structures of two possible structures for adduct between metal complex and the ester reactant**.** Selected distances are given in Å; relative free energies in solution are given in kcal.mol^{-1}. (Some H atoms are omitted for clarity).

bonds are present with distances 1.95 Å and 1.91 Å. **STS1-1** evolves towards **ADD3**, where the Friedel-Crafts product is weakly bound to the catalyst through two hydrogen bonds (1.69 Å and 2.14 Å). **ADD3** is 12.2 kcal.mol^{-1} below the separate reactants. Separation of the product **4** and regeneration of the catalyst **1** is favorable in the free energy scale; the overall exergonicity of the whole process is 13.8 kcal.mol^{-1}. **STS1-1** is the rate-determining transition state for the investigated reaction.

We also consider an alternative mechanism with the involvement of the other proton from the water molecule, which could make another hydrogen atom of water molecule transfer to the ester. This alternative pathway would go through adduct **ADD1´**, which is presented in **Figure 2.4** together with the corresponding adduct **ADD1** in the path discussed above. The structures are qualitatively similar, and the computed energy difference between them is 1.1 kcal.mol^{-1} because of different hydrogen bonds. The hydrogen bonds are stronger in **ADD1** than **ADD1´**. Based on our calculations, we discarded other mechanistic possibilities.

Based on the research of the model and real system above, the catalytic role of the metal complex seems to be the modulation of the acid/base properties of the coordinated water. This water has to be acidic enough to transfer a proton to the pyruvate-indole pair, but the

resulting hydroxyl group has to be basic enough to deprotonate the resulting intermediate. Similar electronic balances seem to be at play in the substrates. Most probably, the presence of the two electron–withdrawing groups, CF_3 and CO_2Et, on the pyruvate carbonyl, precludes direct pyruvate coordination to the metal accompanied by water substitution. However, the carbonyl pyruvate group is nucleophilic enough to establish hydrogen–bonding interactions with one of the water protons, becoming activated for the nucleophilic attack of the indole.

2.5 Stereoselectivity of transition state TS1

The introduction of the real substituent in **TS1** creates a variety of possible isomers, which have to be analyzed.[13] So we tackled next problem of enantioselectivity from a computational point of view. We can classify the conformations according to the four structural dichotomies described in **Figure 2.5**.

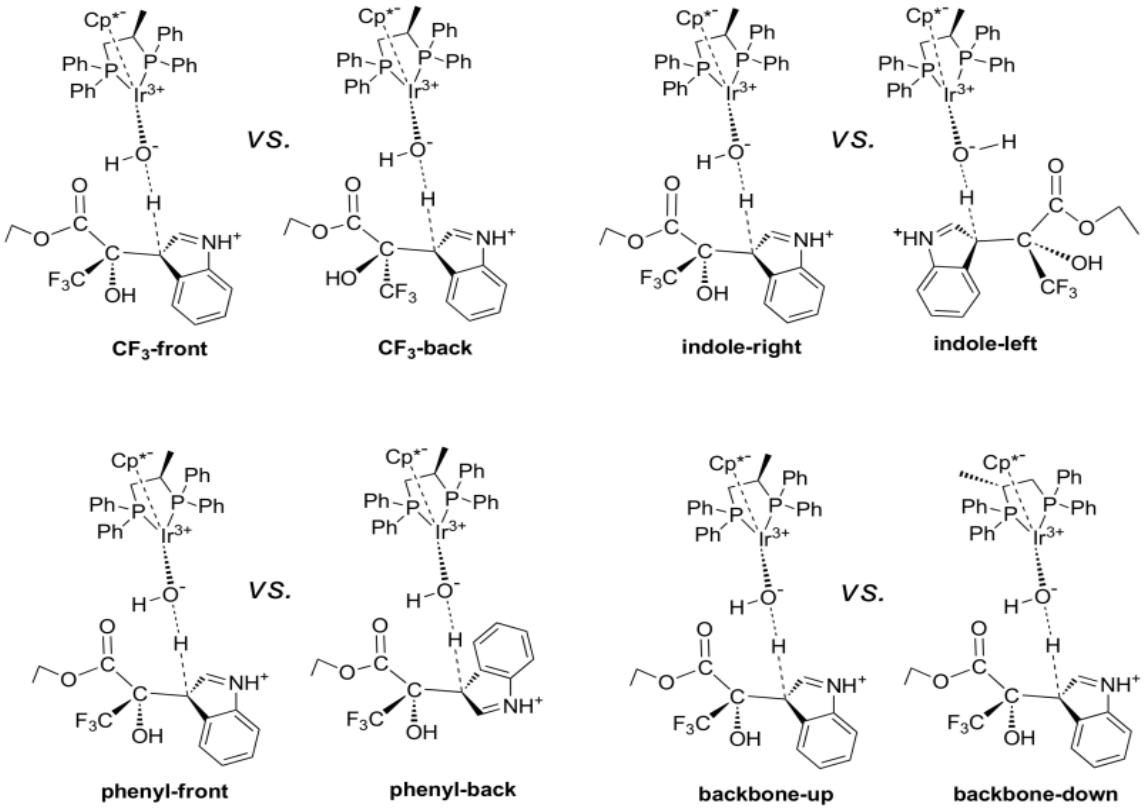

Figure 2.5 Four conformational dichotomies in the definition of the structure for transition state **TS1** in the real system.

The structure of **STS1-1** (**Figure 2.3**) is such that the ester substituent in the newly created stereogenic center is acting as the acceptor and donor of weak hydrogen bonds (1.91 Å and 1.95 Å) from the hydroxyl group bound to the metal, and as such its position is fixed in that direction. As a result, the trifluoromethyl group can point either to the front (CF_3-front) or to the back (CF_3-back) in the representation described in **Figure 2.5**. In this same representation, the indole group can be placed to the right (indole-right) or to the left (indole-left) of this stereogenic carbon. Of course, the combination of the position of CF_3 and indole will define the stereochemistry (*R* or *S*) of the newly formed stereocenter. There are however two other sources of conformational complexity that must be taken into account: the position of the phenyl part of the indole (phenyl-front or phenyl-back), and the arrangement of the diphosphine backbone (backbone-up or backbone-down). The combination of the four dichotomies results in 16 possible isomers of this transition state, which were optimized. Their relative energies are summarized in **Table 2.1**. There are also other conformational complexities associated to the arrangement of the phenyl groups (edge or face) with respect to the Ir-P bonds, or to the involvement of the other hydrogen atom of water in the network of hydrogen bonds. They were also analyzed, and the results presented here correspond only to the most stable arrangement in each case, as shown in **Figure 2.6**.

The relative energies in **Table 2.1** are given with respect to the most stable isomer of the transition state, **STS1-2**. Only the isomers closer in energy to the most stable one will contribute to the overall reaction. And there is a clear separation in the energies; there are five structures within a span of 2.6 kcal.mol^{-1}, the next one having a relative energy of 4.3 kcal.mol^{-1}. So we used these five most stable isomers, **RTS1-4**, **RTS1-8**, **STS1-1**, **STS1-2** and **STS1-6**, to obtain a computed enantiomeric excess at the experimental temperature of -78 ºC. This results in a value of 82% ee in favor of the ***S*** enantiomer. The proper product is predicted, and the computed enantiomeric excess is close to the experimental result of 71 % ee. (About the calculation of the enantiomeric excess, please see **1.2.2.1**).

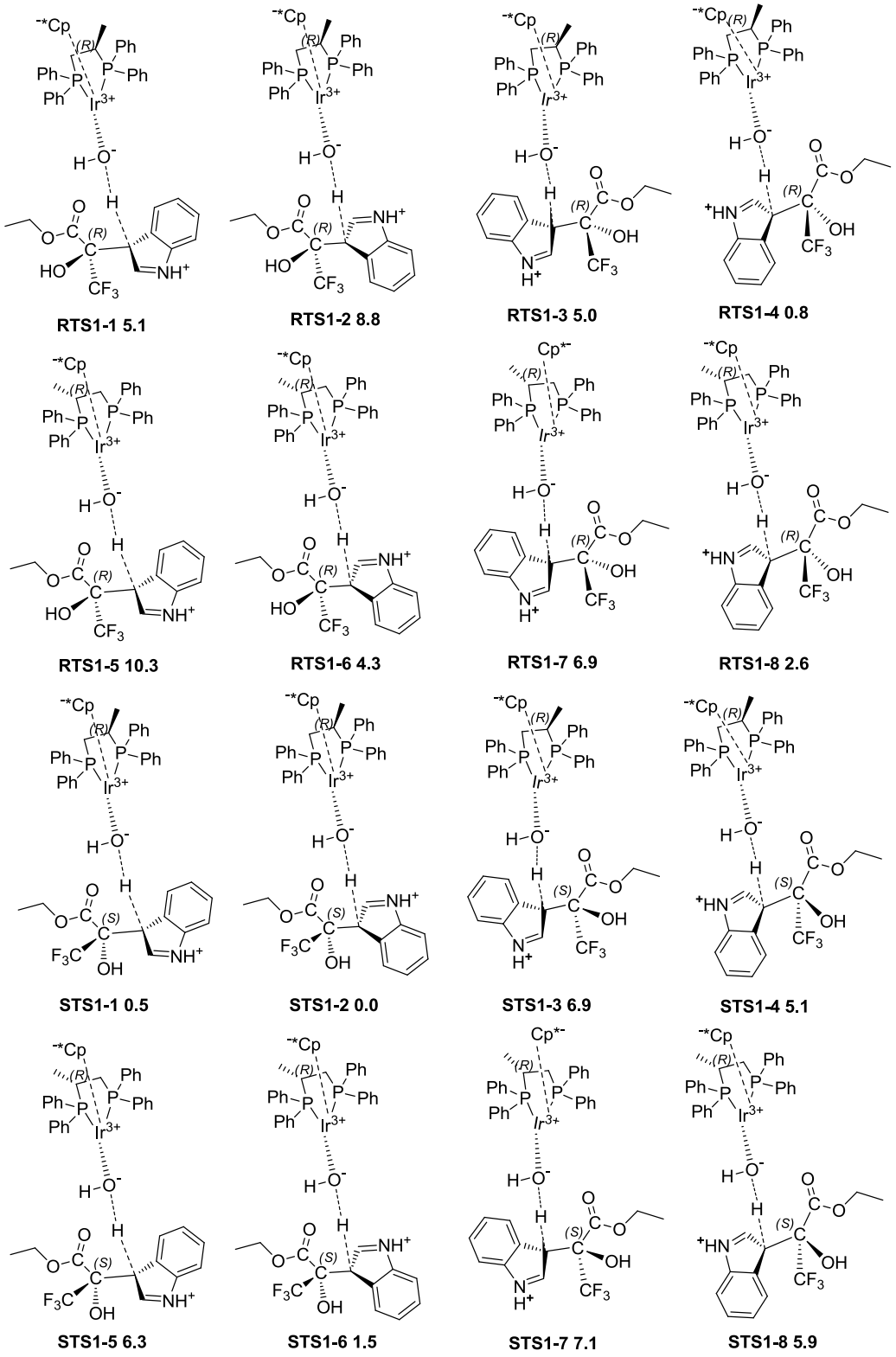

Figure 2.6 All possible isomers and relative free energies (kcal.mol^{-1}) in solution of transition states **STS1**, **RTS1** between ethyl 3,3,3-trifluoroethylpyruvate **2** and indole **3**.

Table 2.1 Computed relative free energies (kcal.mol^{-1}) in solution and conformational identity of the different forms of **TS1**.

Label	Energy	CF_3	Indole	Phenyl	Backbone
RTS1-1	5.1	Back	Right	Back	Up
RTS1-2	8.8	Back	Right	Front	Up
RTS1-3	5.0	Front	Left	Back	Up
RTS1-4	0.8	Front	Left	Front	Up
RTS1-5	10.3	Back	Right	Back	Down
RTS1-6	4.3	Back	Right	Front	Down
RTS1-7	6.9	Front	Left	Back	Down
RTS1-8	2.6	Front	Left	Front	Down
STS1-1	0.5	Front	Right	Back	Up
STS1-2	0.0	Front	Right	Front	Up
STS1-3	6.9	Back	Left	Back	Up
STS1-4	5.1	Back	Left	Front	Up
STS1-5	6.3	Front	Right	Back	Down
STS1-6	1.5	Front	Right	Front	Down
STS1-7	7.1	Back	Left	Back	Down
STS1-8	5.9	Back	Left	Front	Down

The visual analysis of the computed structures is not trivial; the qualitative analysis of the nature of the most stable isomers is informative. In four of the five most stable isomers, both CF_3 and phenyl are in the front arrangement. This means that CF_3 and phenyl point away from the phosphine, and fits well with the intuitive view that CF_3 and phenyl are the bulkier substituents at the pyruvate and indole moieties, respectively, and that the phosphine side is more sterically hindered than the cyclopentadienyl side in the iridium complex. It must be also noticed that the most stable conformations going to the **(*S*)-product** (**STS1-2**) and to the **(*R*)-product** (**RTS1-4**) agree in all the conformational labels but in the indole orientation, which is right for the ***S*** isomer, and left for the ***R*** isomer. This indicates that the right orientation of pyruvate (in the orientation in **Figure 2.6**) is more sterically hindered than the left orientation. This correlates well with the presence of the extra methyl substituent in the diphosphine in this right-hand side, which brings more steric pressure to this part of the system. Therefore the combination of electronic and steric effects places the substituents at the new stereogenic center being formed in a particular

arrangement, deciding the configuration of the product, in a form reminiscent of what happens in asymmetric hydrogenation.[13]

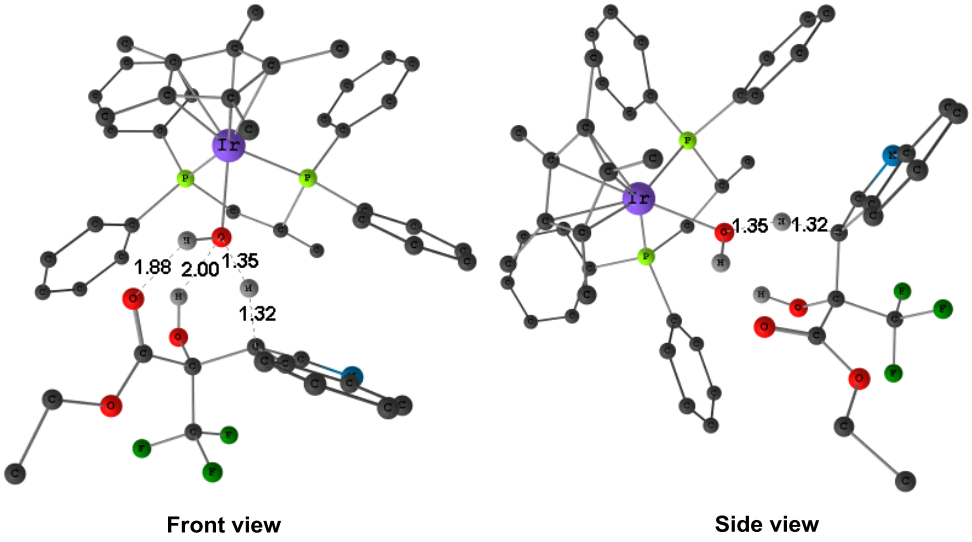

Figure 2.7 Two views of the optimized structure of transition state **STS1-2** (some H atoms are omitted for clarity).

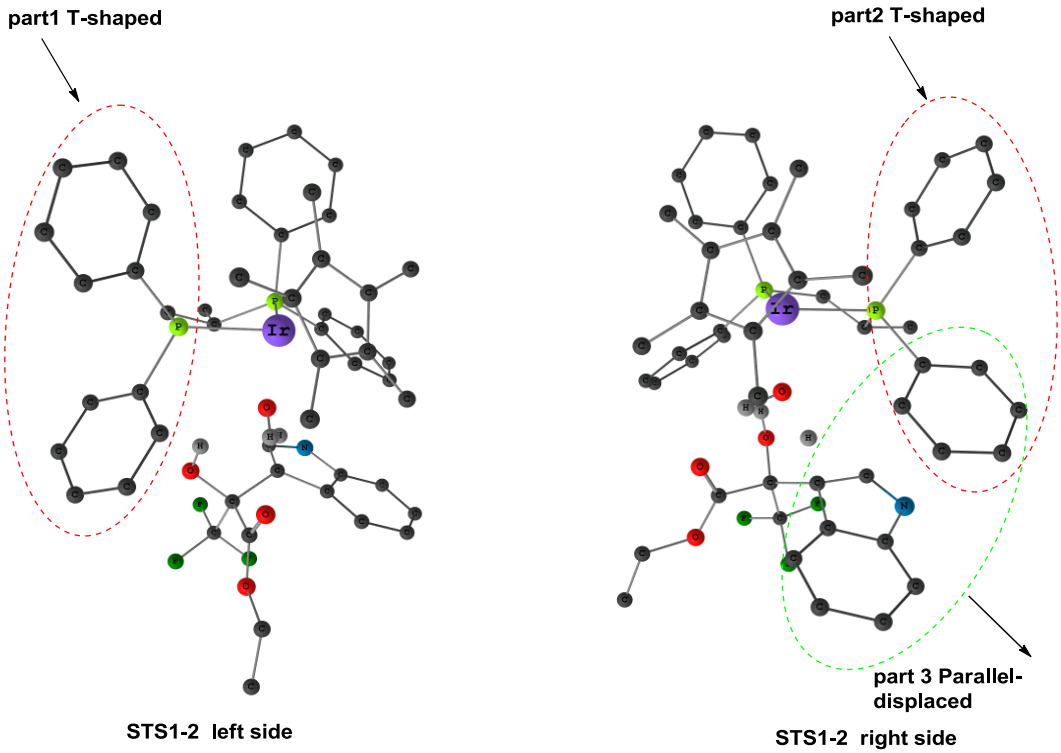

Figure 2.8 Two types of π-π interactions in the geometry of transition state **STS1-2** (some H atoms are omitted for clarity).

The most stable isomer **STS1-2** is shown in **Figure 2.7**. There are hydrogen bonds (O...H distances of 2.00 Å and 1.88 Å) between pyruvate and hydroxyl group of catalyst, but there are not key to enantioselectivity, as they are also present in isomers going to the ***R*** product. π-π interactions among aromatic groups of **STS1-2** play in this case the key role. The π-π interaction between aromatic groups are the most important noncovalent interactions, and influence the stability of many compounds.[14,15] In the structure of **STS1-2** (**Figure 2.8**), we have highlighted as part 1 and part 2 are the "edge-face" T–shaped geometries, and part 3 is the parallel-displaced interactions between the aromatic rings. These π-π interactions contribute to make the **STS1-2** structure the most stable one among all the conformations of **TS1**.

2.6 Conclusions

We have characterized the mechanism of the Friedel–Crafts (FC) reaction between ethyl 3,3,3-trifluoromethylpyruvate and indole catalyzed by iridium complex plus water using M06 method, and explained the catalytic role of the metal complex and water in this reaction. The mechanism of this reaction is stepwise, the first step is the formation of a C-C bond together with the transfer of a proton from water molecule to the substrate; the second step is the rate determining one, which is the transfer of a proton from indole to the -OH moiety of the water molecule. The catalytic role of the metal complex is the modulation of the acid/base properties of the coordinated water, and the water molecule acts as a proton donor and acceptor. We have been also able to explain the origin of the stereoselectivity of the process, which is a result of a subtle combination of the non-covalent interactions, both attractive and repulsive, between catalyst and substrate.

2.7 References

[1]. (a) Schreiner P. R., *Chem. Soc. Rev*, **2003**, 32, 289; (b) Pihko P. M., *Angew. Chem. Int. Ed*, **2004**, 43, 2062; (c) Seayad J., List B., *Org. Biomol. Chem*, **2005**, 3, 719; (d) Takemoto Y., *Org. Biomol. Chem*, **2005**, 3, 4299; (e) Akiyama T., Itoh J., Fuchibe K., *Adv. Synth. Catal*, **2006**, 348, 999; (f) Connon S. J., *Chem. Eur. J*, **2006**, 12, 5418; (g) Taylor M. S., Jacobsen E. N., *Angew. Chem. Int. Ed*, **2006**, 45, 1520; (h) Connon S. J., *Angew. Chem. Int. Ed*, **2006**, 45, 3909; (i) Doyle A. G., Jacobsen E. N., *Chem. Rev*, **2007**, 107, 5713; (j) Akiyama T., *Chem. Rev*, **2007**, 107, 5744; (k) Dondoni A., Massi A., *Angew. Chem. Int. Ed*, **2008**, 47, 4638; (l) Terada M., *Chem. Commun*, **2008**, 4097; (m) Yu X., Wang W., *Chem. Asian. J*, **2008**, 3, 516; (n) Miyabe H., Takemoto Y., *Bull. Chem. Soc. Jpn*, **2008**, 81, 785; (o) Zhang Z., Schreiner P., *Chem. Soc. Rev*, **2009**, 38, 1187; (p) Johnston J. N., Muchalski H., Troyer T. L., *Angew. Chem. Int. Ed*, **2010**, 49, 2290; (q) Terada M., *Bull. Chem. Soc. Jpn*, **2010**, 83, 101; (r) Amarante G. W., Benassi M., Milagre H. M. S., Braga A. A. C., Maseras F., Eberlin M. N., Coelho F., *Chem. Eur. J*, **2009**, 15, 12460.

[2]. Sodeoka M., Hamashima Y., *Chem. Commun*, **2009**, 5787.

[3]. (a) Ishibashi H., Ishihara K., Yamamoto H., *Chem. Rec*, **2002**, 2, 177; (b) Yamamoto H., Futatsugi K., *Angew. Chem. Int. Ed*, **2005**, 44, 1924.

[4]. Carmona D., Lamata M. P., Viguri F., Rodríguez R., Oro L. A., Lahoz F. J., Balana A. I., Tejero T., Merino P., *J. Am. Chem. Soc*, **2005**, 127, 13386.

[5]. (a) Blake J. F., Jorgensen W. L., *J. Am. Chem. Soc*., **1991**, 113, 7430; (b) Blake J. F., Lim D., Jorgensen W. L., *J. Org. Chem*, **1994**, 59, 803.

[6]. Severance D. L., Jorgensen W. L., *J. Am. Chem. Soc*, **1992**, 114, 10966.

[7]. Gruttadauria M., Giacalone F., Noto R., *Adv. Synth. Catal*, **2009**, 351, 33.

[8]. Frisch M. J., Trucks G. W., Schlegel H. B., Scuseria G. E., Robb M. A., Cheeseman J. R., Montgomery J. A., Jr., Vreven T., Kudin K. N., Burant J. C., Millam J. M., Iyengar S. S., Tomasi J., Barone V., Mennucci B., Cossi M., Scalmani G., Rega N., Petersson G. A., Nakatsuji H., Hada M., Ehara M., Toyota K., Fukuda R., Hasegawa J., Ishida M., Nakajima Honda T., Y., Kitao O., Nakai H., Klene M., Li X., Knox J. E., Hratchian H. P., Cross J. B., Adamo C., Jaramillo J., Gomperts R., Stratmann R. E., Yazyev O., Austin A. J., Cammi R., Pomelli C., Ochterski J. W., Ayala P. Y., Morokuma K., Voth G. A., Salvador P., Dannenberg J. J., Zakrzewski V. G., Dapprich S., Daniels A. D., Strain M. C., Farkas O., Malick D. K., Rabuck A. D., Raghavachari K., Foresman J. B., Ortiz J. V., Cui Q., Baboul A. G., Clifford S.,

Cioslowski J., Stefanov B. B., Liu G., Liashenko A., Piskorz P., Komaromi I., Martin R. L., Fox D. J., Gaussian, Inc., Wallingford CT, **2009**. Gaussian 09, Revision A.02.

[9]. Zhao. Y., Truhlar D. G., *Theor. Chem. Acc*, **2008**, 120, 215.

[10]. (a) Fuentealba P., Preuss H., Stoll H., Szentpály L. V., *Chem. Phys. Lett*, **1982**, 89, 418; (b) Dolg M., Wedig U., Stoll H., Preuss H., *J. Chem. Phys*, **1987**, 86, 866; (c) Igel-Mann G., Stoll H., Preuss H., *Mol. Phys*, **1988**, 65, 1321; (d) Andrae D., Haeussermann U., Dolg M., Stoll H., Preuss H., *Theor. Chem. Acc*, **1990**, 77, 123.

[11]. (a) Hehre W. J., Ditchfield R., Pople J. A., *J. Chem. Phys*, **1972**, 56, 2257; (b) Petersson G. A., Bennett A., Tensfeldt T. G., Al-Laham M. A., Shirley W. A., Mantzaris J., *J. Chem. Phys*, **1988**, 89, 2193.

[12]. Marenich A. V., Cramer C. J., Truhlar D. G., *J. Phys. Chem. B*, **2009**, 113, 6378.

[13]. Fjermestad T., Pericàs M. A., Maseras F., *Chem. Eur. J*, **2011**, 17, 10050.

[14]. (a) Askew B., Ballester P., Buhr C., Jeong K. S., Jones S., Parris K., Williams K., Rebek J. Jr., *J. Am. Chem. Soc*, **1989**, 111, 1082; (b) Smithrud D. B., Diederich F., *J. Am. Chem. Soc*, **1990**, 112, 339; (c) Hunter C. A., *Chem. Soc. Rev*, **1994**, 23, 101; (d) Rebek J. Jr., *Chem. Soc. Rev*, **1996**, 25, 255; (f) Claessens C. G., Stoddart J. F., *J. Phys. Org. Chem*, **1997**, 10, 254; (e) Fyfe M. C. T., Stoddart J. F., *Acc. Chem. Res*, **1997**, 30, 393.

[15]. (a) Sinnokrot M. O., Sherrill C. D., *J. Phys. Chem. A,* **2006**, 110, 10656; (b) Sinnokrot M. O., Edward F. V., Sherrill C. D., *J. Am. Chem. Soc*, **2002**, 124, 10887; (c) Tsuzuki S., Uchimaru T., Sugawara K., Mikami M., *J. Chem. Phys*, **2002**, 117, 11216; (d) Tsuzuki S., Honda K., Uchimaru T., Mikami M., *J. Chem. Phys*, **2005**, 122, 144323; (e) Janda K. C., Hemminger J. C., Winn J. S., Novick S. E., Harris S. J., Klemperer W., *J. Chem. Phys*, **1975**, 63, 1419; (f) Steed J. M., Dixon T. A., Klemperer W., *J. Chem. Phys*, **1979**, 70, 4940; (g) Arunan E., Gutowsky H. S., *J. Chem. Phys*, **1993**, 98, 4294; (h) Law K. S., Schauer M., Bernstein E. R., *J. Chem. Phys*, **1984**, 81, 4871; (i) Börnsen K. O., Selzle H. L., Schlag E. W., *J. Chem. Phys*, **1986**, 85, 1726; (j) Scherzer W., Krätzschmar O., Selzle H. L., Schlag E. W. Z., Naturforsch, **1992**, 47A, 1248.

Chapter 2

Chapter 3

Mechanism for the enantioselective synthesis of a Wieland-Miescher ketone

3.1 Experimental background

The Wieland-Miescher (W-M) ketone (**Scheme 3.1**) is a key intermediate for many reactions, for example in the synthesis of terpenoids and steroids.[1] The first example of synthesis of a W-M ketone type compound was reported by Wiechert[2] and co-workers, who used a proline catalyst for intramolecular aldol cyclizations. But the low enantioselectivity of the reaction required recrystallization steps to achieve the enantiomerically pure W-M ketone, with a subsequent drop in overall yield.[3] The efficient preparation of Wieland-Miescher ketone-type compounds with high enantioselectivity is thus a challenging problem in organic chemistry. In an attempt to address this issue, the Bonjoch[4] group reported a highly efficient and enantioselective synthesis of a W-M ketone using N-Ts-(S_a)-Binam-L-prolinamide **1** as the organocatalyst, under solvent-free conditions and the assistance of benzoic acid. The key step is a Robinson annulation reaction, as shown in **Scheme 3.2**., where it corresponds to the conversion from **3** to **4**. The reaction requires 1 mol% triethylamine as the base in the initial Michael process and 1 mol% of N-Ts-(S_a)-binam-L-prolinamide **1** and 2.5 mol% of benzoic acid in the intramolecular aldol process. We were interested in the mechanism of the intramolecular aldol process (from **3** to **4**), and we explained the role of benzoic acid and the origin of the high enantioselectivity.

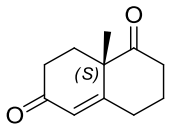

Scheme 3.1 Wieland-Miescher ketone.

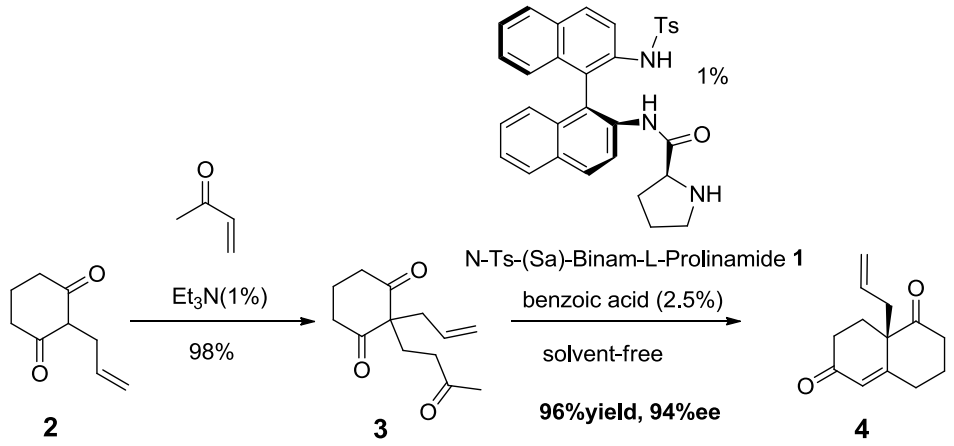

Scheme 3.2 Experimental procedure for the synthesis of the W-M ketone **4**.[4b]

3.2 Mechanistic landscape of the intramolecular aldol reaction

The mechanism of the intramolecular aldol reaction catalyzed by proline has been studied by Houk and co-workers,[5] who proposed a mechanism through a combination of calculation and experiment.[6] The previously controversial mechanism (see **Scheme 1.8**) of aldol reaction catalyzed by proline was thus solved. **Scheme 3.3** shows the proposed pathway by Houk for the (S)-proline catalyzed cyclization. The first step is the formation of a planar iminium structure. Then an enamine intermediate is formed through the intramolecular deprotonation by the carboxylate group in the iminium structure. The subsequent step is the C-C bond formation. After the formation of the C-C bond, the hydrolysis of iminium is achieved in a series of easy steps that lead to the release of the aldol product together with the recovery of the catalyst. In Houk´s study, the carbinolamine, iminium, and enamine formation are three important steps before C-C bond formation, as shown in **Scheme 3.4**, the predicted free energies relative to reactants of transition states for the carbinolamine, iminium, and enamine formation steps are 17.0, 15.3, 26.2 kcal.mol^{-1} at B3LYP/6-31+G(d,p)//B3LYP/6-31G(d) level.

Our system is the intramolecular aldol reaction (from **3** to **4** in **Scheme 3.2**). The experiment shows that this step occurs without base additives, we can only consider the **Houk-List** model (see **1.1.2.2**),[8,5b,6b] where the enamine intermediate is formed from the iminium, not from oxazolidinone (about the oxazolidinone aldol alternative, refer to section **1.1.2.3**). Based on the results above, we carried out computational studies of the

mechanism of intramolecular aldol reaction of triketone catalyzed by prolinamide. We also investigate the role of benzoic acid and the origin of the high enantioselectivity.

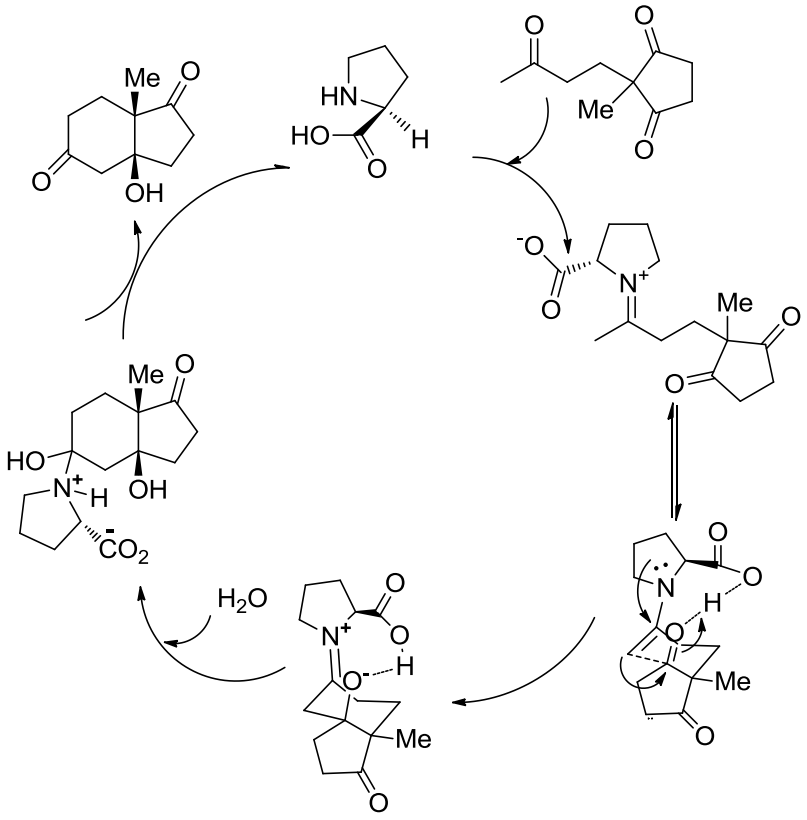

Scheme 3.3 Proposed pathway by Houk for the (S)-proline catalyzed cyclization. Reproduced from reference [7].

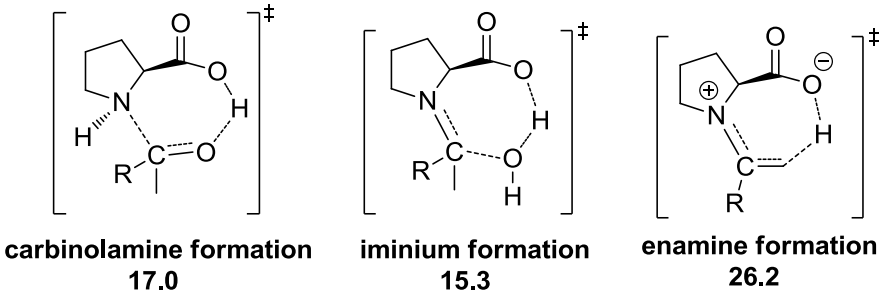

Scheme 3.4 Transition states of the carbinolamine, iminium and enamine formation steps in the proline catalyzed intramolecular aldol reaction of Houk´s paper.[5] The free energy is in kcal.mol^{-1}.

3.3 Computational details

In the first part of the study, concerning the general mechanism, all geometry optimizations and frequency calculations were performed with the B3LYP[9] functional as implemented in the **Gaussian 09**.[10] The 6-31G(d) basis set was used for every atom. Frequency calculations were carried out at the same level to confirm the nature of each stationary point as either a minimum or a transition state (TS). In this system, the most difficult part of the study is to search the most stable geometries for each intermediate and transition state. Monte Carlo Multiple Minimum (MCMM)[11] conformational searches were used to search the conformation in the **Macromodel** program[12] with the MM3 force field.[13] For each species, 10 structures were selected and recalculated at the B3LYP level. For the most stable geometries, the M062x[14]/6-31+G(d,p) single point energies were calculated based on the B3LYP optimized structures. The effect of solvation was incorporated by using the SMD[15] model. The "UltraFine" grid[16] was used in the M062x calculations to minimize integration grid errors. Experiments report that the main solvent is **3** (**Scheme 3.2**), but we could not find the dielectric constant of this compound. We consider that **3** and cyclohexanone are structurally similar, so we consequently chose cyclohexanone as the solvent to study the solvation impact. An error of a few units in the dielectric constant would have after all a very minor effect in the computation results. The free energies in solution are taken from the introduction of gas phase free energy corrections (refer to section **1.2.2.2**).

In the second part, we examined the enantioselectivity, and we used a more refined method. After a method calibration (see below), we settled down on a reoptimization of the key transition states **anti_re_TS** and **syn_si_TS** geometries using a B97D[17]/6-31G(d) method, followed by single point calculations with B97D6-31+G(d,p)(smd, cyclohexanone). We also corrected the final energies for BSSE (basis set superposition error).[18] In particular, we evaluate the BSSE associated with the cleavage of the C-N bond (where N is the cyclic nitrogen atom).

3.4 Results and discussion

3.4.1 Choice of a computational model

The mechanism proposed by Houk is based in the use of proline as catalyst. Both the amine and the carboxylic functions are attached to the same carbon and they play a key role in the catalysis. In Bonjoch's system, the catalyst is prolinamide plus benzoic acid. The fact that there is no carboxylic group attached to the carbon bearing the amine creates a first question on what is the nature of the active catalyst. We have tried four different models, presented in **Scheme 3.5**. In **model1**, prolinamide is the catalyst; **model2a** and **2b** are protonated prolinamides and the two models differ on the protonation site. In **model3**, the catalytic system is composed by the neutral prolinamide with the external assistance of the benzoic acid.

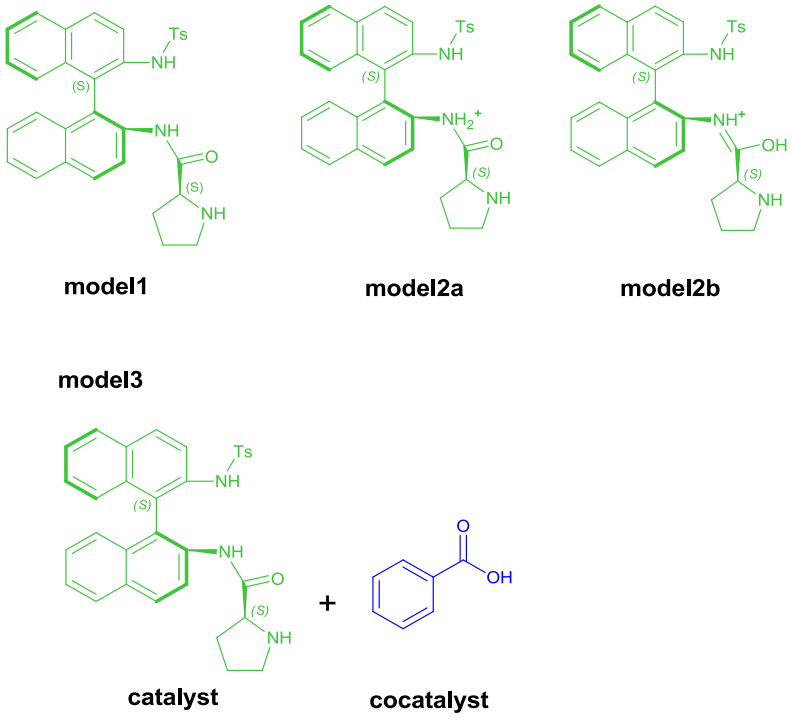

Scheme 3.5 Different catalyst models.

3.4.2 Enamine formation process with every model

3.4.2.1 Enamine formation process with model1

In **model1**, only N-Ts-(S_a)-Binam-L-prolinamide was considered as a catalyst, without the assistance of acid. As shown in **Figure 3.1**, the first step is the C-N bond formation. The catalyst N-Ts-(Sa)-Binam-L-prolinamide attacks the acyclic carbonyl group of the triketone to form a C-N bond. A proton is transferred from the NH group of the prolinamide to the carbonyl of the triketone. The transition state **model1_1** is located with 23.2 kcal.mol^{-1} free energy, and then the carbinolamine intermediate **model1_2** is formed. The second step is the formation of an iminium. **Model1_2** is in equilibrium with **model1_3**. Subsequently, the intermediate **model1_5** is formed with a barrier of 16.3 kcal.mol^{-1}. The transition state **model1_4** is located, and water is formed by a hydrogen

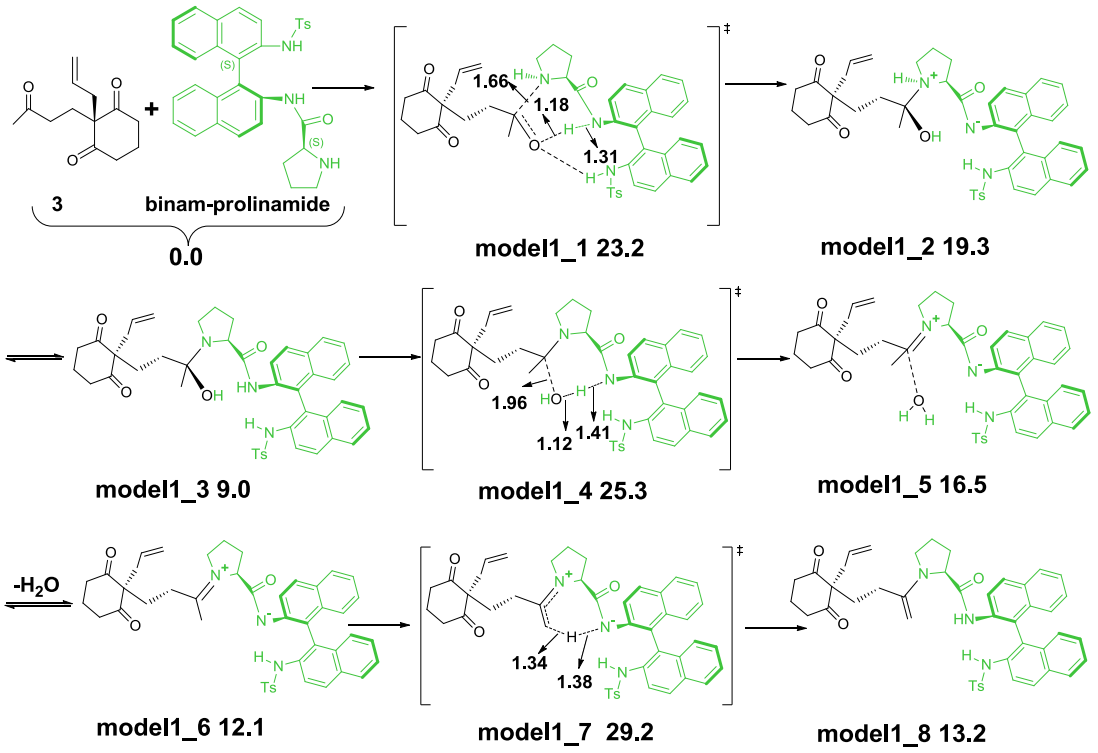

Figure 3.1 Enamine formation process with **model1** and free energies in kcal.mol^{-1} relative to the reactants. Selected distances are given in Å. Geometry B3LYP/6-31G(d), single point energies in cyclohexanone M062x/6-31+G(d,p).

atom of prolinamide and a hydroxyl group of the substrate. After the formation of iminium intermediate, the next step is the formation of enamine. The enamine is formed through an

intramolecular deprotonation process, and the nitrogen atom of prolinamide gets a proton from the methyl group. The free energies of transition states of the carbinolamine, iminium, and enamine intermediates formation are 23.2, 25.3 and 29.2 kcal.mol^{-1} relative to the reactants, respectively. The most difficult step is the formation of enamine with 29.2 kcal.mol^{-1} free energy, which is quite high, so we will consider the role of benzoic acid.

3.4.2.2 Model2a and model2b

We consider two acid assisted catalyst models, see **Figure 3.2**. The first one is **model2a** where the acid protonates the nitrogen atom of the prolinamide to form a quaternary ammonium cation. The second one is **model2b** where the acid protonates the carbonyl of prolinamide to form an iminium cation. **Model2b** is 17.1 kcal.mol^{-1} lower than **model2a**, so we choose **model2b** to study the enamine formation process. Regarding the chemical equilibrium, shown in **Figure 3.3**, for **model2b**, the protonated side of the equilibrium is 27.3 kcal.mol^{-1} higher than the non-protonated side, showing the difficulty of the formation of **model2b**. Because of this high energy, **model2b** is also unlikely, but we computed the corresponding mechanism for the sake of completion.

3.4.2.3 Enamine formation process with model2b

As shown in **Figure 3.4**, the free energies of transition states of the carbinolamine, iminium, and enamine intermediates formation are 11.7, 7.1 and 17.8 kcal.mol^{-1} above the separated reactants. The most difficult step is the formation of enamine, which proceeds through the transition state **model2b_7** with a large barrier of 29.2 kcal.mol^{-1} (from **model2b_6** to **model2b_7**). This large barrier shows that this step is energetically demanding, so we need to consider a new catalytic model, which can be more suitable to this system.

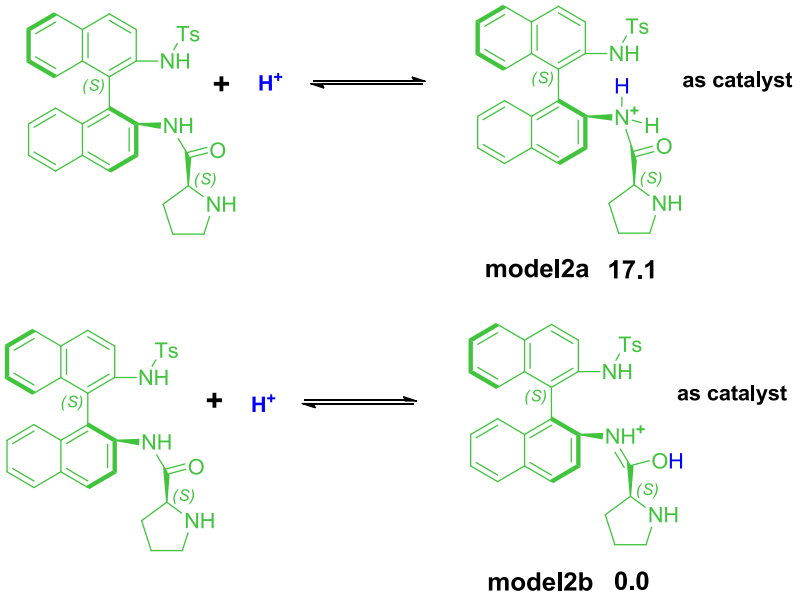

Figure 3.2 Geometries of **model2a** and **model2b**, and free energies in kcal.mol^{-1} relative to **model2b** catalyst. Geometry B3LYP/6-31G(d), single point energies in cyclohexanone M062x/6-31+G(d,p).

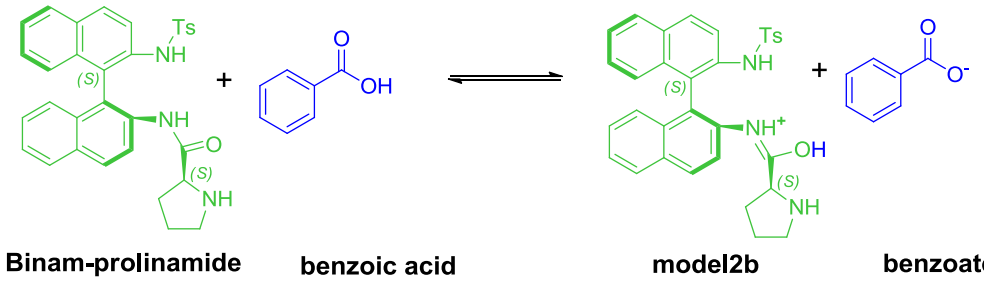

$$\Delta G = G_{(Binam-prolinamide)} + G_{(benzoicacid)} - G_{(model2b)} - G_{(benzoate)} = 27.3 kcal.mol^{-1}$$

Figure 3.3 Chemical equilibrium and free energy of prolinamide, benzoic acid, **model2b** and benzoate. Geometry B3LYP/6-31G(d), single point energies in cyclohexanone M062x/6-31+G(d,p).

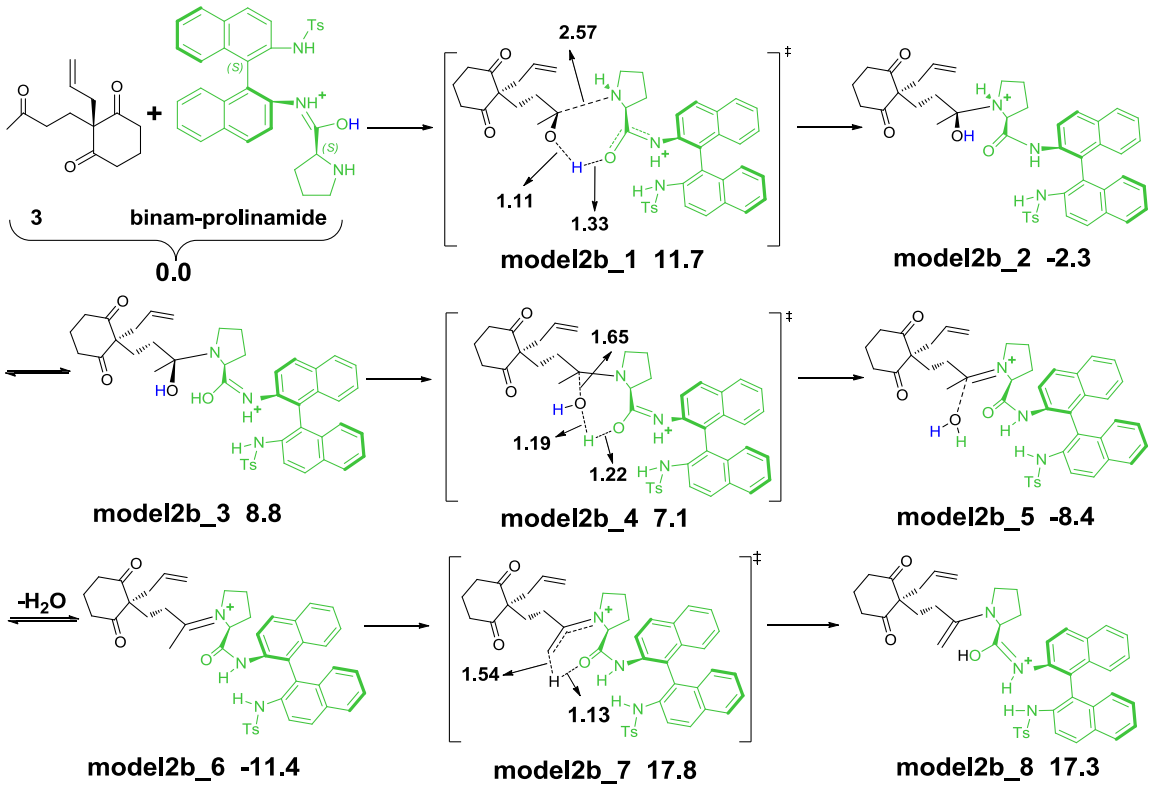

Figure 3.4 Enamine formation process with **model2b**, and free energies in kcal.mol^{-1} relative to the reactants. Selected distances are given in Å. Geometry B3LYP/6-31G(d), single point energies in cyclohexanone M062x/6-31+G(d,p).

3.4.2.4 Enamine formation process with model3

We then investigated the role of benzoic acid, and designed benzoic acid as co-catalyst. Results are summarized in **Figure 3.5**. The first step is the C-N bond formation process. The catalyst prolinamide attacks the acyclic carbonyl group of the triketone to form the C-N bond with an associated proton transferred from benzoic acid to the oxygen atom of carbonyl. Two transition state configurations are located through the C-N bond formation (*trans vs cis*). The one depicted in **Figure 3.6** is the *trans* isomer, which is the most stable one with a free energy of 17.5 kcal.mol^{-1} above the reactants. The *trans* nature of the favored isomer is probably due to the steric repulsion between naphthyl groups of prolinamide and dione in the *cis* geometry. The second step is the iminium formation. Intermediate **model3_2** is in equilibrium with intermediate **model3_3**. The system evolves to intermediate **model3_5** *via* transition state **model3_4**. In transition state **model3_4,** with

a relative energy of 21.3 kcal.mol^{-1}, a water molecule is formed by the binding of a hydrogen atom of the benzoic acid and a hydroxyl group of the substrate. After the formation of iminium intermediate **model3_5**, the system evolves toward the formation of enamine. Enamine is formed through an intramolecular deprotonation process. There are two competitive pathways. In **pathway a**, after the dissociation of a molecular H_2O, the

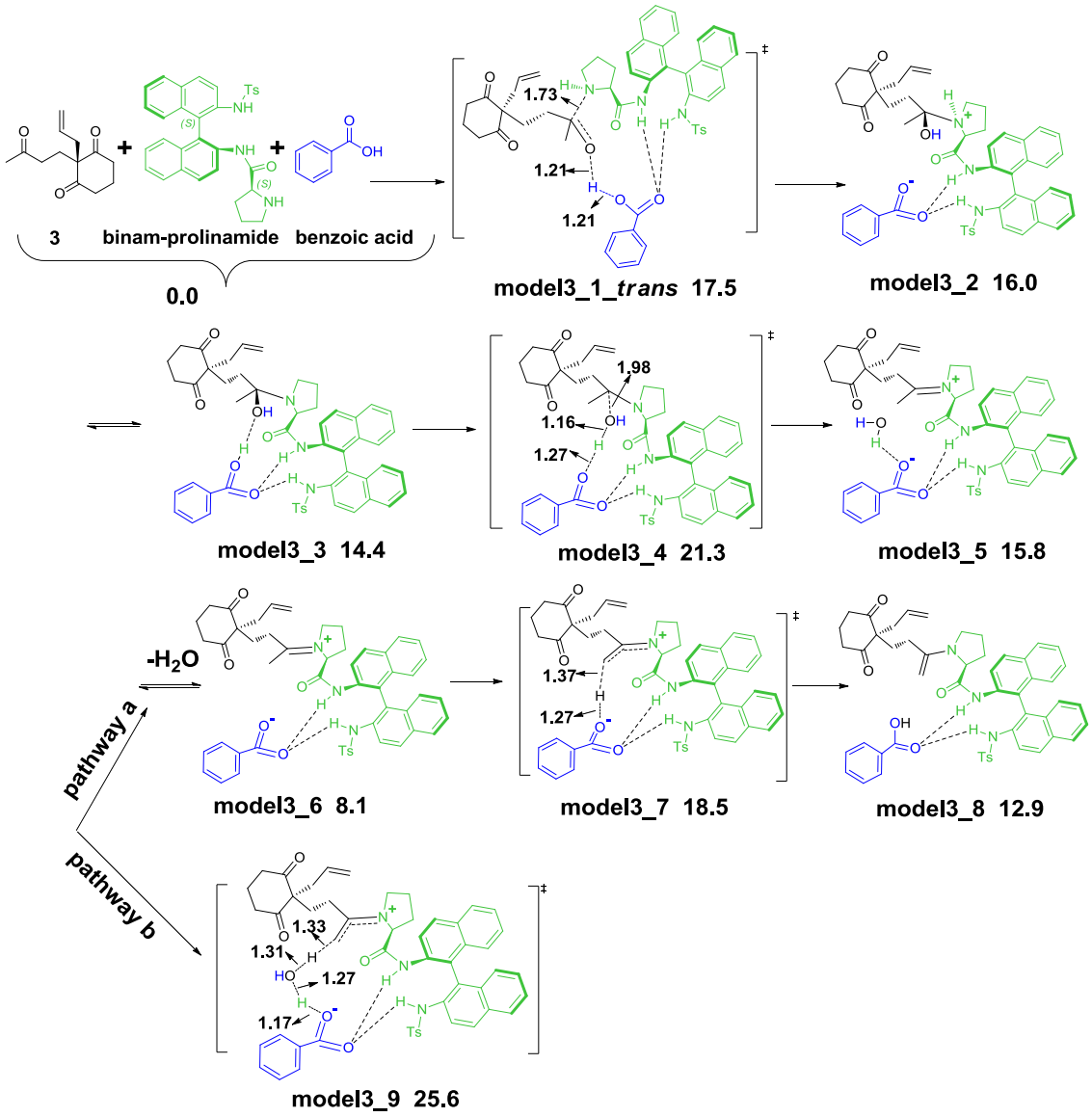

Figure 3.5 Enamine formation process with **model3** and free energies in kcal.mol^{-1} relative to the reactants. Selected distances are given in Å. Geometry B3LYP/6-31G(d), single point energies in cyclohexanone M062x/6-31+G(d,p).

benzoate moiety gets a proton from the methyl to form the enamine **model3_8** with a barrier of 10.4 kcal.mol^{-1}. **Pathway b** shows a H_2O assisted process. This process locates the transition state **model3_9**, where the benzoate moiety gets a proton from the water molecule, and the water molecule gets a proton from the methyl group to form the enamine. The free energies of the transition states of **pathway a** and **pathway b** are respectively 18.5 and 25.6 kcal.mol^{-1}. This difference of energy indicates that the enamine is preferentially formed without the assistance of water. The energies of transition states of the carbinolamine, iminium, and enamine intermediates formation are 17.5, 21.3 and 18.5 kcal.mol^{-1}. The iminium formation step is the most difficult one among these three steps. The energy demands are thus moderate, and compatible with experiment. We settled thus on **model3** for the studies that follow.

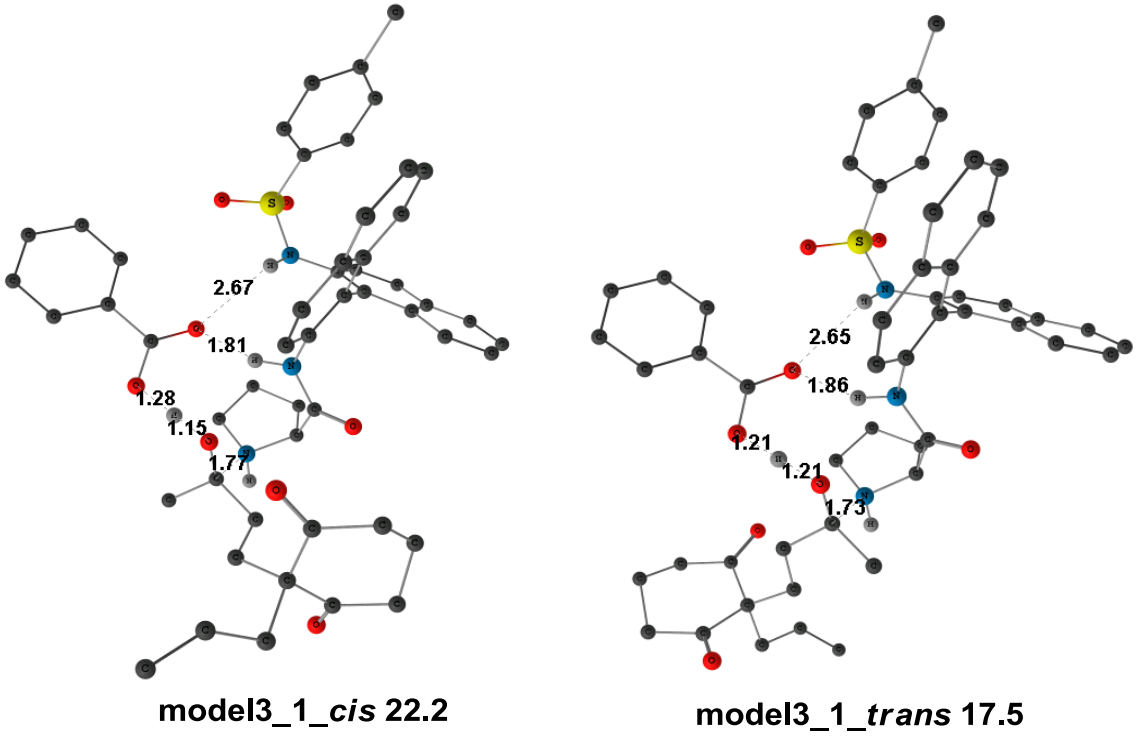

Figure 3.6 *Cis* and *trans* geometries of the carbinolamine transition state of **model3** and free energies in kcal.mol^{-1} relative to the reactants. Selected distances are given in Å. Geometry B3LYP/6-31G(d), single point energies in cyclohexanone M062x/6-31+G(d,p).

3.4.3 C-C bond formation process with model3

After the enamine intermediate formation, the next process is the C-C bond formation. The enamine attacks the carbonyl of the dione to form the C-C bond. As depicted in **Figure 3.7**, there are two different pathways. **Pathway c** is going with benzoic acid as co-catalyst, whereas **pathway d** is not assisted by benzoic acid. In **pathway c**, the proton goes from the benzoic acid moiety to the carbonyl oxygen atom of dione with the formation of a C-C bond. A six-membered chair ring is formed through the transition state **model3_11** with a free energy of 20.0 kcal.mol^{-1}. However, in **pathway d**, the C-C bond formation and the proton migration steps are not simultaneous processes. First the enamine attacks the carbonyl of the dione to form a C-C bond through the transition state **anti_re_TS** with the free energy of 17.3 kcal.mol^{-1}, which is lower than **model3_11**. Therefore, the C-C bond formation step should proceed through **anti_re_TS** transition state. After the formation of **model3_15**, the proton transfer follows. This step also involves two alternative pathways. In **pathway d1**, the NH group of prolinamide transfers a proton to the carbonyl oxygen atom of the dione *via* transition state **model3_16** to arrive to the **model3_17** intermediate, which has a free energy of 8.8 kcal.mol^{-1}. In **pathway d2**, the benzoic acid transfers a proton to the carbonyl oxygen atom of dione to produce **model3_12** directly without energy barrier. **Model3_12** is more stable than **model3_17**, so this process should proceed through **model3_12**. In all, the C-C bond formation process is going through the formation of the C-C bond and the proton transfer in two separate steps. The C-C bond is formed without benzoic acid as co-catalyst, and the proton is transferred to the carbonyl oxygen atom from benzoic acid.

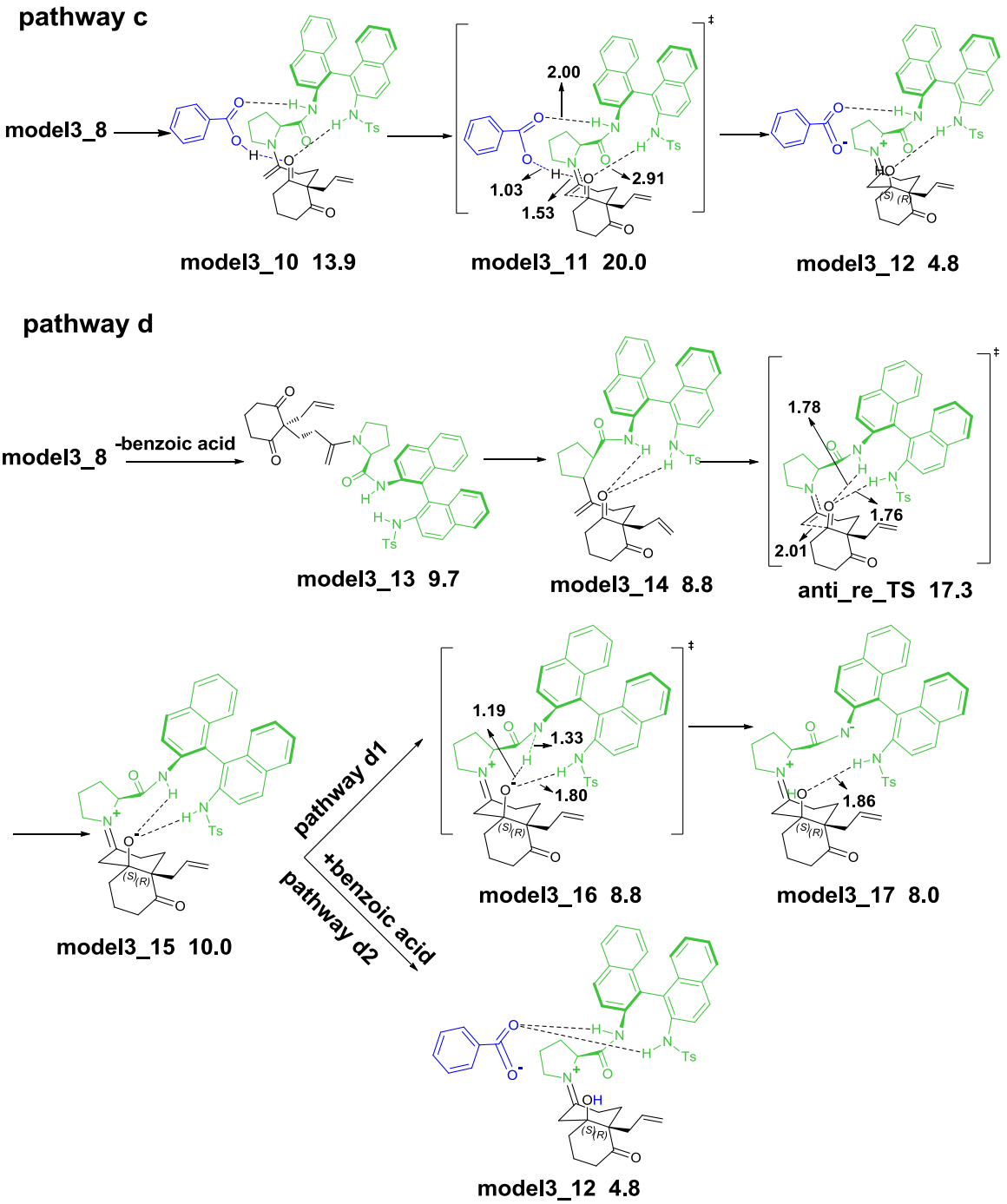

Figure 3.7 C-C bond formation process with **model3** and free energies in kcal.mol^{-1} relative to the reactants. Selected distances are given in Å. Geometry B3LYP/6-31G(d), single point energies in cyclohexanone M062x/6-31+G(d,p).

3.4.4 Hydrolysis process with model3

After the formation of the C-C bond, the hydrolysis of the iminium **model3_12** intermediate is achieved in a series of easy steps that leads to the release of the aldol product and the recovery of the prolinamide and benzoic acid. As shown in **Figure 3.8**, these steps are analogous with the formation of carbinolamine and iminium intermediates, but in reverse order. **Model3_12** rearranges to **model3_18**, and then a water molecule offers a proton to the benzoate moiety and a hydroxyl group to the iminium, resulting in transition state **model3_19** with an energy barrier of 17.2 kcal.mol^{-1}. **Model3_20** is in equilibrium with **model3_21**. The last step is the regeneration of prolinamide and benzoic acid, and the release of the product. The carboxylate group gets a proton from the hydroxyl

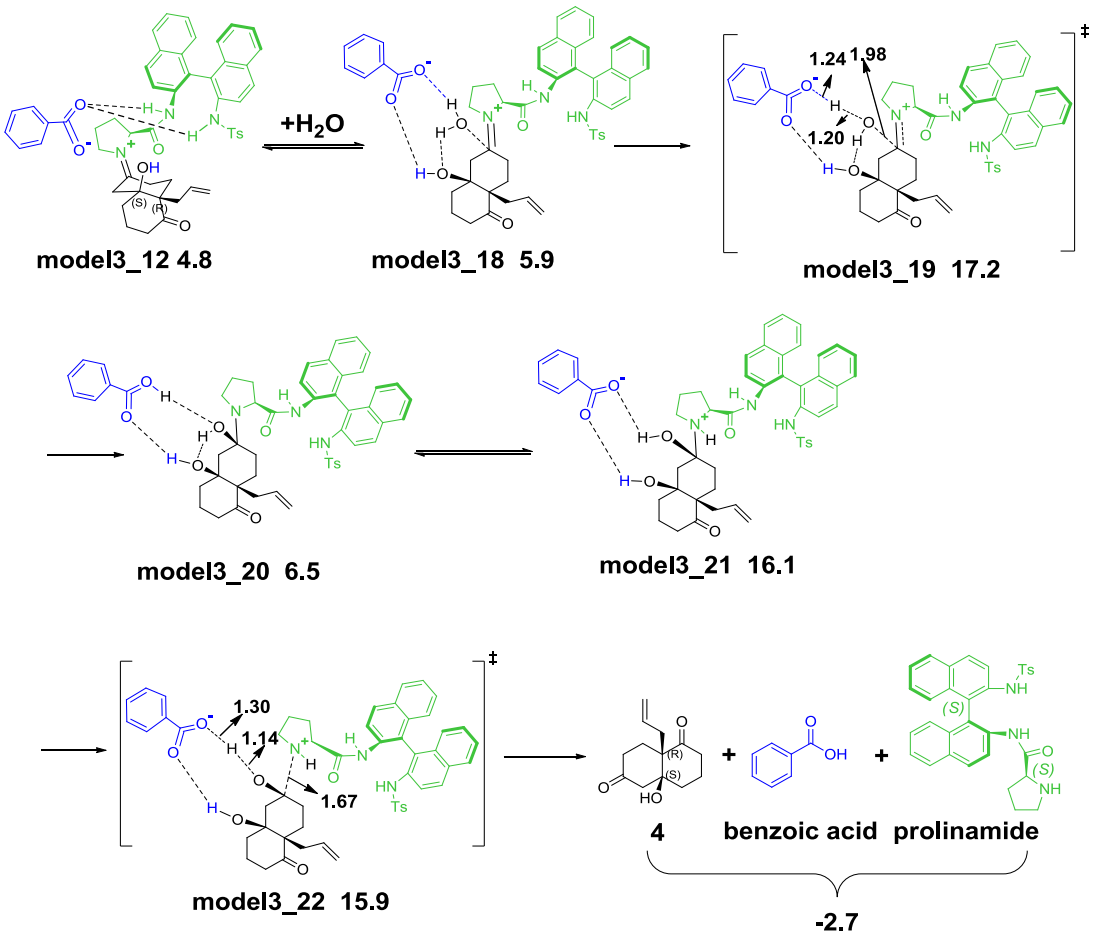

Figure 3.8 Hydrolysis process with **model3** and free energies in kcal.mol^{-1} relative to the reactants. Selected distances are given in Å. Geometry B3LYP/6-31G(d), single point energies in cyclohexanone M062x/6-31+G(d,p).

group of **model3_21**, as the prolinamide catalyst moves away from the aldol product. The transition state for this process, **model3_22**, has a free energy 15.9 kcal.mol^{-1} above the separate reactants. The highest energy transition state during the hydrolysis process is **model3_19**, 17.2 kcal.mol^{-1} above reactants. This is lower than the energies required for enamine formation, and the hydrolysis step does not have thus kinetic relevance.

.

3.4.5 Overall reaction scheme with model3

Following the discussion above, we propose a complete mechanism of the intramolecular aldol cyclization reaction in **Figure 3.9**. The highest energy corresponds to the transition state **model3_4** for the formation of the iminium intermediate with a free energy of 21.3 kcal.mol^{-1} above the reactants. **Model3_4** is thus the rate-determining transition state. The stereochemistry-determining step is the C-C bond formation through transition state **anti_re_TS**. Benzoic acid is present on transition state **model3_4** and has thus an effect on the rate of the reaction. However, it is absent from transition state **anti_re_TS**, and has thus no role on the enantioselectivity. This is fully consistent with the experimental data reported in **Table 3.1**. Changes in the nature of carboxylic acid affect the reaction rate, but not the enantiomeric excess. In this reaction, the carboxylic acid plays an important role in the proton transfer processes, whereas prolinamide catalyst determines the stereoselectivity.

Table 3.1 Screening of different acids (experimental data from Prof. Bonjoch group)

Entry	Acid	pKa	Time/d	Yield	ee%
1	benzoic	4.2	5-6	97	90
2	4-chlorobenzoic	4.0	5	91	90
3	formic	3.77	3	97	90
4	2-fluorobenzoic	3.27	3	97	90
5	2-chlorobenzoic	2.94	3	94	89

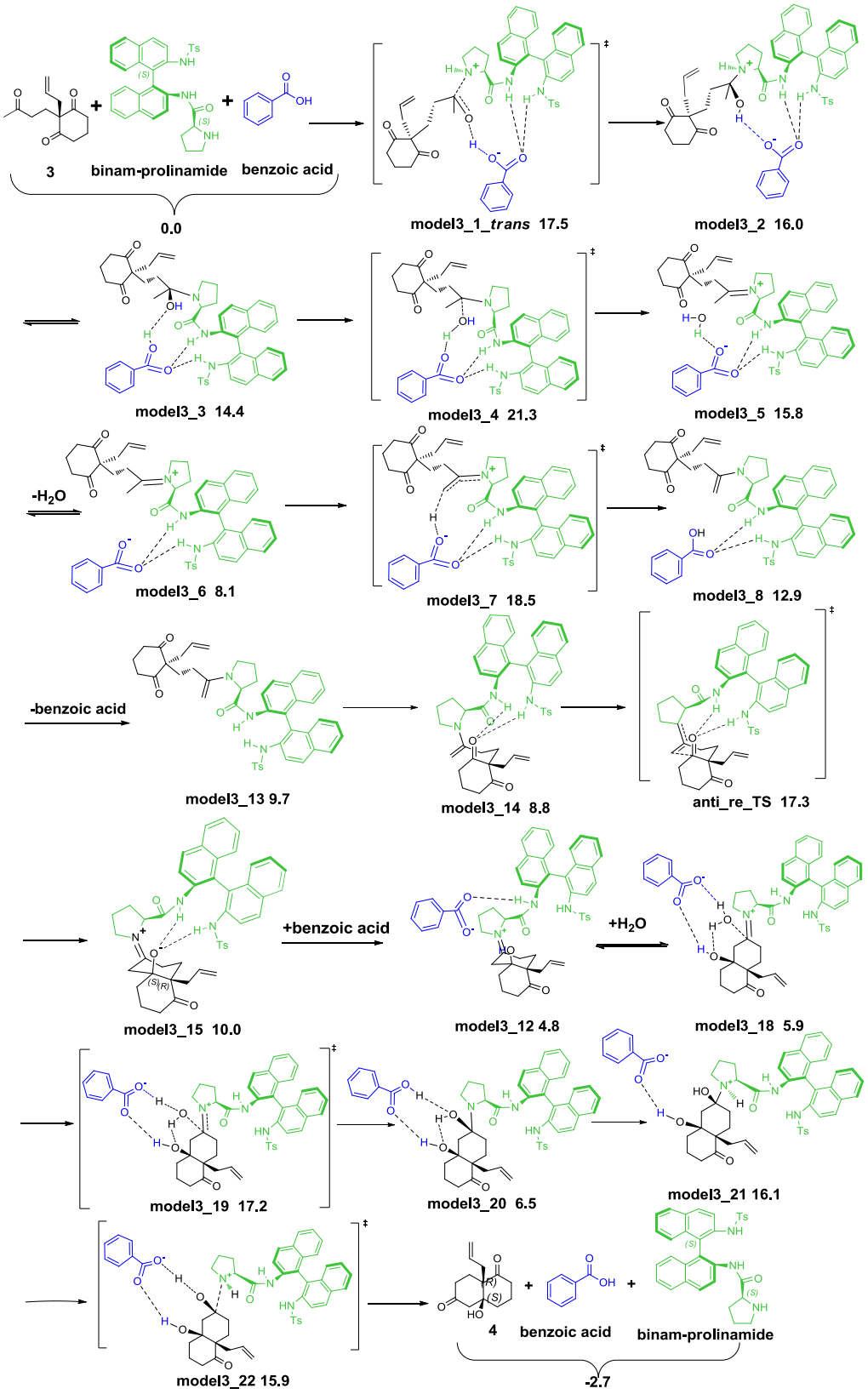

Figure 3.9 The whole pathway with **model3** and relative free energies in kcal.mol^{-1} relative to the reactants. Selected distances are given in Å. Geometry B3LYP/6-31G(d), single point energies in cyclohexanone M062x/6-31+G(d,p).

3.4.6 Enantioselectivity of this reaction

The stereochemistry-determining step (C-C bond formation step) has two main isomers (**anti_re_TS** and **syn_si_TS**), each one has many conformations. We combined **Gaussian 09** with **Macro model** to search their most stable geometries. As shown in **Figure 3.10**, the two six-membered rings (red and black colour) prefer the chair conformation, one oxygen atom of dione forms two hydrogen bonds with two NH bonds of the prolinamide, supported by the strong $^{\delta+}$NH……O$^{\delta-}$ electrostatic interactions. In **anti_re_TS** and **syn_si_TS** geometries, the C=C bond attacks the carbonyl group of dione to form the six-membered chair ring. The carboxylic acid is absent, in agreement with its lack of effect on enantioselectivity. The **anti_re_TS** geometry is more stable with 4.5 kcal.mol^{-1} than **syn_si_TS**, which would favour **anti_re_TS** structure with almost 100% enantiomeric excess (ee) value. The identity of the major product is correct, but our computed ee value

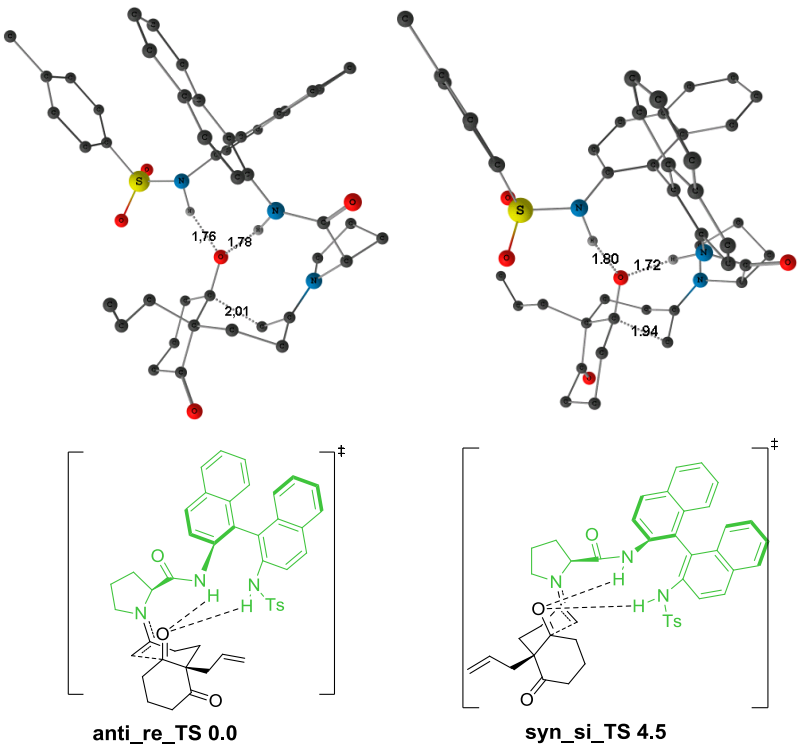

Figure 3.10 Structures of **anti_re_TS** and **syn_si_TS** (some H atoms are omitted for clarity). Relative free energies in kcal.mol^{-1}, selected distances are given in Å. Geometry B3LYP/6-31G(d), single point energies in cyclohexanone M062x/6-31+G(d,p).

overestimates by 2 kcal.mol^{-1} compared with the expected energy difference. Because of this, we tried to refine the method in order to improve the quantitative agreement.

Table 3.2 Relative free energies (ΔG) [kcal.mol^{-1}] between **anti_re_TS** and **syn_si_TS** geometries at the different theory levels.

isomer	method1	method2	method3	method4	method5
ΔG(syn_si_TS-anti_re_TS)	4.5	5.1	4.1	3.2	2.8
ee value	99.9%	100%	99.8%	99.1%	98%

method1: Geometry B3LYP/6-31g(d), single point energies in solution M062x/6-31+g(d,p).
method2: Geometry B3LYP/6-31g(d), single point energies in solution B97D/6-31+g(d,p).
method3: Geometry M062x/6-31g(d), single point energies in solution M062x/6-31+g(d,p).
method4: Geometry B97d/6-31g(d), single point energies in solution B97d/6-31+g(d,p).
method5: Geometry B97d/6-31g(d), single point energies in solution B97d/6-31+g(d,p), BSSE B97d/6-31+g(d,p) in gas phase.

An obvious limitation of our initial set of calculations is the limited introduction of dispersion effects. They are absent from the geometry optimization, and introduced only through the M062x method in single point calculations. Dispersion may be important to describe properly the interaction between the substrate and the sulphonamide and naphthyl groups of binam, which should be important in enantioselectivity. Another more subtle limitation is that we have not considered basis set superposition error (BSSE). After all, we have the interaction between two fragments, and in these cases BSSE should be important.

In order to address these limitations, we evaluated the additional methods depicted in **Table 3.2**. We optimized the **anti_re_TS** and **syn_si_TS** geometries using methods including dispersion (M062x and B97D), and we introduced BSSE. As shown in **Table 3.2**, the best result is provided by **method 5**, B97D optimization with a posteriori BSSE correction, with an ee value of 98%. The experiment group can get 97% ee value when using 2.5 mol% prolinamide and 1 mol% benzoic acid.[4a] The ee value with **method 5** is close to the experimental results. The introduction of dispersion effects in the course of the geometry optimization has the relevant side effect of introducing two new conformers to the discussion. During the search of **anti_re_TS** and **syn_si_TS** geometries using **method 5**, we found two other geometries (**anti_re_TS_2** and **syn_si_TS_2)**, which are also depicted in **Figure 3.11**. They are more stable than **anti_re_TS** and **syn_si_TS** for this particular combination of substrate and catalyst. The main difference between the **anti_re_TS** and **anti_re_TS_2** geometries is in the orientation of SO_2R group. Joint

consideration of these four structures (**anti_re_TS**, **anti_re_TS_2**, **syn_re_TS** and **syn_re_TS_2)** leads to an ee value of 97%, very consistent with the experiment result. In the next section, we will use these four geometries (**anti_re_TS**, **anti_re_TS_2**, **syn_re_TS** and **syn_re_TS_2)** to discuss the effect of different sulfonamide groups on the ee value with **method 5**.

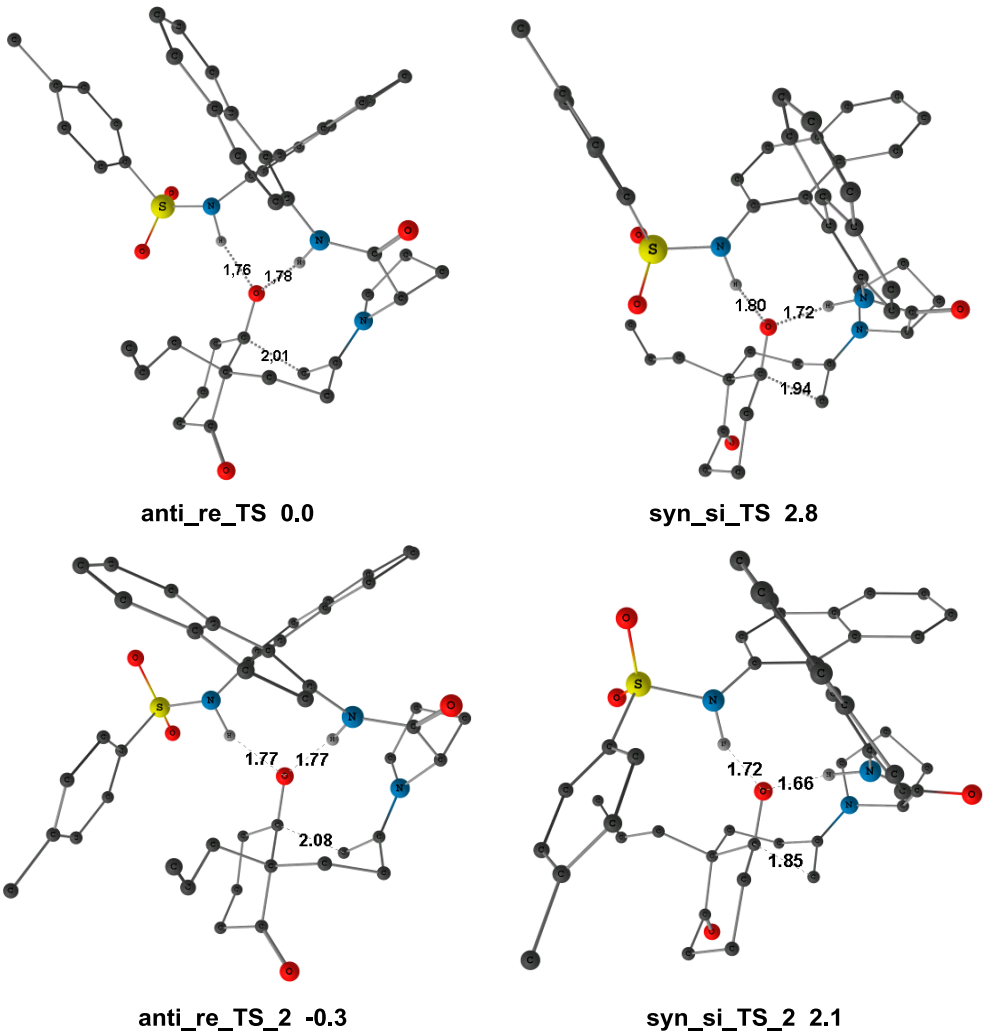

Figure 3.11 The views of **anti_re_TS**, **anti_re_TS_2**, **syn_si_TS** and **syn_si_TS_2** (some H atoms are omitted for clarity). Relative free energies in kcal.mol^{-1}, selected distances are given in Å. Geometry B97D/6-31g(d), single point energies in cyclohexanone B97D/6-31+G(d,p), including BSSE B97d/6-31+G(d,p) corrections in gas phase.

Once we reproduce the experimental result in terms of enantiomeric excess, it is important to understand the reason why the origin of this enantioselectivity. From the examination of

the structures in **Figure 3.11**, this origin is not clear. The hydrogen bonds play an obvious role in the shape of this transition states, as they are rather strong, but there is not a clearly pattern connecting the O...H distances to the stability of the transition states. Moreover, there is no obvious non-bonding interaction, either repulsive or attractive, between groups in substrate and catalyst that can explain in a simple way the discrimination between the diastereomeric transition states.

We approached the problem by carrying out the energy decomposition analysis outlined in the thermodynamic cycle in **Figure 3.12**. The idea is to separate the system in two fragments, catalyst and substrate, and to have a quantitative measure of how distorted they are and how strongly they interact. The analysis is complicated by the presence of a double bond between the two fragments. We solved this problem by having the C=N bond present in both fragments, being capped in each case by two hydrogen atoms, marked in pink in the Figure. These hydrogen atoms were optimized in the calculations, but the rest of the atoms were kept at the positions they have in the transition states. The discussion is limited to potential energies, as they capture already the main changes, and avoid computational artifacts related to the artificial fragmentation of the system. For the sake of simplicity, we will limit the discussion to the comparison of two structures: **anti_re_TS** and **syn_si_TS**. As discussed above, they are not the most stable conformations for this particular system, but they follow the general trend, and they are the most stable ones in other examples that will be discussed in the next section.

The results of this energy decomposition analysis are summarized in **Figure 3.12**. Fragment A, the prolinamide fragment, is practically unchanged in the two transition states, being only 0.4 kcal.mol^{-1} more stable in **anti_re_TS** ($\Delta E_{DIST(A)}$ is 0.4 kcal.mol^{-1}). For fragment B, the substrate, the energy difference, $\Delta E_{DIST(B)}$ is 2.9 kcal.mol^{-1}, much larger. The interaction energies cannot be evaluated independently, but completing the thermodynamic cycle we obtain an $\Delta E_{INT(syn)}$-$\Delta E_{INT(anti)}$ of 1.1 kcal.mol^{-1}. 2.9 plus 0.4 minus 1.1 yields the 2.2 kcal.mol^{-1} difference in potential energy that exists between the two transition states. This result is remarkable; the direct interactions between substrate and catalyst would favour the major enantiomer. The key is in the distortion terms that are significantly larger in this major enantiomer. The asymmetry in these distortions terms contains in our opinion the key to the explanation. The most important term is $\Delta E_{DIST(B)}$,

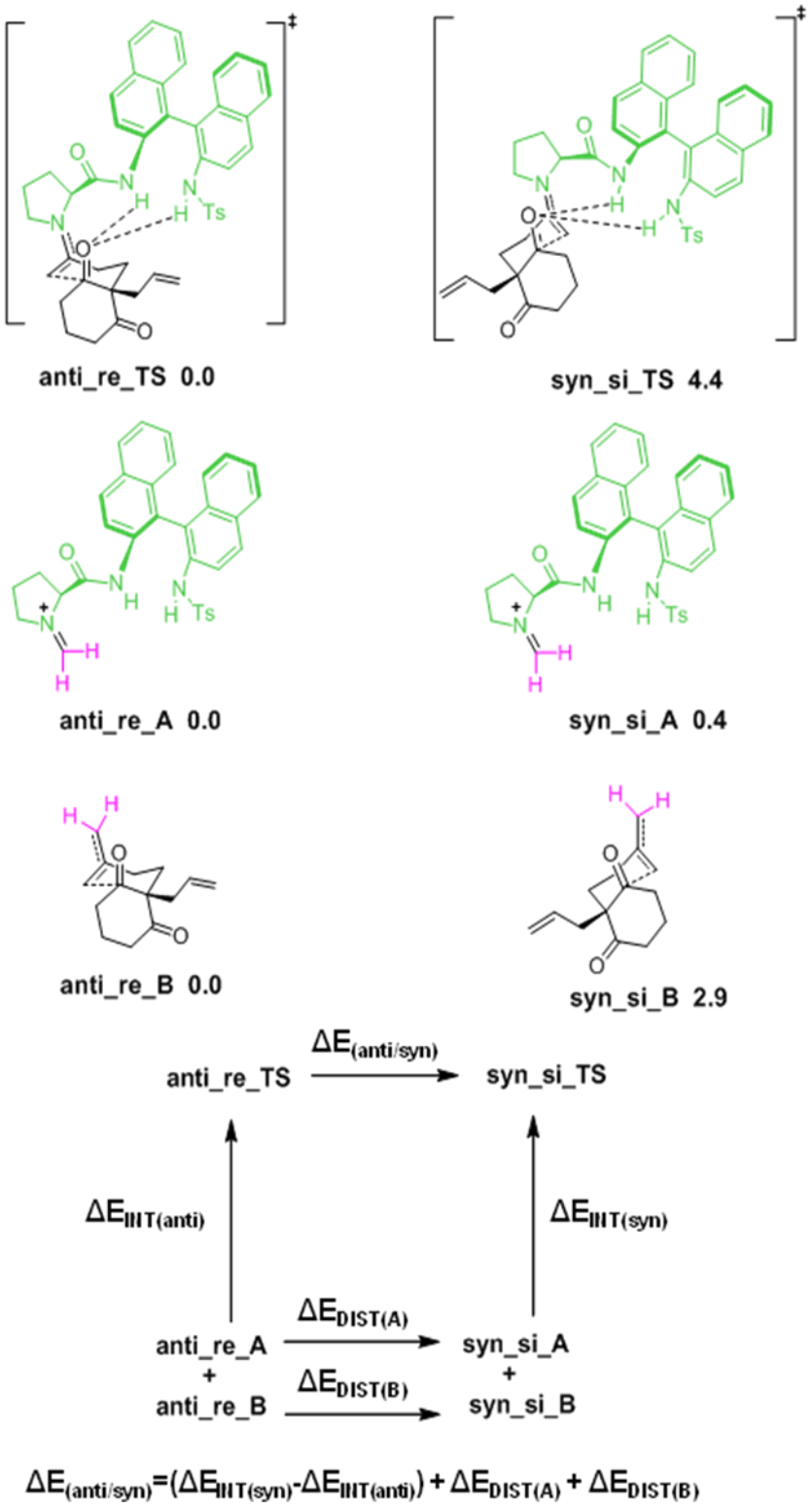

Figure 3.12 Schematic structures and relative potential energies of **anti_re_TS**, **syn_si_TS** and the **A** and **B** fragments of them relative to the **anti_re** geometries. Geometry B97D/6-31g(d), single point energies in cyclohexanone B97D/6-31+G(d,p). The energy decomposition diagram used is also presented.

with $\Delta E_{DIST(A)}$ being much smaller. This means that the A fragment, the catalyst, is practically rigid. This is consistent with the known structural features of the binaphthyl group. The B fragment, with its two fused six-membered rings is in contrast more flexible, and distorts to obtain a better interaction with the catalyst. To understand this distortion we examine again the structure of the transition state. There are two regions of contact between catalyst and substrate. The first of them is the C=N double bond, the second are the two hydrogen bonds between the acidic N-H groups in the catalyst and the oxygen developing a negative charge in the substrate. In the rigid structure of the catalyst, both interactions are pointing to precise regions in the space, and the substrate distorts to allow for these interactions. This distortion is smaller in the case of **anti_re_TS**, and this is why it leads to major product.

The origin of enantioselectivity in this particular system is therefore not in the interaction of a particular region of the catalyst with a particular region of the substrate, but in the rigidity of the catalyst. This rigidity of the catalyst favors a certain arrangement of the substrate that leads to the major product.

3.4.7 Impact of the substituents in the catalyst on the enantioselectivity

As shown in **Figure 3.13**, the R groups on the prolinamide have an effect on the ee values obtained for a related reaction where an allyl group in the reactant is replaced by a methyl. We computed the key transition states for these systems with the methods outlined above. The ee values of our computational studies are presented in **Table 3.3**. All of our results overestimate the ee value compared with the experimental results, but the energy order is consistent with the experimental results.

As we were able to reproduce the trends, we repeated the energy decomposition analysis presented in the previous section for these new catalysts in order to check if the origin of enantioselectivity was the same. This could help the experimental group to design new sulfonamide ligands that could give better ee values. The energy decomposition analysis is presented in **Table 3.4**. Two groups can be clearly distinguished in the results reported in this Table. Systems **5**, **6**, **7**, **8** follow the same trend outlined above for the model system. The distortion energy $\Delta E_{DIST(B)}$ is larger than the other energy terms, while $\Delta E_{DIST(A)}$ of them is small, which means that the fragment A of these system is rigid. Therefore, the

origin of the enantioselectivity for systems **5**, **6**, **7**, **8** comes from the differences in the distortion of fragment B. The explanation is thus the same outlined above; the rigidity of the catalyst is the key to enantioselectivity. This is fully consistent with the similar experimental enantioselectivity for these systems. All these catalysts follow a same pattern in terms of rigidity. And there are then some minor differences which favor rigidity in the case of the bulky naphthyl substituent on sulfur, or the presence an electron-withdrawing nitro group favoring stronger hydrogen bonds.

Systems **9** and **10** follow, in contrast, a different pattern. The energy differences between **anti_re_TS** and **syn_si_TS** come mostly from the interaction energies ($\mathbf{\Delta E_{INT(syn)}}$-$\mathbf{\Delta E_{INT(anti)}}$), so the origin of the enantioselectivity of them comes from the interaction between the fragments. This is a more conventional situation in enantioselective catalysis. We will analyze the reason for this behavior in detail in the case of system **10**, which is more extreme than **9**. As shown in **Figure 3.14**, in **anti_re_TS** geometry of system **10**, the C=O group of the dione has three interactions, one with the NH bond and two with methyl groups of prolinamide, the O...H distances being 1.70, 2.58 and 2.46 Å, respectively. In contrast, in **syn_si_TS** geometry, the C=O group only interacts with a NH bond and a methyl group of prolinamide, O…H distances being 1.71 and 2.22 Å, respectively. The anti structure has thus more attractive interactions between fragments A and B than the syn structure. This is the reason for the enantioselectivity in system **10**. The mechanism operating in systems **5** to **8**, based on the rigidity of the catalyst, is thus absent in system **10**. $\Delta E_{DIST(A)}$ of system **10** is larger than the other systems, which means that fragment A (prolinamide) is less rigid. The reasons are clear when examining the structure, the absence of the second N-H unit makes the structure more flexible, as there is no constrain associated with this second hydrogen bond. The case of **9** is more subtle, but the absence of the SO_2R group gives also more flexibility. It is therefore clear that the key to high enantioselectivity in these prolinamide systems is in the rigidity of the binam fragment, which should not be reduced if one wants to keep selectivity. This is why systems **9** and **10** are steps in the wrong direction.

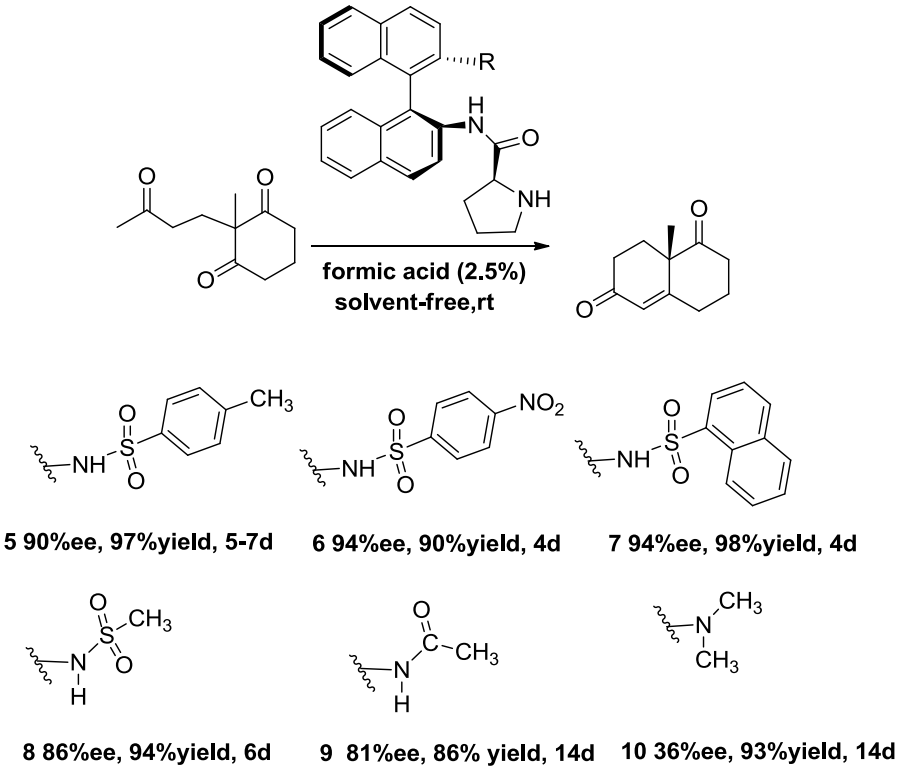

Figure 3.13 Screening of modified Binam-prolinamide catalyst (experimental data from Prof. Bonjoch).

Table 3.3 Relative free energy ΔG (kcal.mol^{-1}) between **anti_re_TS**, **anti_re_TS_2**, **syn_si_TS** and **syn_si_TS_2** geometries with different **R** groups. Geometry B97D/6-31g(d), single point energies in cyclohexanone B97D/6-31+G(d,p), including BSSE B97d/6-31+G(d,p) corrections in gas phase.

isomer	**5**	**6**	**7**	**8**	**9**	**10**
anti_re_TS	1.9	0.0	0.0	0.0	0.0	0.0
anti_re_TS_2	0.0	0.7	0.6	-	-	-
syn_si_TS	4.3	3.6	4.6	2.9	2.6	0.7
syn_si_TS_2	4.7	4.3	3.5	-	-	-
ee value	100%	100%	100%	99%	98%	42%
experimental ee value	90%	94%	94%	86%	81%	36%

Table 3.4 Relative potential energies of **anti_re_TS**, **syn_si_TS** for the different R group and the **A** and **B** fragments of them relative to the **anti_re** geometries. Geometry B97D/6-31g(d), single point energies in cyclohexanone B97D/6-31+G(d,p).

	5	6	7	8	9	10
$\Delta E_{DIST(A)}$	0.6	0.4	1.9	0.3	-0.8	-2.6
$\Delta E_{DIST(B)}$	3.7	3.5	3.6	2.8	0.9	-0.8
$\Delta E_{INT(syn)}$-$\Delta E_{INT(anti)}$	-1.6	-0.5	-0.4	-0.6	3.0	3.9
$\Delta E_{(anti/syn)}$	2.7	3.4	5.1	2.5	3.1	0.5

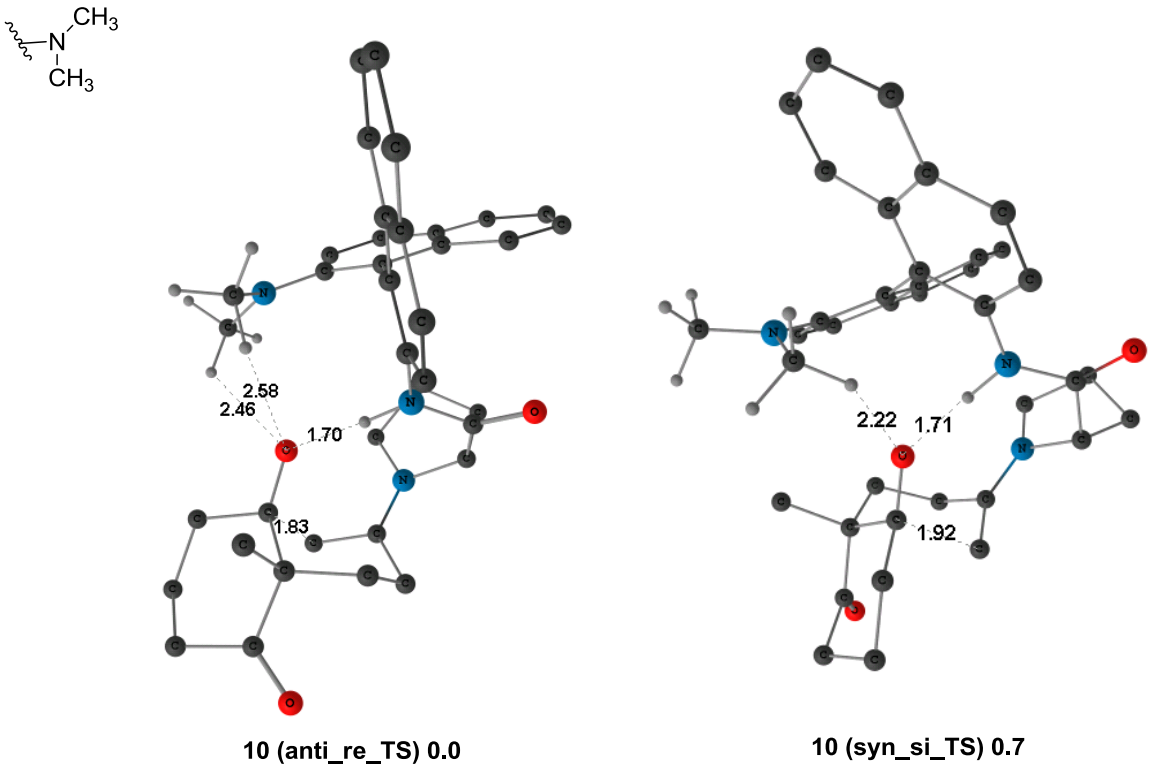

Figure 3.14 The most stable transition geometries of system **10** (some H atoms are omitted for clarity). Relative free energies in kcal.mol^{-1}, selected distances are given in Å. Geometry B97D/6-31g(d), single point energies in cyclohexanone B97D/6-31+G(d,p), including BSSE B97d/6-31+G(d,p) corrections in gas phase.

3.5 Conclusion

The N-Ts-(Sa)-binam-L-prolinamide catalyzed intramolecular aldol reaction leading to Wieland-Miescher ketones has been investigated with density functional theory. We have been able to clarify the mechanism of the reaction with prolinamide. It follows the general trends of the mechanism with proline, with the important caveat that the presence of a carboxylic acid as co-catalyst is mandatory in the initial steps of the reaction, in particular for the formation of the iminium intermediate. In contrast, the carboxylic acid has no effect on the enantioselectivity, as it departs the system after enamine formation, and is absent in the transition state leading to C-C bond formation, where the enantioselectivity of the reaction is decided. The origin of the enantioselectivity of the reaction has been also clarified. It is based on the rigidity of the catalyst, which has two anchoring points for the substrate, the C=N double bond in the enamine intermediate, and the N-H...O hydrogen bonds between catalyst and substrate. The substrate has to distort to bind properly to these anchoring points, and this distortion is smaller for the transition state leading to the favored enantiomer.

.

3.6 References

[1]. (a) Ley S.V., *Proc. Natl. Acad. Sci*, USA **2004**, 101, 12073; (b) Diaz S., Gonzalez A., Bradshaw B., Cuesta J., Bonjoch J., *J. Org. Chem*, **2005**, 70, 3749; (c) Waters S. P., Tian Y., Li Y-M., Danishefsky S. J., *J. Am. Chem. Soc*, **2005**, 127, 13514; (d) Takikawa H., Imamura Y., Sasaki M., *Tetrahedron*, **2006**, 62, 39; (e) Kaliappan K. P., Ravikumar V., *Org. Lett*, **2007**, 9, 2417; (f) Chanu A., Safir I., Basak R., Chiaroni A., Arsenyyadis S., *Org. Lett*, **2007**, 9, 1351.

[2]. (a) Eder U., Sauer G., Wiechert R., German Patent, DE 2104757, Oct. 7, **1971**; (b) Eder U., Sauer G., Wiechert R., *Angew. Chem*, **1971**, 83, 492; *Angew. Chem. Int. Ed. Engl*, **197**1, 10, 496.

[3]. (a) Gutzwiller J., Buchschacher P., Fürst A., *Synthesis*, **1977**, 167; (b) Buchschacher P., Fürst A., *Org. Synth*, **1985**, 63, 37; (c) Harada N., Sugioka T., Uda H., Kuriki T., *Synthesis*, **1990**, 53.

[4]. (a) Bradshaw B., Etxebarria-Jardia G., Bonjoch J., Viozquez S. F., Guillena G., Najera C., *Adv. Synth. Catal*, **2009**, 351, 2482; (b) Bradshaw B., Etxebarria-Jardıa G., Bonjoch J., *J. Am. Chem. Soc*, **2010**, 132, 5966.

[5]. (a) Fernando R. C., Houk K. N., *Angew. Chem. Int. Ed*, **2004**, 43, 5766; (b) Cheong P. H-Y., Legault C. Y., Um J. M., Çelebi-Ölcüm N., Houk K. N., *Chem. Rev*, **2011**, 111, 5042.

[6]. (a) List B., Hoang L., Martin H. J., *Proc. Natl. Acad. Sci*, USA, **2004**, 101, 5839; (b). Hoang L., Bahmanyar S., Houk K. N., List B., *J. Am. Chem. Soc*, **2003**.125, 16.

[7]. Strategic Applications of Named Reactions in Organic Synthesis, 1st Edition, Eds: Kürti. L., Czakó. B., Elsevier academic press, New York, **2005**, 192.

[8]. Bahmanyar S., Houk K. N., Martin H. J., List B., *J. Am. Chem. Soc*, **2003**, 125, 2475.

[9]. (a) Becke A. D., *J. Chem. Phys*, **1993**, 98, 5648; (b) Lee C., Yang W., Parr R. G., *Phys. Rev. B*, **1988**, 37, 785.

[10]. Frisch M. J., Trucks G. W., Schlegel H. B., Scuseria G. E., Robb M. A., Cheeseman J. R., Montgomery J. A., Jr., Vreven T., Kudin K. N., Burant J. C., Millam J. M., Iyengar S. S., Tomasi J., Barone V., Mennucci B., Cossi M., Scalmani G., Rega N., Petersson G. A., Nakatsuji H., Hada M., Ehara M., Toyota K., Fukuda R., Hasegawa J., Ishida M., Nakajima Honda T., Y., Kitao O., Nakai H., Klene M., Li X., Knox J. E., Hratchian H. P., Cross J. B., Adamo C., Jaramillo J., Gomperts R., Stratmann R. E., Yazyev O., Austin A. J., Cammi R., Pomelli C., Ochterski J. W., Ayala P. Y., Morokuma K., Voth G. A., Salvador P., Dannenberg J. J., Zakrzewski V. G., Dapprich S., Daniels A. D., Strain M. C., Farkas O., Malick D. K., Rabuck A. D., Raghavachari K., Foresman J. B., Ortiz J. V., Cui Q., Baboul A. G., Clifford S.,

Cioslowski J., Stefanov B. B., Liu G., Liashenko A., Piskorz P., Komaromi I., Martin R. L., Fox D. J., Gaussian, Inc., Wallingford CT, **2009**. Gaussian09, Revision A.02.

[11]. (a) Chang G., Guida W. C., Still W. C., *J. Am. Chem. Soc*, **1989**, 111, 4379; (b) Saunders M., Houk K. N., Wu Y. D., Still W. C., Lipton M., Chang G., Guida W. C., *J. Am. Chem. Soc*, **1990**, 112, 1419.

[12]. Mohamadi F., Richards N. G. J., Guida W. C., Liskamp R., Lipton M., Caufield C., Chang G., Hendrickson T., Still W. C., *J. Comp. Chem*, **1990**, 11, 440.

[13]. Allinger N. L., Yuh Y. H., Li J. H., *J. Am. Chem. Soc*, **1989**, 111, 8551.

[14]. Zhao Y., Truhlar D. G., *Theor. Chem. Acc*, **2008**, 120, 215.

[15]. Marenich A. V., Cramer C. J., Truhlar D. G., *J. Phys. Chem. B*, **2009**, 113, 6378.

[16]. Wheeler S. E., Houk K. N., *J. Chem. Theory. Comput*, **2010**, 6, 395.

[17]. Grimme S., *J. Comp. Chem*, **2006**, 27, 1787.

[18]. Balabin R. M., *J. Chem. Phys*, **2008**, 129, 164101.

Chapter 4

Mechanism of [4+2] cycloaddition reaction catalyzed by chiral phosphoric acid derivatives

4.1 Mechanistic landscape of chiral phosphoric acid–catalyzed reaction

BINOL-phosphoric acid derivatives are well-known catalysts with excellent yield and enantioselectivity in many organic reactions as indicated in **Chapter 1**. Computational studies for the organocatalytic reactions of BINOL-phosphoric acid have been carried out by a number of research groups, including those of the Goodman,[1] You,[2] Yamanaka,[3] Himo[4] and Shi.[5] Chiral phosphoric acid derivatives bearing both Brønsted acidic and Lewis basic sites allow for bifunctional catalysis to activate simultaneously both electrophiles and nucleophiles, as indicated in **Scheme 4.1**. These phosphoric acid derivatives may interact with substrates in different ways, and each of them may affect enantioselectivity: (i) formation of hydrogen bonds with one of the phosphoric acid oxygens, (ii) formation of hydrogen bonds with two of the phosphoric acid oxygens, in what has been labeled as dicoordination, (iii) non-covalent interactions between the substrate and the phosphoric acid substituents. A strong hydrogen bond will almost always be present, but it will not be able to induce enantioselectivity by itself. This will be thus caused by either a second hydrogen-bond interaction or non-covalent interactions with the substituents.

In this chapter, we will study a reaction catalyzed by chiral phosphoric acid derivatives that gives rise to different products responding to seemingly minor changes in the catalyst.

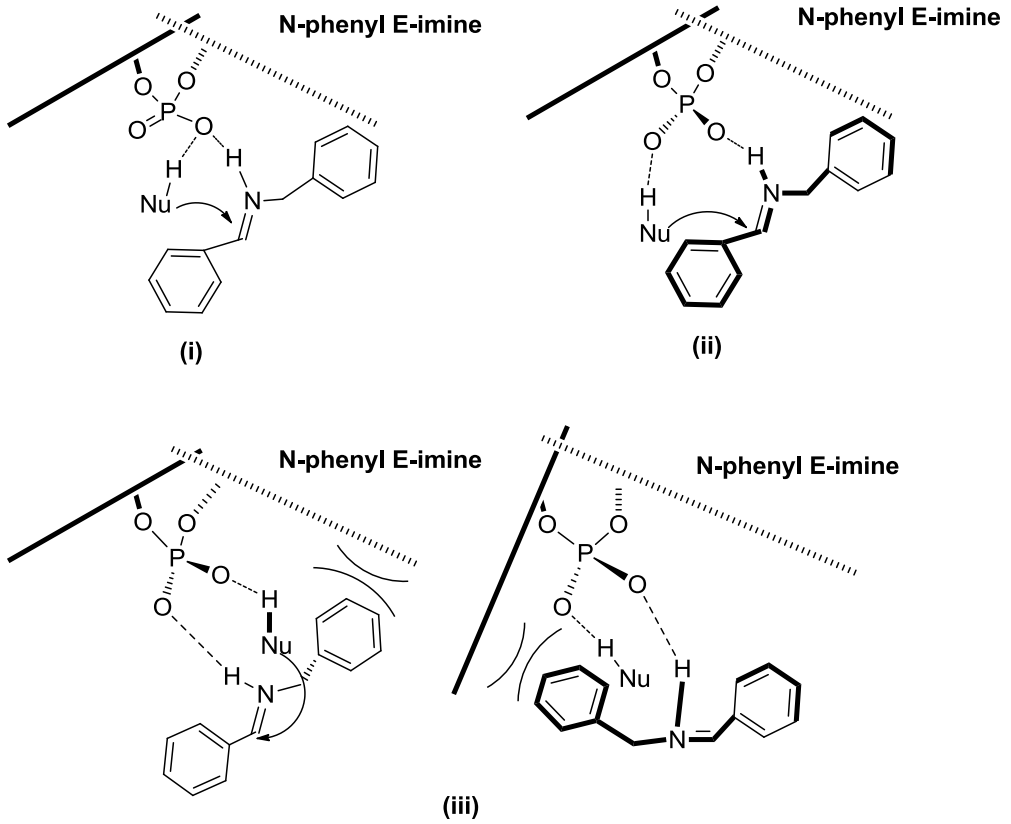

Scheme 4.1 Different types of the interaction between the phosphoric acid derivatives and substrates.[8a]

4.2 [4+2] cycloaddition reaction

N- and O-containing heterocyclic compounds are prominent in nature and exhibit a wide range of interesting biological properties, including antihypertensive and anti-ischemic behavior.[6] 4-aminobenzopyrans (see **Scheme 4.2**) and their derivatives have drawn considerable attention in the last decade as the modulators of potassium channels influencing the activity of the heart and blood pressure.[7] Owing to the importance of the benzopyran framework, their synthesis has attracted considerable attention.[8]

Pyranobenzopyran and furanobenzopyran frameworks, containing three fused rings are particularly interesting. An appealing approach to the synthesis of these compounds is a [4+2] cycloaddition between a hydroxybenzaldimine and a furan, as depicted in **Scheme 4.3**. This reaction is catalyzed by phosphoric acid derivatives. There are some recent puzzling results which we would like to analyze. In 2010, Rueping and Lin[9] reported the

synthesis of the *trans*-fused furanobenzopyrans (labeled as **4** in **Scheme 4.3**) through inverse-electron-demand (IED) [4+2] cycloaddition of *o*-hydroxybenzaldimines **1** with 2,3-dihydro-2H-furan (DHF) catalyzed by (*S*)-BINOL-N-triflylphosphoramide. In the same year, Fochi and co-workers reported the synthesis of *cis*-fused furanobenzopyrans (labeled as **3** in **Scheme 4.3**) obtained through an analogous reaction, but catalyzed in this case by (*S*)-BINOL-phosphoric acid.[10] The same reactants and slightly different catalysts produced different diastereomers of the product. As can be seen in **Scheme 4.3**, the catalysts are based in an identical (*S*)-BINOL phosphorus framework, with minor differences in the substituents on the binol group and in presence of a NTfH substituent on phosphorus for the Rueping system. The origin of this different behavior is not clear, and because of this we decided to analyze the topic from a computational point of view.

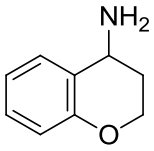

Scheme 4.2 4-aminobenzopyrans

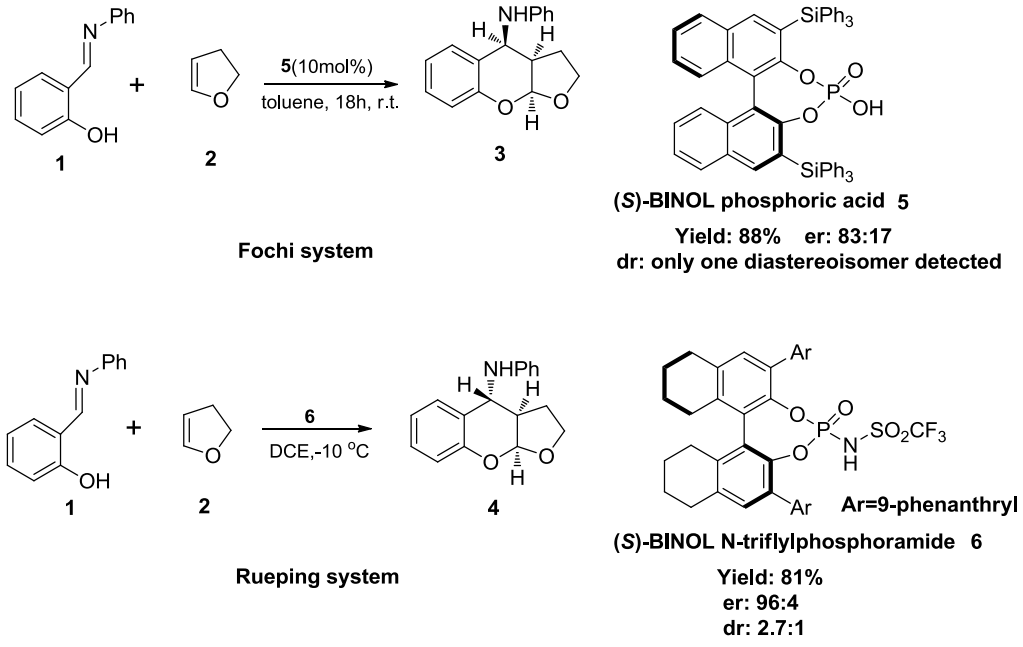

Scheme 4.3 [4+2] cyclization of *o*-hydroxybenzaldimine with 2,3-dihydro-2H-furan(DHF) catalyzed by (*S*)-BINOL phosphoric acid[10] and N-triflylphosphoramide.[9]

4.3 Computational details

Calculations were carried out with the **Gaussian 09**[12] suite of programs. Structures were fully optimized and their natures were characterized by frequency calculations using a two-layered ONIOM[11] description. B3LYP/6-31G(d,p) was used for the high layer, and the UFF[13] force field was used for the low layer. The combination of DFT and UFF has previously been shown to give excellent results when used to describe reactions catalyzed by chiral phosphoric acids derivatives.[1a,1b,1d] The QM/MM partition is shown in **Scheme 4.4**. The reactants, the phosphoric acid and the N-triflylphosphoramide moiety were included in the high-layer, and the remaining regions of the catalyst were treated as the low-layer.

After the ONIOM geometry optimization, the final energy was obtained by single point calculations at the full QM level. The M062x[14]/6-31+G(d,p) single point energies in solution were calculated based on the ONIOM optimized geometries. The effect of solvation was incorporated using the SMD[15] model. Following the experimental data, the solvent was toluene for the Fochi system and dichloroethane for the Rueping system. MonteCarlo Multiple Minimum (MCMM) conformational searches[16] were used to search the conformation of this system in the **Macromodel**[17] program with the MM3[18] force field.

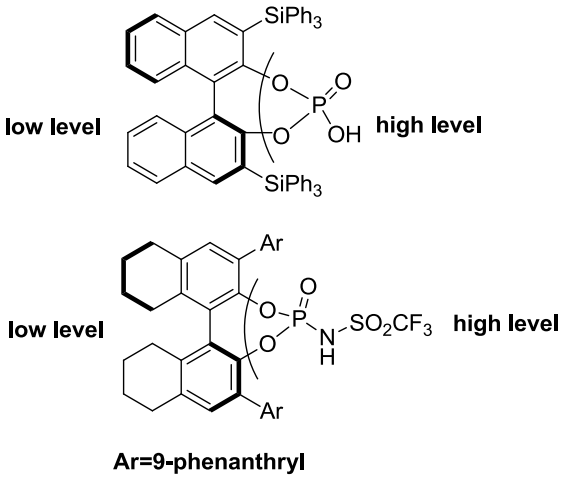

Scheme 4.4 QM/MM partition used in the ONIOM calculations.

4.4 Isomeric diversity

As shown in **Scheme 4.5**, [4+2] cyclization of *o*-hydroxybenzaldimine with 2,3-dihydro-2H-furan (DHF) can yield four different products, two *cis*-fused and two *trans*-fused pyranobenzopyrans. The two major experimental products, **3** and **4**, have the labels already defined in **Scheme 4.3**, and we have used **3´** and **4´** for the other two. There is also isomeric complexity in the reactant, and this will translate into the transition states which we want to analyze. There are four main geometries of *o*-hydroxybenzaldimine (in **Scheme 4.6**). There are two sources of isomeric diversity for the reactants. The first of them is the N=C bond, which may produce *E* and *Z* isomers. And then there is the placement of the OH substituent in the phenyl ring, which we have represented by labels **1** and **2**. The (*Z*)-imine is less stable than (*E*)-imine according to our calculations, but Himo and Goodman[4b,1b] group reported the transition states in which the imine is in *Z* configuration was more stable. Therefore, we should consider both (*E*) and (*Z*)-imine for the transition geometries studied of this reaction.

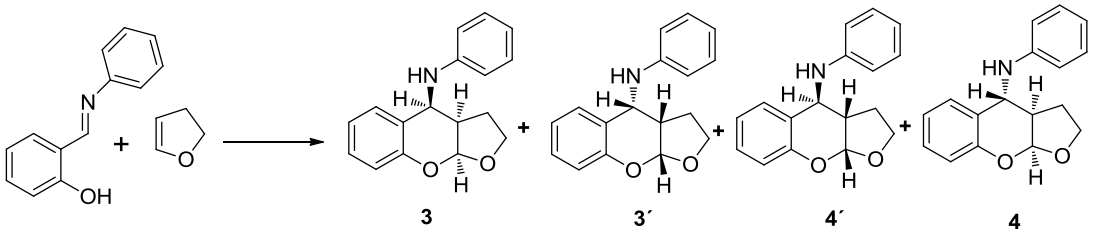

Scheme 4.5 Product geometries.

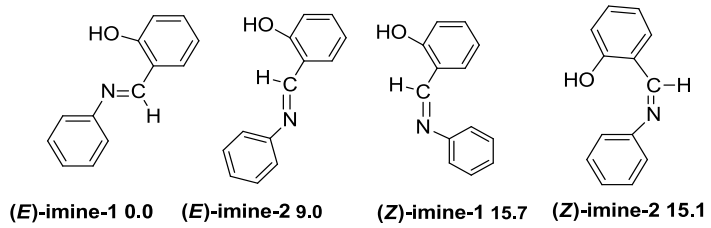

Scheme 4.6 *o*-hydroxybenzaldimine geometries and relative free energies (kcal.mol^{-1}) in gas phase relative to (*E*)-imine-1 at the B3LYP/6-31G(d,p) level.

It may seem awkward to assume equilibria involving rotation around a double bond, but this can be explained by assuming the intermediacy of the amines represented in **Scheme 4.7**. The transformation from imine to amine resembles formally a keto-enol interconversion, and has a very low barrier. The reaction is mildly endergonic in gas phase, and the transition state is only 0.2 kcal.mol^{-1} above the amine product in gas phase. When solvation effects are introduced the transition state ends up below the amine, as indicated in **Scheme 4.7**. This is associated to the lack of optimization in solution, and we interpret it as meaning that the transition state is very low. The key numbers are thus the energy differences between imine and amine, and they are smaller than 6.0 kcal.mol^{-1} for the most stable amine. Afterward, the amine interconversions involve only rotation around a single bond.

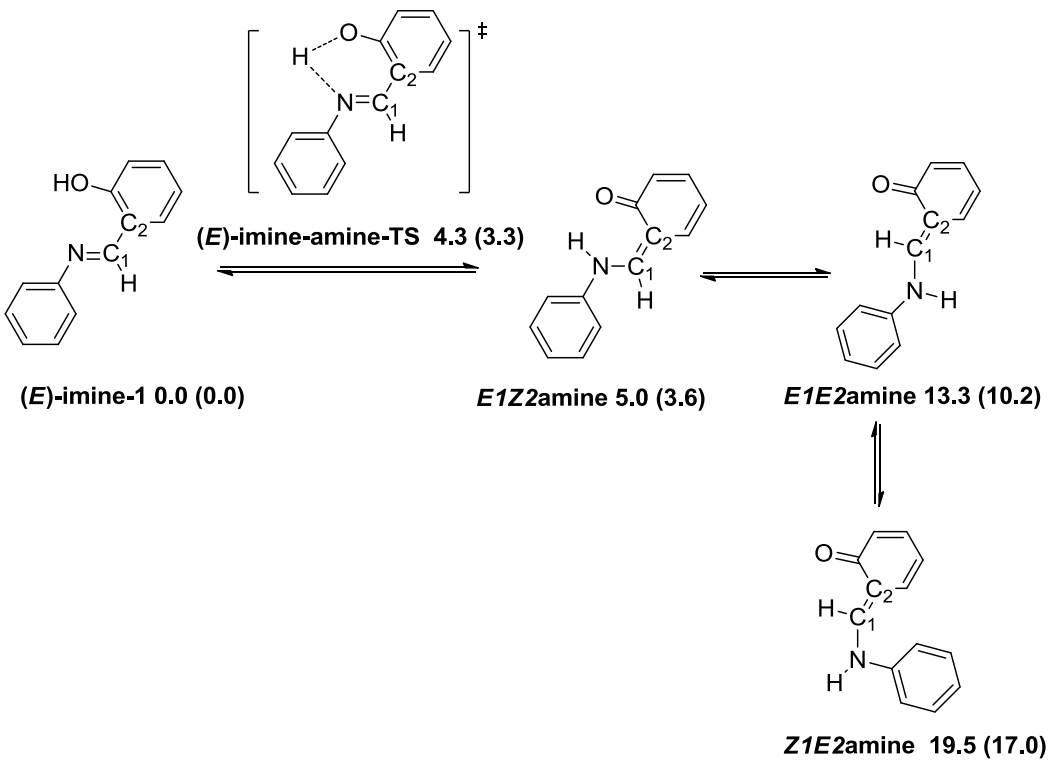

Scheme 4.7 The transformation from imine to amine. Geometry optimization at the B3LYP/6-31G(d,p) level, single-point energy in toluene (dichloroethane) solution at the M06-2X/6-31+G(d,p).

As we will see below, these amines participate in the energy profile, as they allow the placement of four electrons in the diene π system. To label their isomeric forms we take

into account the arrangement around the N-C1 and C1-C2 bonds (see labels in **Scheme 4.7**). The N-C1 bond, formally single, conserves some double bond character, and the substituents can be distributed around it on *Z* or *E* arrangements. These same arrangements also exist for the C1-C2 bond, already formally a double bond. There exist thus four isomers of this amine: *E1Z2*, *E1E2*, *Z1E2*, *Z1Z2*. The first three of them will be considered in the calculations that follow. Their relative energies with respect to (*E*)-imine-1 are 5.0, 13.3 and 19.5 kcal.mol^{-1} in toluene, respectively. The *Z1Z2* isomer was not considered because the steric strain increases too much the energy.

4.5 The reaction with the (*S*)-BINOL-derived phosphoric acid catalyst (Fochi system)

4.5.1 Overall reaction pathway

There is little mechanistic information available on this [4+2] cyclization. The most remarkable proposal is that put forward by Rueping and Lin, and shown in **Scheme 4.8**.[9] The assumption is that an iminium intermediate is formed by protonation from the phosphoric acid, but it is unclear how the cycloaddition can take place as the four π electrons in the diene part cannot be easily identified.

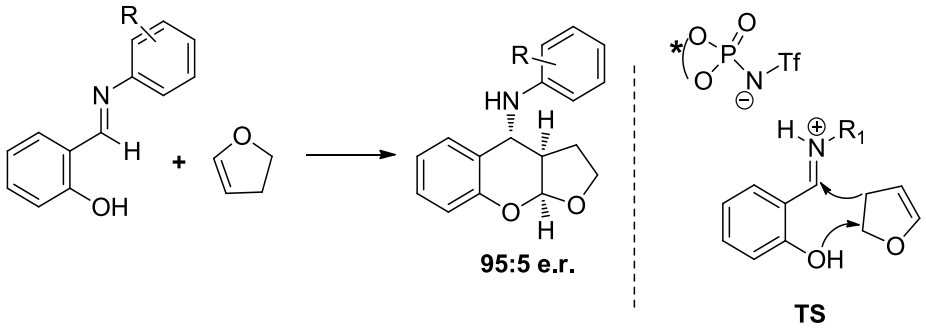

Scheme 4.8 Mechanistic proposal for the reaction of [4+2] cyclization of *o*-hydroxybenzaldimines with DHF catalyzed by chiral N-triflylphosphoramide suggested by Rueping group.[9]

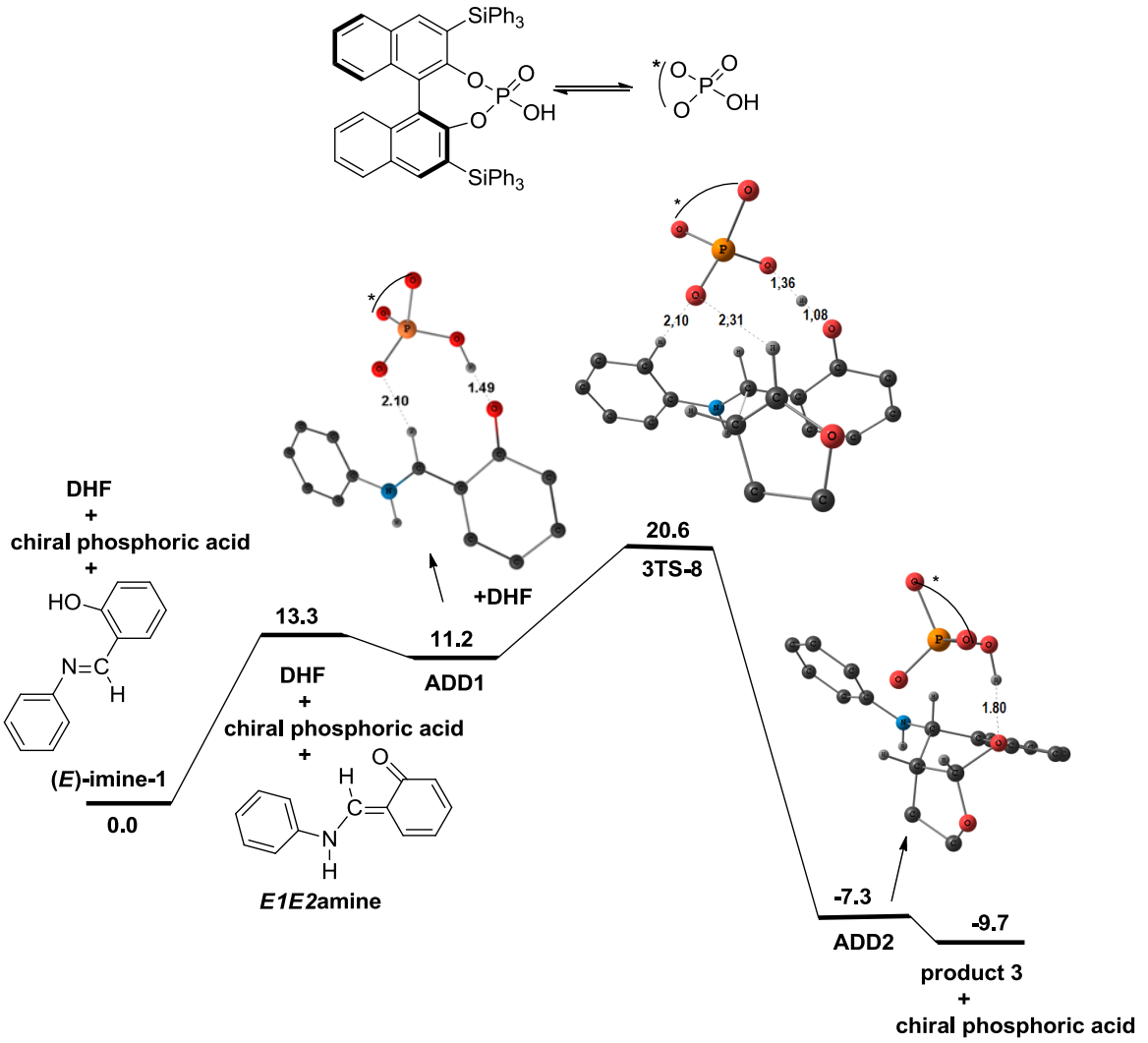

Figure 4.1 Computed free energy profile of the [4+2] cyclization of *o*-hydroxybenzaldimine with 2,3-dihydro-2H-furan(DHF) catalyzed by (*S*)-BINOL-derived phosphoric acid. Free energies in toluene relative to the reactants in kcal.mol^{-1}. Selected distances are given in Å.

We carried out an initial calculation on the system which produced the free energy profile presented in **Figure 4.1**. First the initial imine is transformed into an amine through relocation of a hydrogen atom. This has a modest energy cost of 13.3 kcal.mol^{-1}. After, the phosphoric acid binds to the amine through a strong hydrogen bond (POH-O being 1.49 Å), resulting in adduct **ADD1**. In the next step, dehydrofuran (DHF) attacks the amine *via* a transition state with a barrier of 20.6 kcal.mol^{-1} in free energy. In this transition state, the new C-C and C-O bonds are made. The resulting adduct **ADD2** releases the product and

the catalyst with a modest free energy gain of 2.4 kcal.mol^{-1}. The overall energy barrier just above 20 kcal.mol^{-1} is consistent with the experimental results of the reaction occurring at room temperature. The overall exergonicity of 9.7 kcal.mol^{-1} is also consistent with experimental result. It is worth noticing that the transition state is an ionic pair, with full transfer of the phosphoric acid proton to the reacting system, and that there is one single hydrogen bond between the catalyst and the system in this transition state. There are of course many isomeric forms of this transition state possible, which will lead to different diastereomers and enantiomers of the product. The following sections will present our search of these structures.

4.5.2 A preliminary classification of the transition states

We used a systematic approach to search the transition states. It is easier to understand the results by outlining first a classification of these transition state structures. We will use for this the isomeric forms of the amine intermediates that lead to them, that have been discussed above and shown in **Scheme 4.7**. There are three families of transition states, each of them connected to one of the amine isomers. They are shown in **Scheme 4.9**.

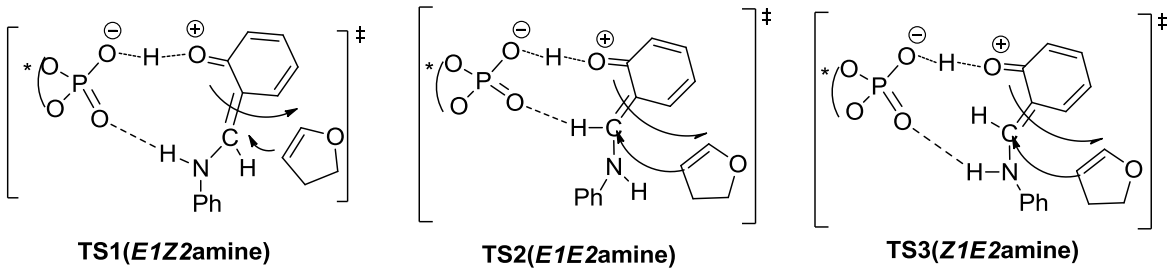

Scheme 4.9 Each isomer of the amine intermediate gives rise to a family of transition states

In the *E1Z2*amine family, the P=O and the P-O-H groups of the catalyst are oriented to form two hydrogen bonds with the NH bond and the C=O groups of the amine, resulting in a ten-membered hydrogen bonded ring. At the same time, the C=C double bond of the DHF attacks the amine to form the pyran ring. In the *E1E2*amine family, there is a clear possibility of hydrogen bond between the P-O-H group of the catalyst and the C=O group

of the amine, but the P=O group of the catalyst can only interact with a CH bond. If this latter bond could be considered a hydrogen bond, there would be a nine-membered ring. In the *Z1E2* family, the P=O and P-O-H groups of catalyst are in principle well arranged to form two hydrogen bonds with the NH bond and the C=O group of amine, and a ten-membered ring may be formed.

4.5.3 Transition states leading to product 3 and its enantiomer 3´

Figure 4.2 shows a schematic presentation of eleven of the lower energy transition states leading to product **3**. Seven of them correspond to the *E1Z2*amine family, three from the *E1E2*amine family, and one from the *Z1E2*amine family. The most stable transition state from the *E1Z2*amine family is **3TS-1**. It contains a ten-membered ring involving two hydrogen bonds. There is a clear hydrogen bond between the P-OH group and the C=O group of the amine, involving in fact hydrogen transfer, with PO-H being 1.36 Å and CO-H being 1.09 Å, respectively. Another hydrogen bond between the P=O group and the NH bond of amine seems weak only bond is also observable with a O…H distance of 1.69 Å. The transition states from the *E1Z2*amine family have in any case a minor role in the reaction, as they have energies more than 7.3 kcal.mol^{-1} above those of the most stable transition state, that comes from family *E1E2*amine. This is **3TS-8**. In **3TS-8**, the P-OH group forms a strong hydrogen bond with the C=O group of the amine (PO-H 1.36 Å, CO-H 1.08 Å). This is however the only strong hydrogen bond in this structure. The P=O group has only weak long distance interactions with the CH bond of the DHF and the phenyl CH bond of the amine. Simultaneously, the C=C bond of DHF attacks the amine to form a pyran ring. The eleven-membered hydrogen bonded ring that could be associated to family *E1E2*amine is therefore also absent. For family *Z1E2*amine, we only show the most stable geometry **3TS-11**. There are in this case two hydrogen bonds, but they seem to be quite weak according to the distances. The P=O group forms a hydrogen bond with the NH bond of the amine, and the P-OH group forms a hydrogen bond with the C=O group of the amine. The energy of **3TS-11** is also much higher (9.3 kcal mol^{-1}) than that of **3TS-8**.

There are two remarkable results in the structures reported in **Figure 4.2**. The first of them is that the lowest energy transition sate **3TS-8** corresponds to the *E1E2*amine family. This is remarkable because this transition state derives from amine *E1E2*, which was 8.3

kcal.mol^{-1} in toluene above amine *E1Z2* (see **Scheme 4.7**). The preference for the *E1E2*amine family in the transition state is moreover not minor, with the lowest energy transition state (**3TS-1)** from family *E1Z2*amine 7.3 kcal.mol^{-1} above **3TS-8**. There is therefore a very heavy advantage in this transition state that is able to overcome the inferior stability of the corresponding amine. The second remarkable aspect in **Figure 4.2** is that the superior stability of **3TS-8** is not associated to its hydrogen bond network. There is only one hydrogen bond in the structure, while **3TS-1** has two. Moreover, it seems clear from the reported geometrical parameters that hydrogen bonds in **3TS-1** are stronger. The reasons for the superior stability of **3TS-8** are associated to dispersion type interactions between the catalyst and the substrate, and they will be analyzed in detail later on.

Figure 4.3 shows a schematic presentation of nine of the lower energy transition states leading to product **3´**. Five of them correspond to the *E1Z2* family, three to the *E1E2* family, and one to the *Z1E2*amine family. The most stable transition state from the *E1Z2*amine family is **3´TS-1**. It contains a ten-membered ring including two hydrogen bonds. There is a clear hydrogen bond between the P-OH group and the C=O group of the amine, involving in fact hydrogen transfer, with PO-H being 1.36 Å and CO-H being 1.08 Å, respectively. Another hydrogen bond between P=O group and NH bond of amine has a O-H distance of 1.85 Å. The transition states from the *E1Z2*amine family have a minor role in the reaction, as they have energies more than 3.3 kcal.mol^{-1} above those of the most stable transition state **3´TS-6**, that comes from family *E1E2*amine. In **3´TS-6**, the P-OH group forms a strong hydrogen bond with the C=O group of the amine (PO-H, 1.49 Å; CO-H 1.04 Å). This is however the only strong hydrogen bond in this structure. The P=O group has only weak long distance interactions with the CH bond of the DHF. For the *Z1E2*amine family, we only show the most stable geometry **3´TS-9**. There are in this case two hydrogen bonds: the P=O group forms a hydrogen bond with the NH bond of the amine, and the P-OH group forms a hydrogen bond with the C=O group of the amine. The energy of **3´TS-9** is also much higher (6.7 kcal mol^{-1}) than that of **3´TS-6**.

Transition states leading to product **3** (in **Figure 4.2**) are systematically lower in energy than those leading to its enantiomer **3´** (in **Figure 4.3**). There are however similarities between the two sets of transition states. The most stable structures are in family *E1E2*amine, followed by family *E1Z2*amine, with the *Z1E2* amine family having the highest energies. This energy ordering in the transition states is remarkable because it is contrary to the relative stabilities of the corresponding amines. Amine *E1E2* is 8.3

kcal.mol^{-1} above amine *E1Z2* in toluene solution (see **Scheme 4.7**). This means that the interaction between substrate and catalyst is much favorable in family *E1E2*amine.

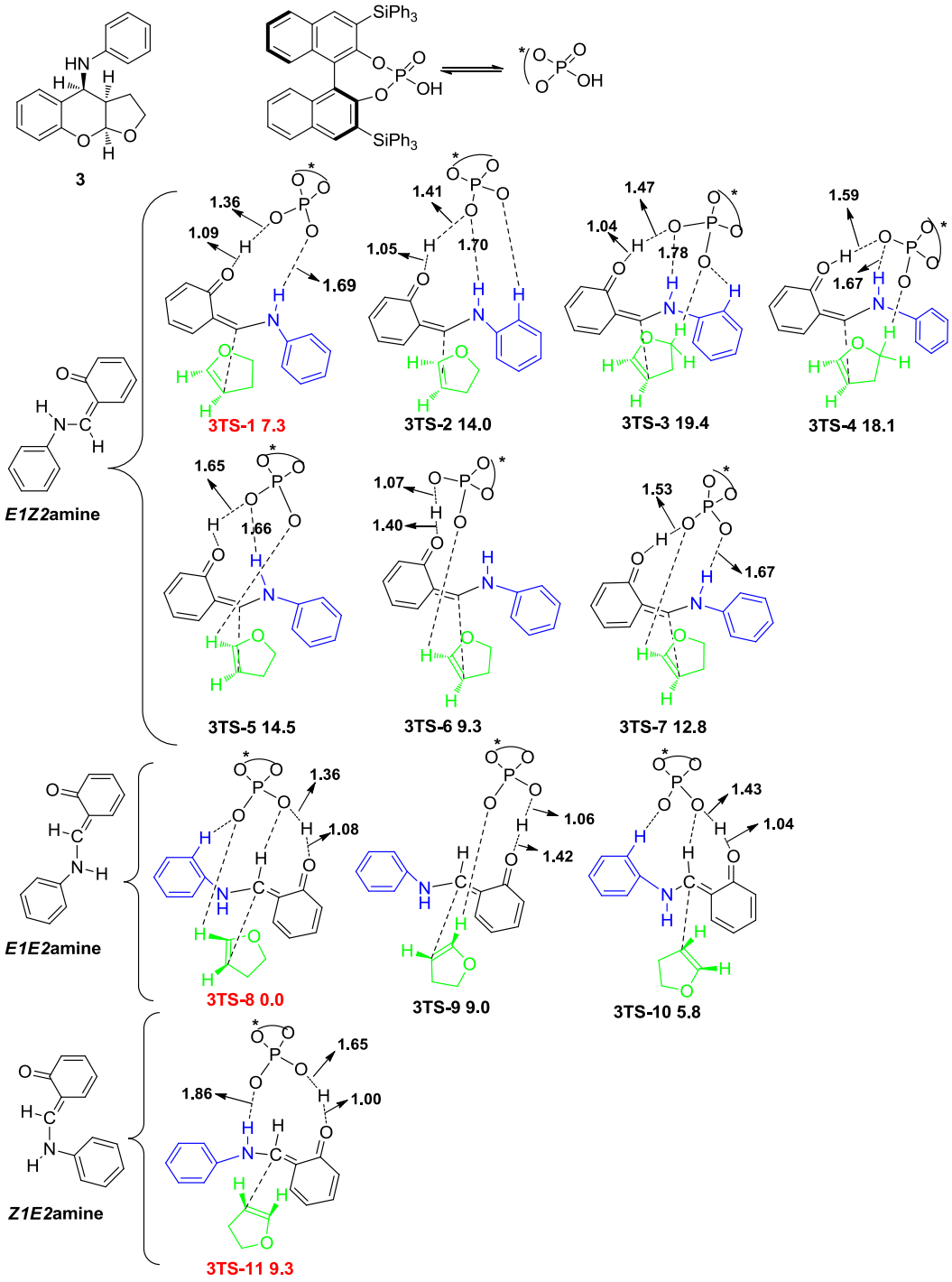

Figure 4.2 Main geometries of transition state for product **3** with the Fochi catalyst. Relative free energies (kcal.mol^{-1}) in toluene based on the most stable geometry **3TS-8**. Selected distances are given in Å.

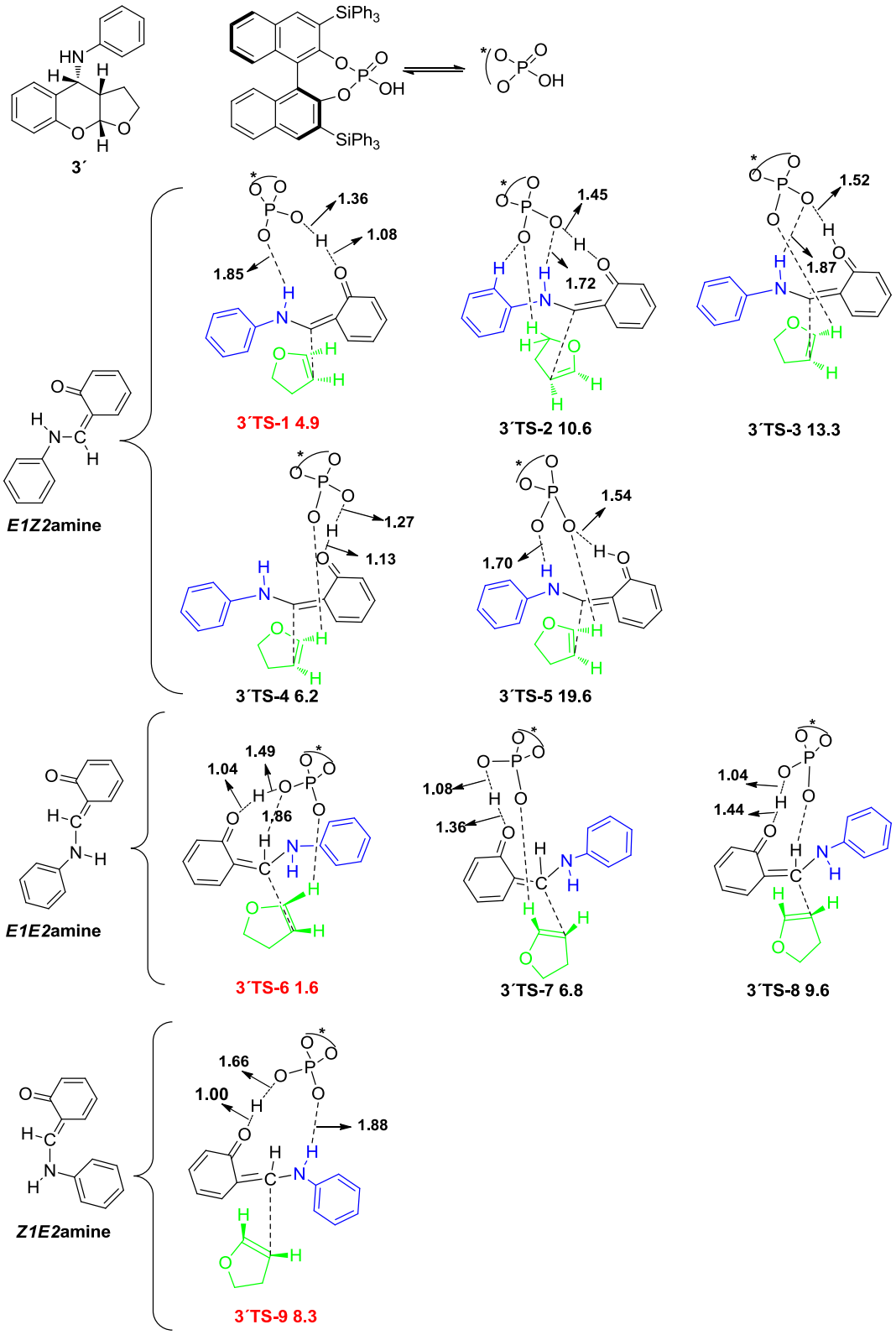

Figure 4.3 Main transition states leading to product **3´** with the Fochi catalyst. Relative free energies (kcal.mol^{-1}) in toluene based on the most stable geometry **3TS-8**. Selected distances are given in Å

4.5.4 Transition states leading to product 4 and its enantiomer 4´

Figure 4.4 shows a schematic presentation of nine of the lower energy transition states leading to product **4´**. Five of them correspond to the *E1Z2*amine family, three from the *E1E2*amine family, and one from the *Z1E2*amine family. The most stable transition state from the *E1Z2*amine family is **4´TS-1**. It contains a ten-membered ring including two hydrogen bonds. One hydrogen bond is the interaction between the P-OH group and the C=O group of the amine, involving in fact hydrogen transfer, with PO-H being 1.43 Å and CO-H being 1.06 Å, respectively. Another hydrogen bond is the interaction between a P=O group and the NH bond of amine, the O-H distance being 1.61 Å. The most stable transition state from the *E1E2*amine family is **4´TS-6**. There is only one strong hydrogen bond in this structure. The P-OH group forms a hydrogen bond with the C=O group of the amine (PO-H, 1.34 Å; CO-H 1.09 Å). The P=O group has only weak long distance interactions with the CH bonds of the DHF. The transition states from the *E1E2*amine family have a minor role in the reaction, as they have energies more than 6.6 kcal.mol^{-1} above those of the most stable transition state **4´TS-1**. For family *Z1E2*amine, we only show the most stable geometry **4´TS-9**. There are in this case two hydrogen bonds. The energy of **4´TS-9** is much higher (11.7 kcal mol^{-1}) than that of **4´TS-1**.

Figure 4.5 shows a schematic presentation of nine of the lower energy transition states leading to product **4**. Five of them correspond to the *E1Z2*amine family, three from the *E1E2*amine family, and one from the *Z1E2*amine family. The most stable transition state from the *E1Z2*amine family is **4TS-1**. It contains a ten-membered ring structure including two hydrogen bonds. One hydrogen bond is the interaction between the P-OH group and the C=O group of the amine, involving in fact hydrogen transfer, with PO-H being 1.41 Å and CO-H being 1.06 Å, respectively. Another hydrogen bond is the interaction between P=O group and NH bond of amine, the PO-H distance being 1.80 Å. The most stable transition state from the *E1E2*amine family is **4TS-6**. There is only one hydrogen bond in this structure, that between the P-OH group in the catalyst and a C=O group in the amine (PO-H, 1.32 Å; CO-H 1.10 Å). The P=O group has only weak long distance interactions with the CH bond of the DHF. The transition states from the *E1E2*amine family have a minor role in the reaction, as they have energies more than 7.0 kcal.mol^{-1} above those of the most stable transition state **4TS-1**. For family *Z1E2*amine, we only show the most stable geometry **4TS-9**. There are in this case two hydrogen bonds. The relative energy of

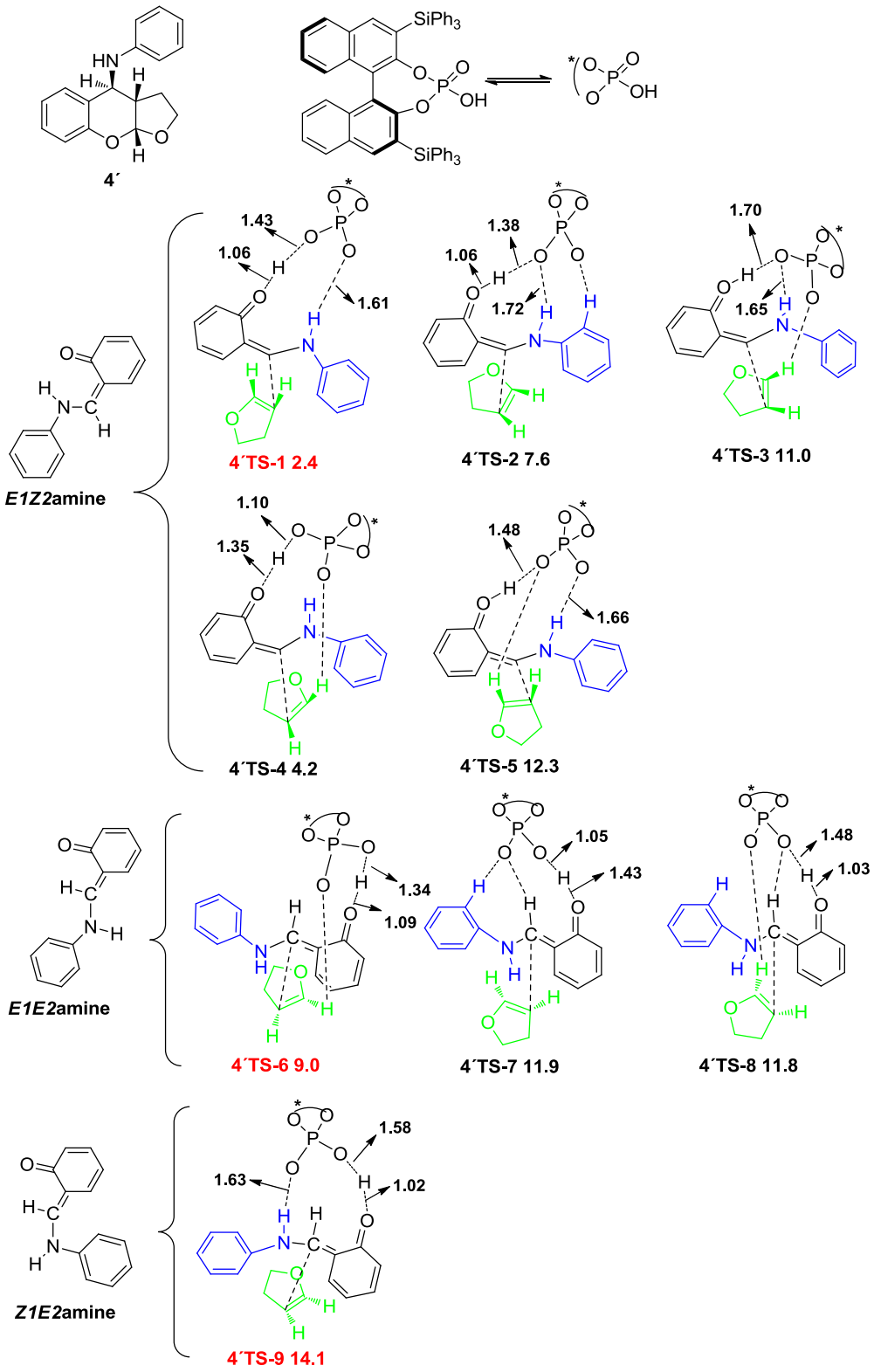

Figure 4.4 Main transition states leading to product **4´** with the Fochi catalyst. Relative free energies (kcal.mol^{-1}) in toluene based on the most stable geometry **3TS-8**. Selected distances are given in Å

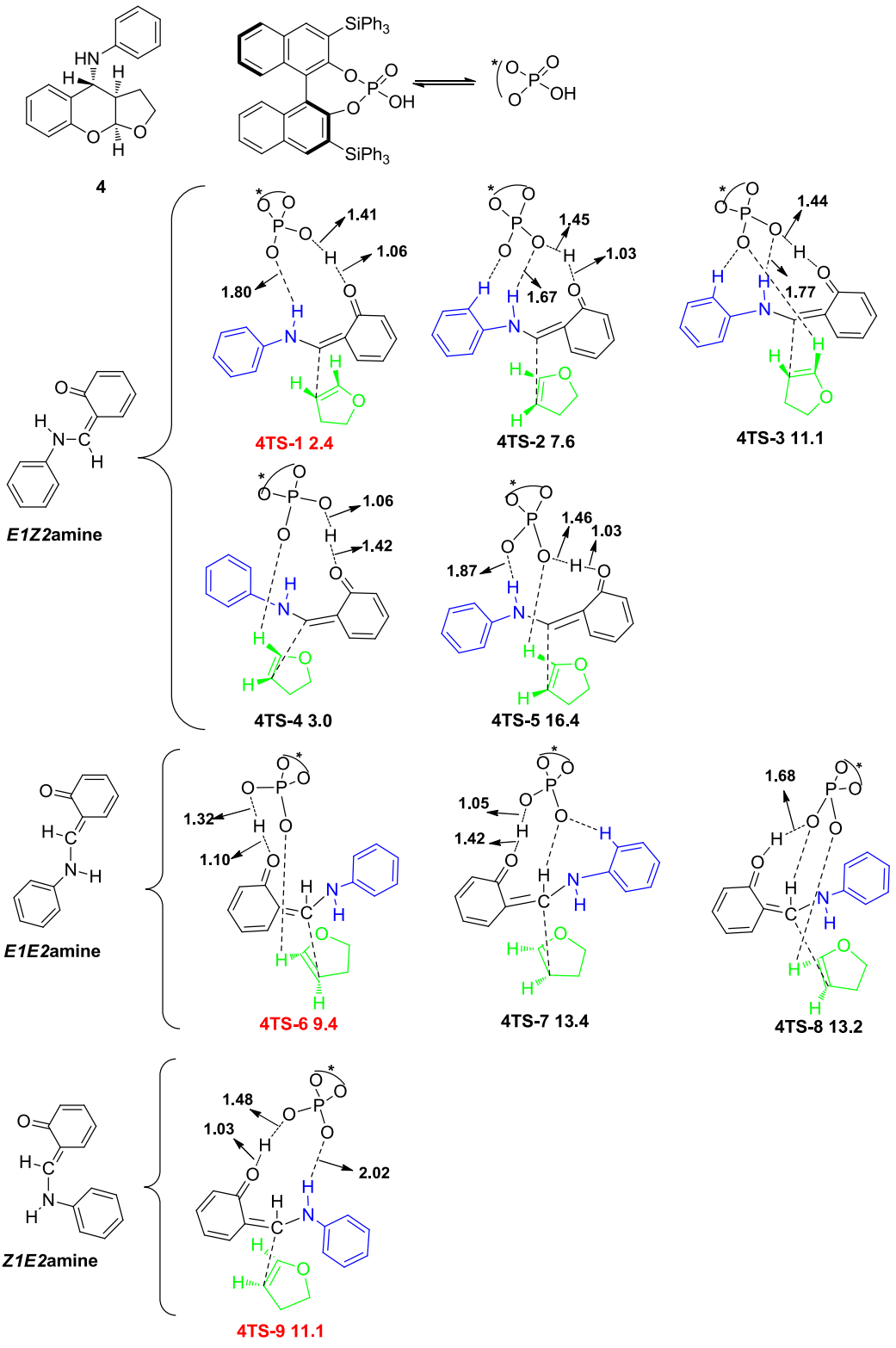

Figure 4.5 Main transition states leading to product **4** with the Fochi catalyst. Relative free energies (kcal.mol^{-1}) in toluene based on the most stable geometry **3TS-8**. Selected distances are given in Å

4TS-9 is even higher (8.7 kcal mol^{-1}).

Transition states leading to **4** have a lower energy than those going to **4´**. There is in any case a shared pattern between both sets, as the more stable transition states come always from the *E1Z2*amine family. Remarkably, this is not happened for transition states leading to **3** and **3´**, which have been discussed in the previous section, where the *E1E2*amine family was systematically preferred. There is thus a different balance between hydrogen bonds and π–π interactions in the different sets of transition states.

4.5.5 The origin of selectivity in the Fochi system

In this section, we will compare the structures and energies of the most stable transition states leading to each of the four products, as their relative stabilities are the key to the reaction selectivity. These transition states are **3TS-8**, **3´TS-6**, **4´TS-1** and **4TS-1** (**Figure 4.6**). Their relative energies are 0.0, 1.6, 2.4 and 2.4 kcal.mol^{-1} respect to **3TS-8**. These energy differences correspond to an enantiomeric excess of 87% and a diastereomeric excess of 97% in favour of product **3**. The experimental results show an er value of 83:17 (ee value of 66%) and only one diastereoisomer was detected (de 100%), see **Scheme 4.3**. The agreement between the experimental ee and de values and the computational ones is thus quite reasonable.

Figure 4.6 presents the four key transition states in this reaction. From inspection of these geometries, it is clear that the key to selectivity is not in the hydrogen-bond networks. **3TS-8** and **3´TS-6** have only one hydrogen bond, albeit strong, while **4´TS-1** and **4TS-1** have two. Although the hydrogen bond is weaker in **3TS-8**, **3TS-8** is the lowest energy transition state in the Fochi system.

Since the key to selectivity is not in the hydrogen bonds, we decided to examine other geometrical features. Two important sources of non-covalent interactions are the π–π and the CH–π interactions. The hydroxybenzaldimine substrate has two aromatic rings, and the furan is also a mostly planar ring. The rings in the substrates are thus able to interact with the phenyl rings in the two triphenylsilyl substituents of the catalyst. It is not simple to fully characterize these interactions from a structural view, as they depend on the distance between the rings, their relative orientations and their degree of overlap. However, a first impression of their importance can be obtained by tabulating the shortest distances

between the rings in the substrates and those in the catalyst.

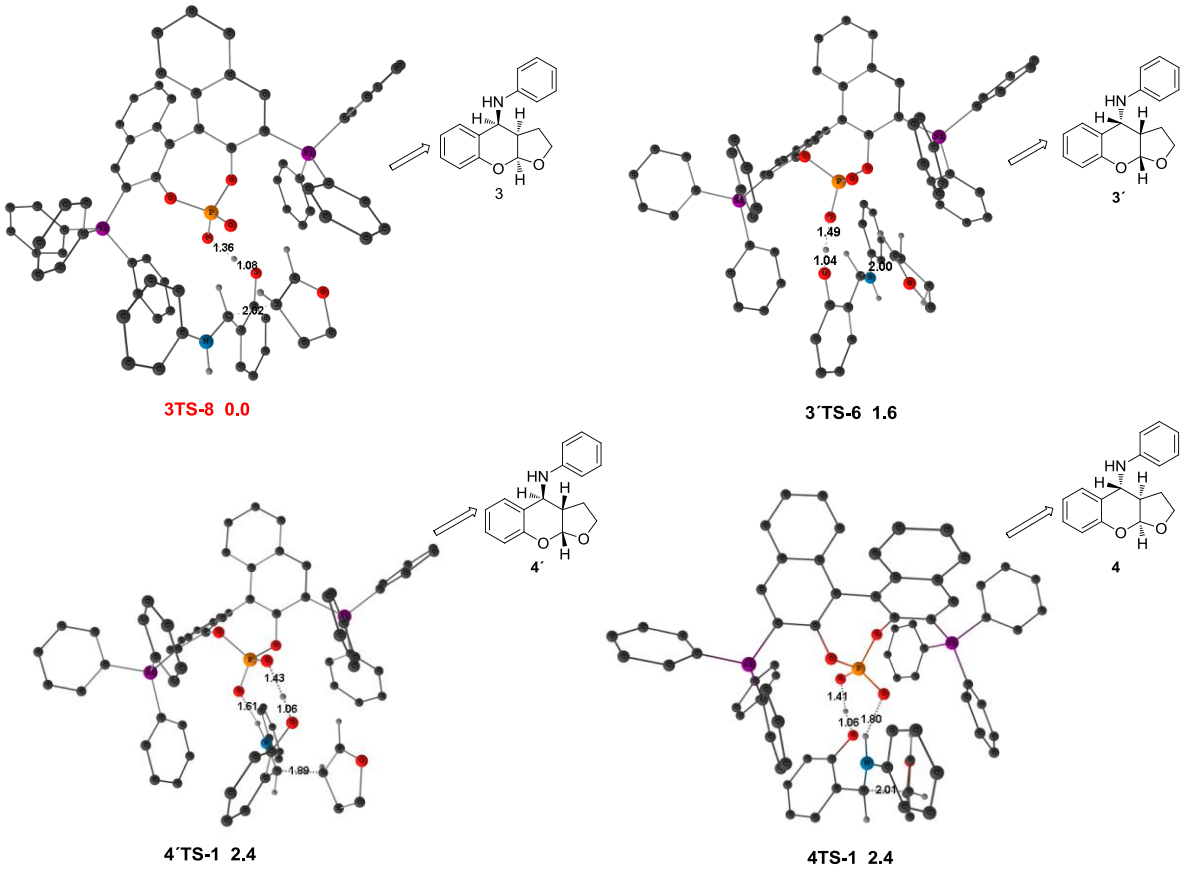

Figure 4.6 Structure of the most stable transition state leading to each of the four possible products. Relative free energies in toluene (kcal.mol^{-1}) are based on the most stable geometry **3TS-8**. Selected distances are given in Å.

Table 4.1 Shortest ring-ring distances (Å) for the key transition states in the reaction with the Fochi system. Relative energies are also provided in kcal.mol^{-1}

	3TS-8	**3'TS-6**	**4'TS-1**	**4TS-1**
ΔG	0.0	1.6	2.4	2.4
N-ring	3.44	3.52	3.49	3.44
O-ring	3.35	3.51	3.70	3.56
Furan	3.50	3.29	3.64	3.50

We have collected in **Table 4.1** the shortest ring-ring contacts between substrates and catalyst. Hydroxybenzaldimine has two aromatic rings (see for instance compound **1** in **Scheme 4.3**). We label the one that is directly bound to nitrogen as N-ring, and the one that contains the hydroxyl group that is afterwards deprotonated as O-ring. We have measured the shortest C-C distance between each of these two rings and the phenyl rings of the substrate. We have also repeated the operation for furan, which is the other reactant. All C-C values collected in **Table 4.1** are between 3 and 4 Å. This may seem long but it is in agreement with the optimal distance obtained from high level calculations on the benzene dimer,[19] which is 3.9 Å for the sandwich configuration, leading to an attractive interaction energy of 1.8 kcal.mol^{-1}. The structural features are also in agreement with the empirical observation[20] of distances in the range 3.3-3.6 Å between aromatic rings in crystal structures. The main interactions are depicted in **Figures 4.7** and **4.8**, where the interacting phenyl rings in the catalyst have been highlighted.

A structural pattern can be recognized which agrees with the energy order of the transition states. The shortest distances between the aromatic rings of hydroxybenzaldimine (N-ring and O-ring) and the substrate correspond to **3TS-8**, which has the lowest energy. The distance associated to the furan ring is larger, but interactions with this non-aromatic ring should be weaker. The analysis of the data for the other three transition states is more complicated, but their energies are in a small range of 0.8 kcal.mol^{-1}.

We conclude thus that the preferred formation of compound **3** is associated to the presence more favorable π–π interactions in the corresponding transition state. The selectivity is thus ruled in this case by the attractive interactions between catalyst and substrate.

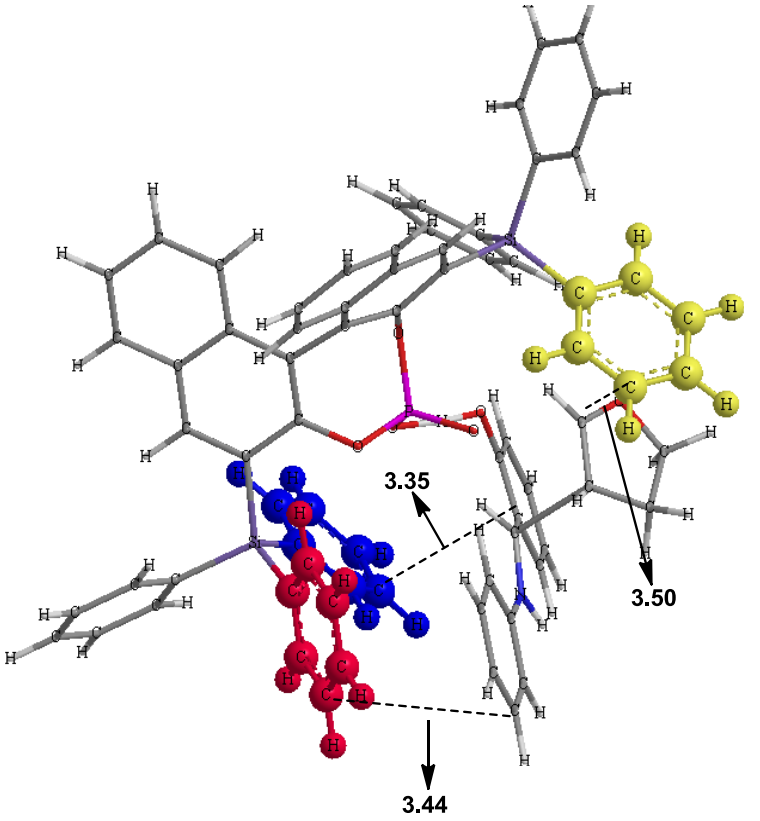

3TS-8

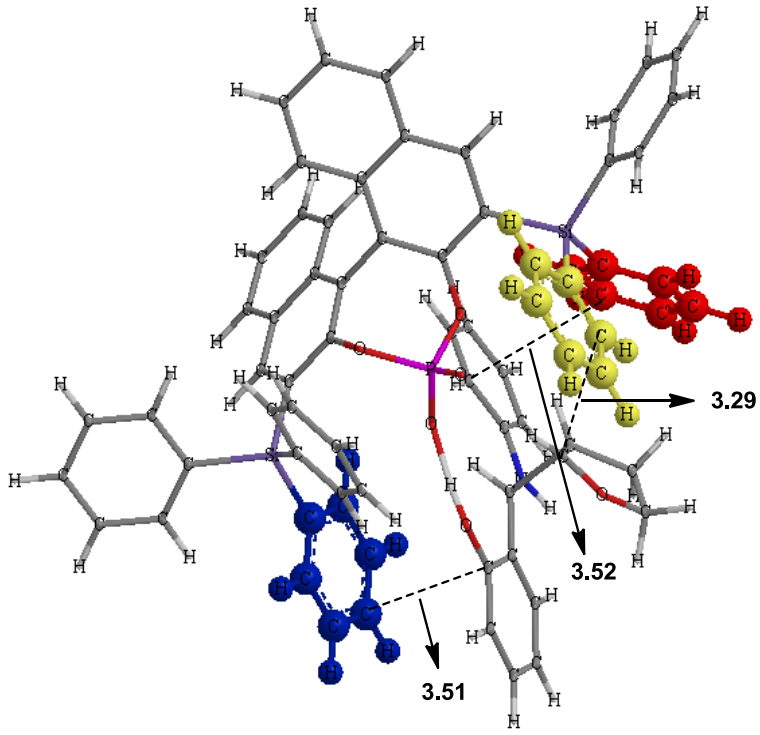

3´TS-6

Figure 4.7 The views of **3TS-8 and 3´TS-6.** Selected distances are given in Å.

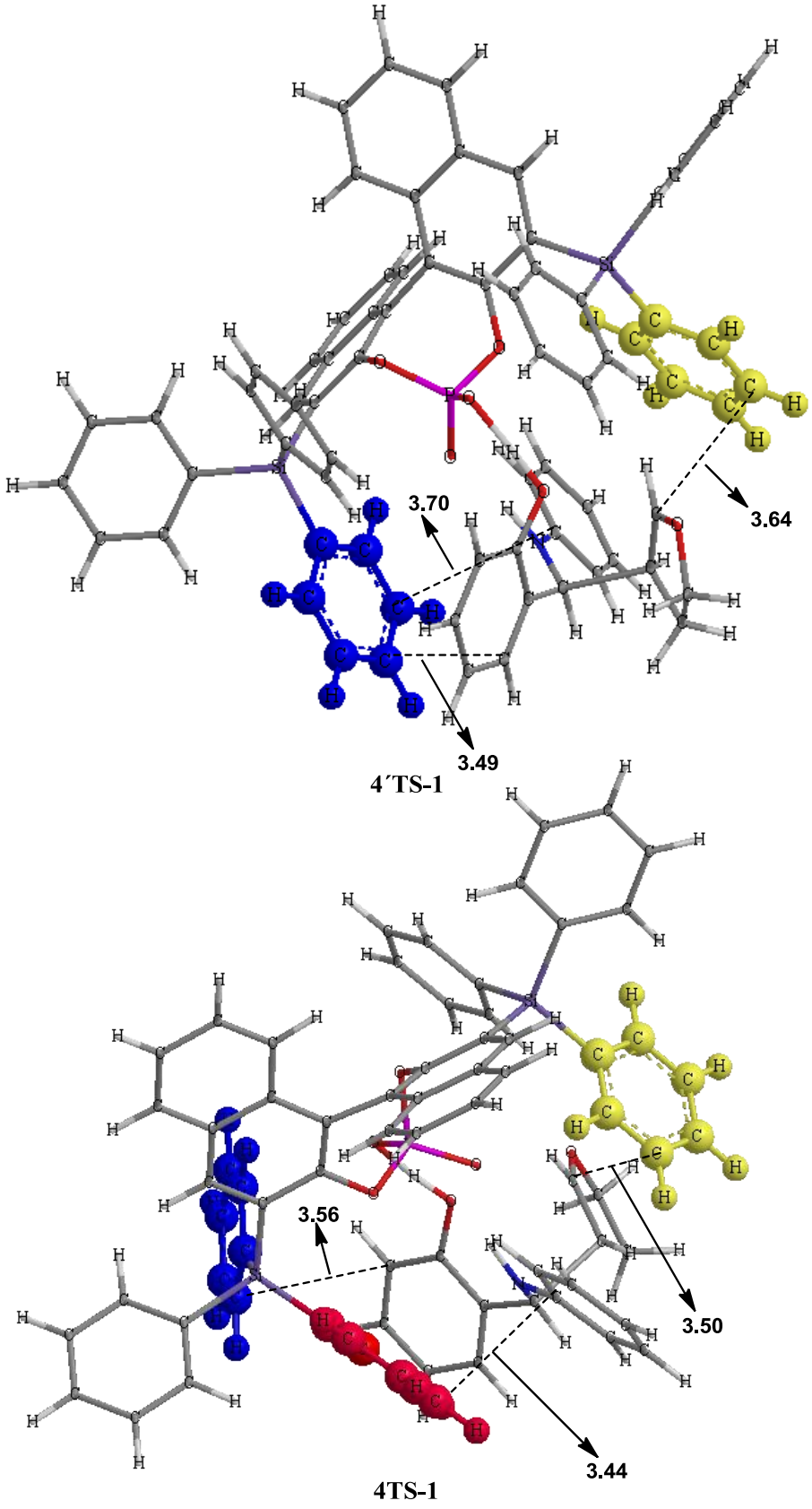

Figure 4.8 The views of **4´TS-1 and 4TS-1.** Selected distances are given in Å.

4.6 The reaction with the (*S*)-BINOL-derived catalyst N-triflylphosphoramide (Rueping system)

4.6.1 Overall reaction pathway

We carried out an initial calculation on the system which produced the free energy profile in **Figure 4.9**. It is similar to that described above for the Fochi system. First the initial imine is transformed into an amine through relocation of a hydrogen atom, with a modest energy cost of 3.6 kcal.mol^{-1}. After, NH bond of the catalyst binds to the amine through a strong hydrogen bond (NTfH-O being 1.59 Å), resulting in adduct **ADD1new**. In the next step, dehydrofuran (DHF) attacks the amine *via* a transition state with a barrier of 12.1 kcal.mol^{-1} in free energy. In this transition state, the new C-C and C-O bonds are made. The resulting adduct **ADD2new** releases the product and the catalyst with a modest free energy gain of 7.1 kcal.mol^{-1}. The overall energy barrier just 12.1 kcal.mol^{-1} is consistent with the experimental results of the reaction occurring at -10^{0}C temperature. The overall exergonicity of 11.8 kcal.mol^{-1} is also consistent with experimental result. The transition state is an ionic pair, with full transfer N-triflylphosphoramide proton to the reacting system, and that there is one hydrogen bond between the catalyst and the system in this transition state. There are also many isomeric forms of this transition state possible, which will lead to different diastereomers and enantiomers of the product. The rest of this section will present our search of these structures for Rueping system, as well as the analysis of the most stable ones.

4.6.2 A preliminary classification of the transition states

We will use of the Rueping system the same labeling scheme defined above for the Fochi system. We will omit the calculation of the *Z1E2*amine family of transition states, because it always had the highest energy. Two families of transition states will thus be computed, those present in **Scheme 4.10**, *E1Z2*amine and *E1E2*amine. The only qualitative difference between the Fochi and Rueping systems is that in the latter one of the potential hydrogen bond donors is NTf-H. We will use the "new" label in the transition states for the Rueping

system to distinguish them from those in the Fochi system.

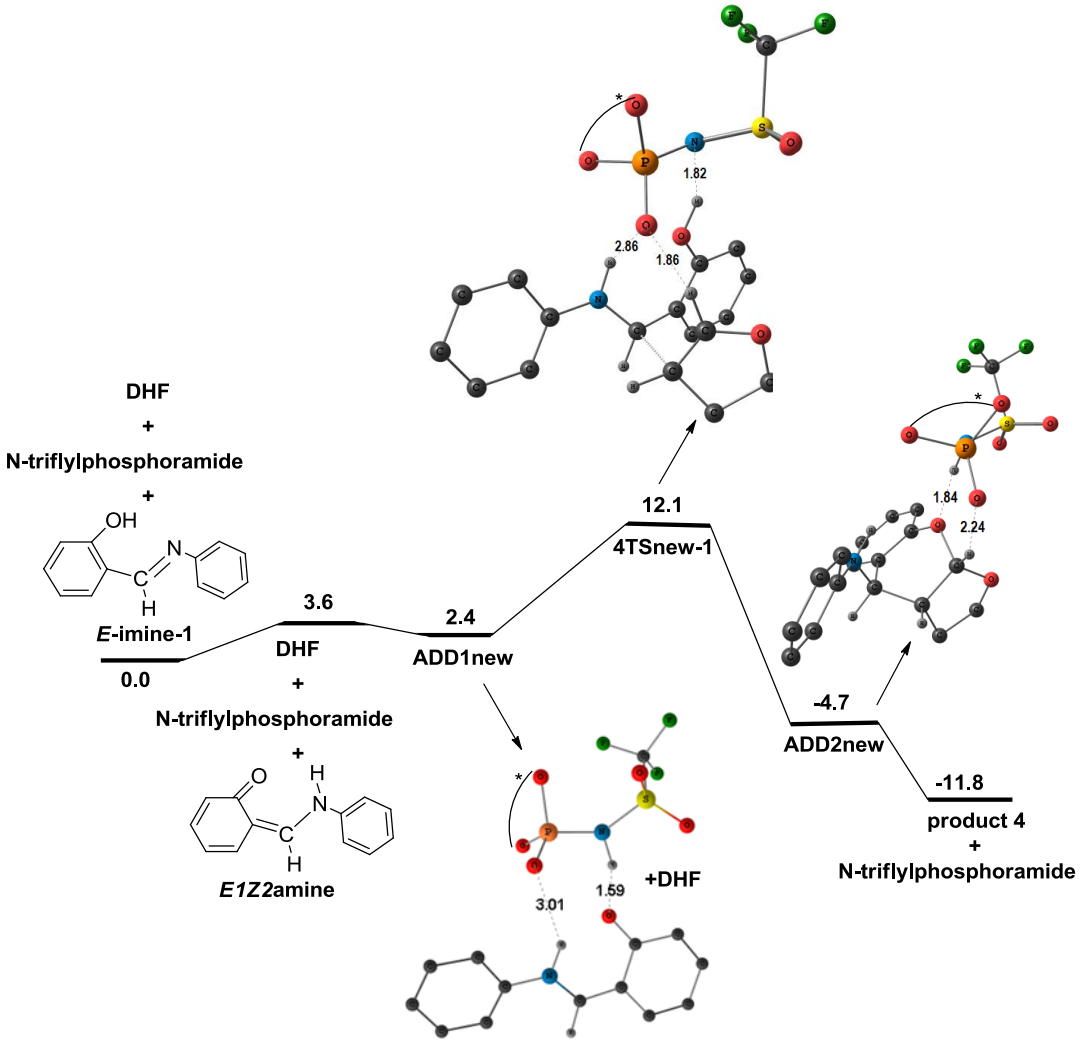

Figure 4.9 Computed free energy profile of the [4+2] cyclization of *o*-hydroxybenzaldimine with 2,3-dihydro-2H-furan(DHF) catalyzed by (*S*)-BINOL-derived N-triflylphosphoramide. Free energies in dichloroethane relative to the reactants in kcal.mol^{-1}. Selected distances are given in Å.

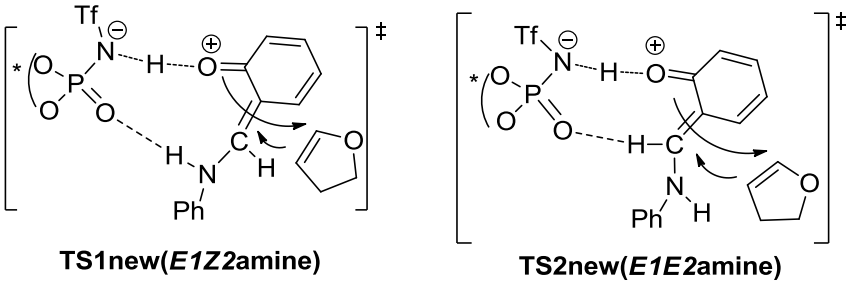

Scheme 4.10 Each isomer of the amine intermediate gives rise to a family of transition states.

4.6.3 Transition states leading to product 3 and its enantiomer 3´

Figure 4.10 shows a schematic presentation of seven of the lower energy transition states leading to product **3**. Four of them correspond to the *E1Z2*amine family, three to the *E1E2*amine family. The most stable transition state from the *E1Z2*amine family is **3TSnew-4**. It has only one hydrogen bond, that between the NTfH and C=O groups. This interaction involves in fact a hydrogen transfer, with NTf-H being 1.54 Å and CO-H being 1.04 Å, respectively. The P=O group has only weak long distance interactions with the CH bond of the DHF. Remarkably, **3TSnew-4** has an energy significantly lower (by 3.7 kcal.mol^{-1}) than **3TSnew-1**, which is in the same *E1E2*amine family but has two hydrogen bonds. **3TSnew-1** has an interaction between NTfH and C=O similar to that on **3TSnew-4**, and has besides a hydrogen bond between the P=O group in the catalyst and the NH bond of amine, the O-H distance being 1.95 Å. The most stable transition state from family *E1E2*amine, and the preferred one among those leading to product **3**, is **3TSnew-7**. In **3TSnew-7**, the NTfH group forms a single hydrogen bond with the C=O group of the amine (NTf-H 1.56 Å, CO-H 1.04 Å).

The relative energies reported in **Figure 4.10** are clear proof that hydrogen bonds are not the key to the stability of these transition states. The most stable transition state (relative energy of 0.8 kcal.mol^{-1}) is **3TSnew-7** with only one hydrogen bond. The most stable transition state in the *E1Z2*amine family, **3TSnew-4** (relative energy of 2.9 kcal.mol^{-1}) has also a single hydrogen bond. In contrast, the lowest energy transition state with two hydrogen bonds is **3TSnew-1**, also in family *E1Z2* amine, with an energy of 6.6 kcal.mol^{-1}. The reasons for the superior stability of **3TSnew-7** are associated to dispersion type interactions between the catalyst and the substrate, and they will be analyzed in detail in section **4.6.5**.

Figure 4.11 shows a schematic presentation of six of the lower energy transition states leading to product **3´**. Three of them correspond to the *E1Z2*amine family and three from the *E1E2*amine family. The most stable transition state from the *E1Z2*amine family is **3´TSnew-1**. There is a clear hydrogen bond between the NTf-H group and the C=O group of the amine, involving in fact hydrogen transfer, with NTf-H being 1.60 Å and CO-H being 1.02 Å, respectively. A potential hydrogen bond between P=O group and NH bond of amine is very weak, the O-H distance being 2.15 Å. The most stable transition state from the *E1E2*amine family is **3´TSnew-6**. In **3´TSnew-6**, the NTfH group forms a single

hydrogen bond with the C=O group of the amine (NTf-H, 1.56 Å; CO-H 1.03 Å). The P=O group has only weak long distance interactions with the CH bond of the DHF.

Transition states leading to product **3** are systematically lower in energy than those leading to product **3´**, but a same pattern is followed in the two sets. The *E1E2*amine family is always favored with respect to the *E1Z2*amine family.

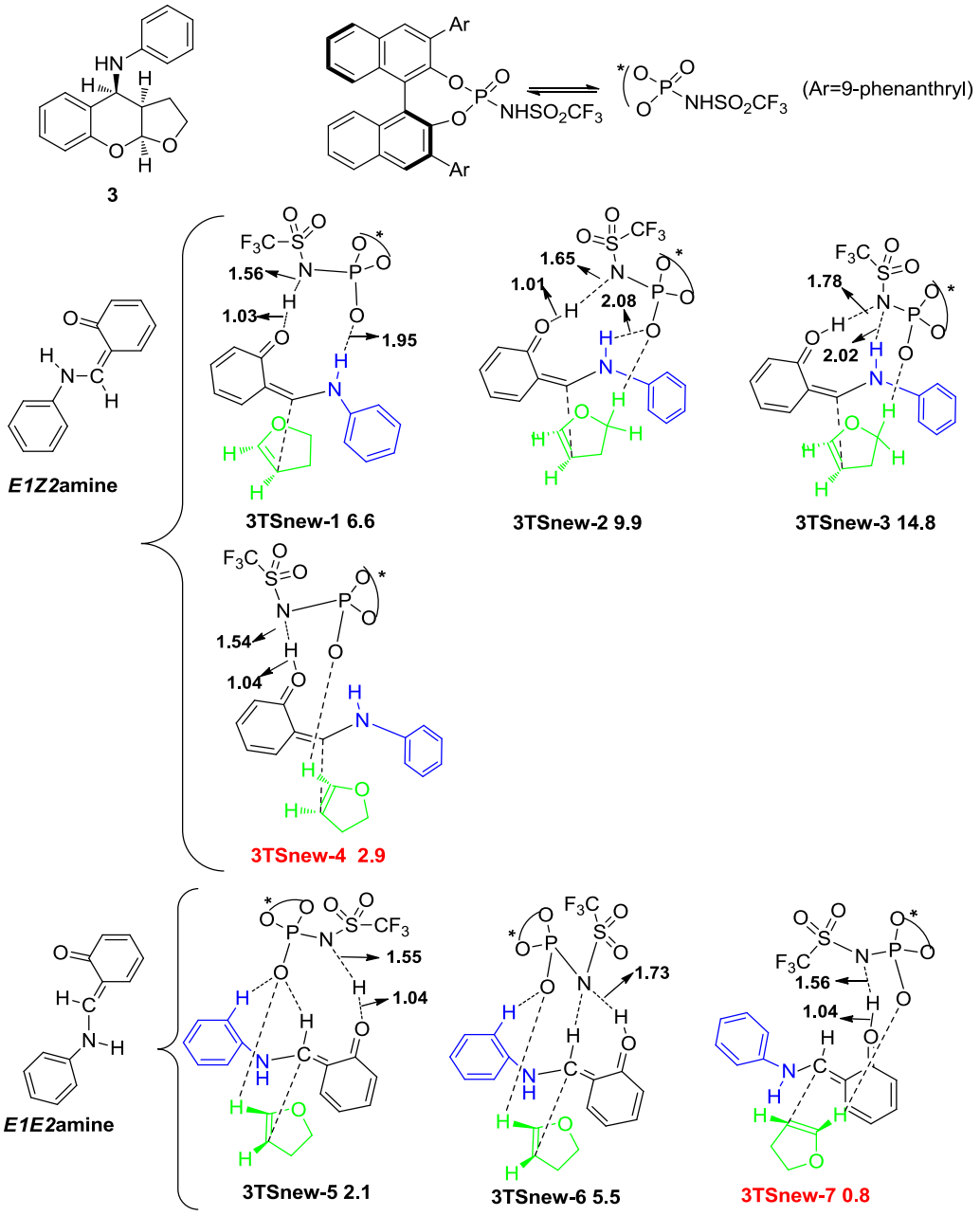

Figure 4.10 Main transition states leading to product **3** with the Rueping catalyst. Relative free energies (kcal.mol^{-1}) in dichloroethane based on the most stable geometry **4TSnew-1**. Selected distances are given in Å.

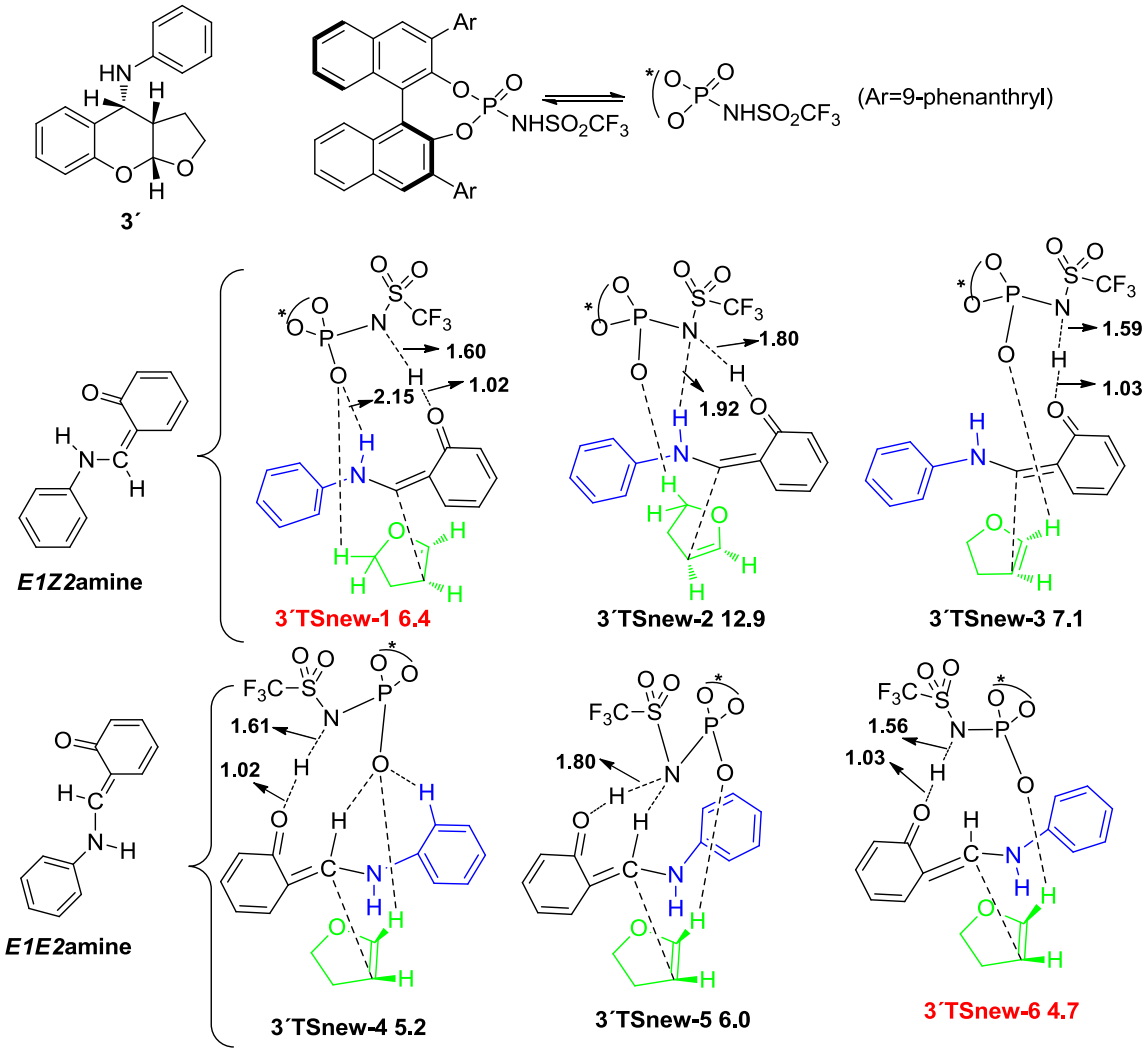

Figure 4.11 Main transition states leading to product **3´** with the Rueping catalyst. Relative free energies (kcal.mol^{-1}) in dichloroethane based on the most stable geometry **4TSnew-1**. Selected distances are given in Å.

4.6.4 Transition states leading to product 4 and its enantiomer 4´

Figure 4.12 shows a schematic presentation of seven of the lower energy transition states leading to product **4´**. Three of them correspond to the *E1Z2*amine family, and four from the *E1E2*amine family. The most stable transition state from the *E1Z2*amine family is **4´TSnew-3**. It has only one hydrogen bond, that between the NTfH group and the C=O group of the amine, involving in fact hydrogen transfer, with NTf-H being 1.55 Å and CO-H being 1.04 Å, respectively. The P=O group has only weak long distance interactions

with the CH bond of the DHF. **4´TSnew-1** contains a ten-membered ring including two hydrogen bonds but has a higher energy (5.0 *vs* 3.2 kcal.mol^{-1}). The most stable transition state from the *E1E2*amine family is **4´TSnew-7**. It has also only one strong hydrogen bond, that of the NTfH group with the C=O group of the amine (NTfH 1.60 Å, CO-H 1.03 Å). The P=O group has only weak long distance interactions with the CH bond of the DHF. The transition states from the *E1E2*amine family have a minor role in the reaction, as they have energies more than 3.3 kcal.mol^{-1} above those of the most stable transition state **4´TSnew-3**, that comes from the *E1Z2*amine family.

Figure 4.13 shows a schematic presentation of seven of the lower energy transition states leading to product **4**. Three of them correspond to the *E1Z2*amine family, and four to the *E1E2*amine family. The most stable transition state from the *E1Z2*amine family is **4TSnew-1**, which is also the transition state with the lowest energy of those involved in the Rueping system, thus leading to the major product. There is only one hydrogen bond in **4TSnew-1**, that between the NTfH group and the C=O group of the amine, involving a hydrogen transfer, with NTf-H being 1.82 Å and CO-H being 1.00 Å, respectively. The P=O group has very weak hydrogen bond with NH bond of amine being 2.86 Å.

The most stable transition state from the *E1E2*amine family is **4TSnew-7**. This structure has also only one hydrogen bond. The NTfH group connects with the C=O group of the amine (NTf-H 1.58 Å, CO-H 1.03 Å). The P=O group has only weak long distance interactions with the CH bond of the DHF. The transition states from the *E1E2*amine family have a minor role in the reaction, as they have energies more than 4.1 kcal.mol^{-1} above those of the most stable transition state **4TSnew-1**.

The joint analysis of the transition states leading to **4´** and **4** summarized in **Figures 4.12** and **4.13** shows a pattern where the lower energy structures come from the *E1Z2*amine family. This is in contrast to what happened for the transition states leading to **3** and **3´**, discussed in the section above, where the *E1E2*amine family was favored. The Rueping system shows thus an identical pattern to that of the Fochi system discussed above (section **4.5**) in terms of the family of transition states favored for each of the four products. The difference between both systems is of course in the relative energy of the transition states leading to **3** and **4**, and this will be discussed in section **4.7**.

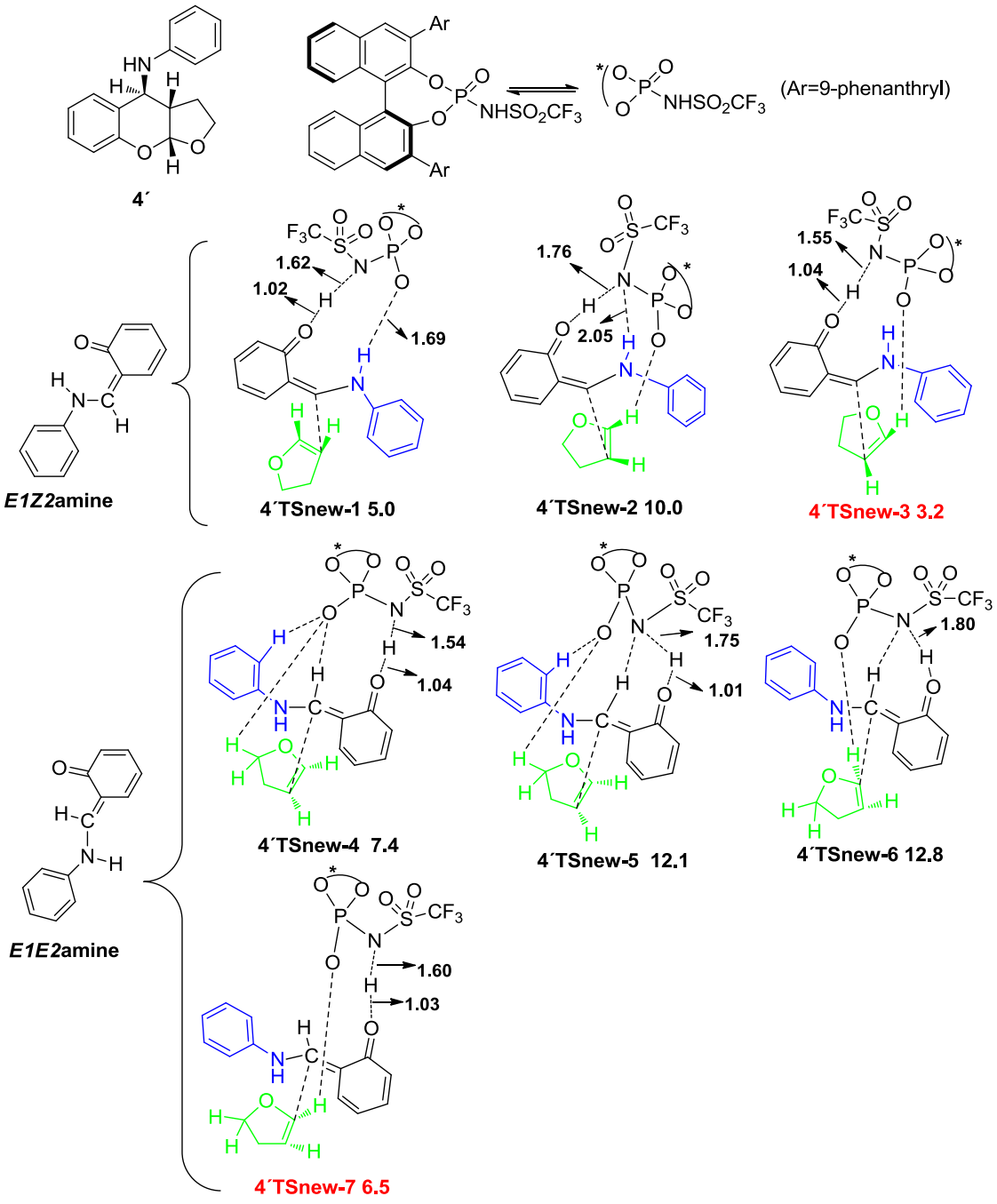

Figure 4.12 Main transition states leading to product **4´** with the Rueping catalyst. Relative free energies (kcal.mol^{-1}) in dichloroethane based on the most stable geometry **4TSnew-1**. Selected distances are given in Å.

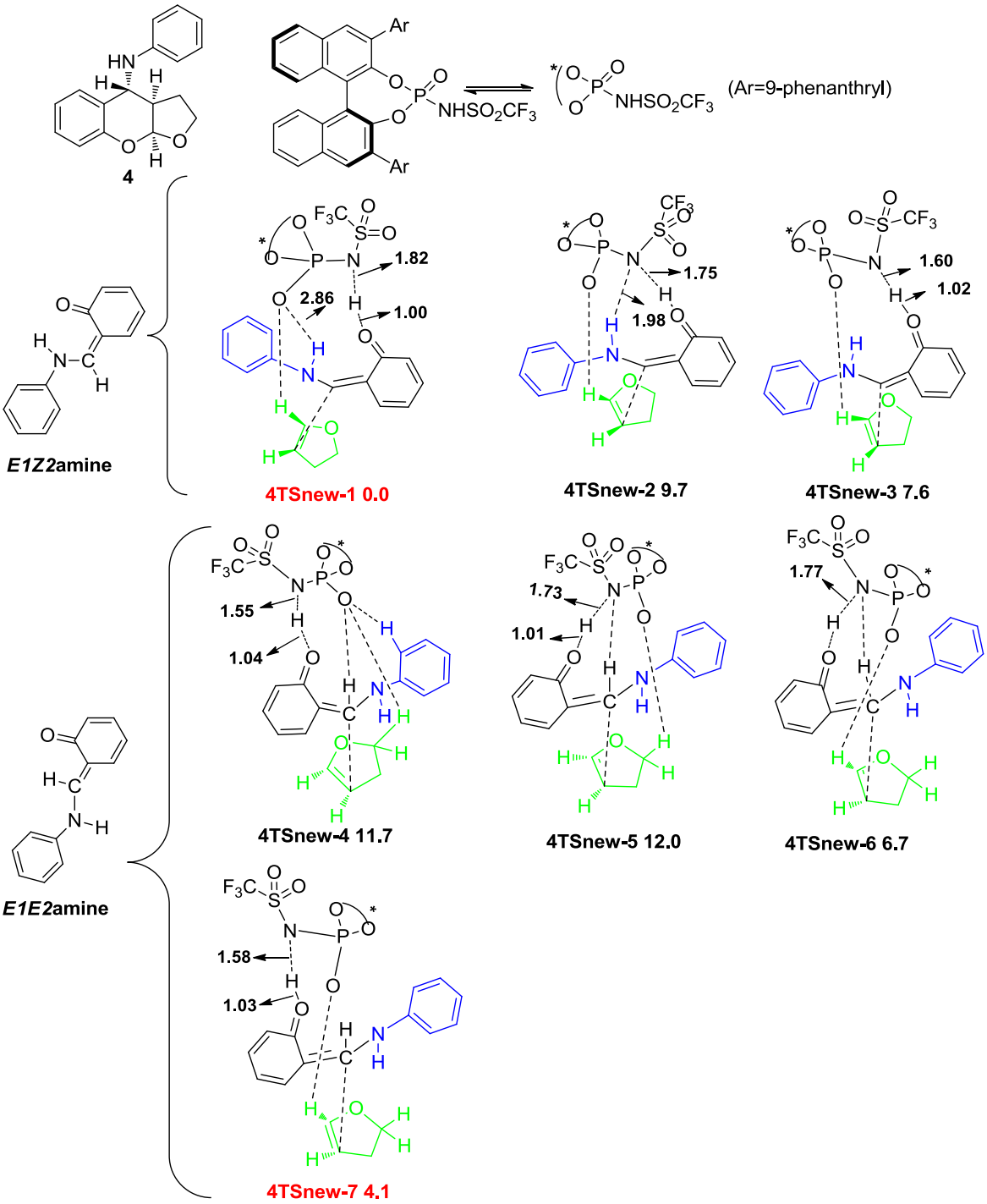

Figure 4.13 Main transition states leading to product **4** with the Rueping catalyst. Relative free energies (kcal.mol^{-1}) in dichloroethane based on the most stable geometry **4TSnew-1**. Selected distances are given in Å.

4.6.5 The origin of selectivity in the Rueping system

The key transition states are the most stable ones leading to each of the four possible products. These transition states are **3TSnew-7**, **3´TSnew-6**, **4´TSnew-3** and **4TSnew-1** (**Figure 4.14**). Their relative energies are 0.8, 4.7, 3.2 and 0.0 kcal.mol^{-1}. These energy differences represent an enantiomeric excess of 99 % and a diastereomeric excess of 59% in favour of product **4**. The experimental results show an er value of 96:4 (ee value of 92%) and a dr value of 2.7:1 (de value of 46%), see **Scheme 4.3**. Again there is good agreement between experiment and calculation.

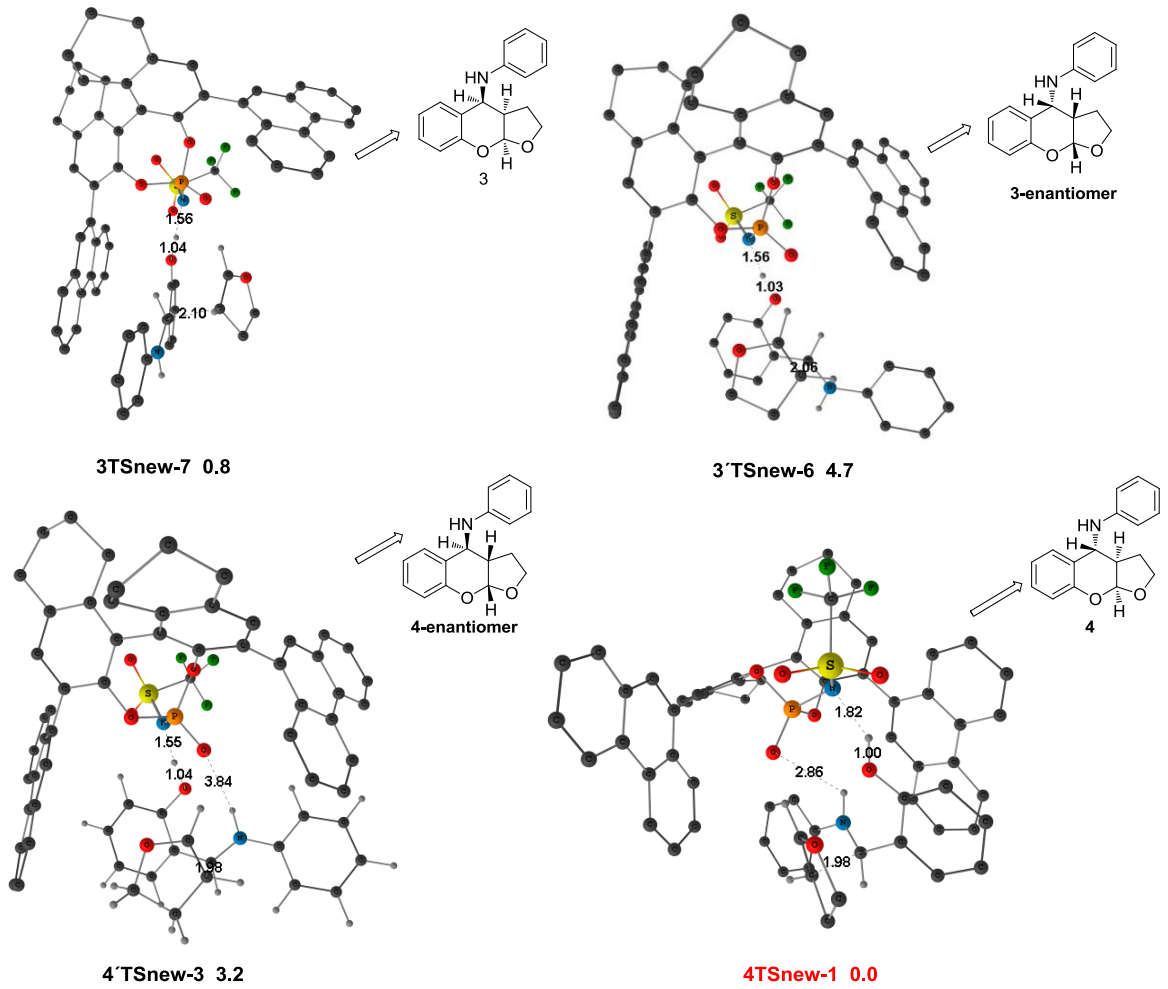

Figure 4.14 Structure of the most stable transition states leading to each of the four possible products. Relative free energies in dichloroethane (kcal.mol^{-1}) based on the most stable geometry **4TSnew-1**. Selected distances are given in Å.

As was the case for the Fochi system, the hydrogen networks, although structurally relevant, do not correlate with the relative energies. Because of this, we decided to examine again the ring-ring interactions following the same scheme reported above for the Fochi system. In the Rueping system, the interactions are with the phenanthryl rings instead of triphenylsilyl substituents, but the overall analysis is similar. The results are summarized in **Table 4.2**, and the key interactions are highlighted in **Figures 4.15** and **4.16**.

Table 4.2 Shortest ring-ring distances (Å) for the key transition states in the reaction with the Rueping system. Relative energies are also provided in kcal.mol^{-1}

	3TSnew-7	**3'TSnew-6**	**4'TSnew-1**	**4TSnew-1**
ΔG	0.8	4.7	3.2	0.0
N-ring	3.36	4.29	3.59	3.78
O-ring	3.40	3.56	3.59	3.36
Furan	5.29	4.76(3.69)	4.60(3.49)	3.89

In **Table 4.2**, there are two values for the ring-ring distance associated to furan for the cases of **3´TSnew-6** and **4´TSnew-1.** The value in parenthesis is shorter, but corresponds to a C-C interaction between rings that are not in a parallel orientation (see **Figure 4.15** and **4.16**), and involving one of the CH_2 groups, instead of the CH group as was the case for the other systems. Because of this, we consider this interaction not significant, and we concentrate on the shortest distance involving the CH carbon. If we take this into account, there is again agreement between ring-ring distances and relative energies. The only transition state with distances below 4.0 Å for all three substrate rings is **4TSnew-1**, which leads to major product **4**. The interaction with the furan ring, although likely less important because it is not aromatic, is completely absent in the other three transition states, and has thus a discriminating role. The shortest distances associated to the N-ring and O-ring systems are associated to transition state **3TSnew-7**, with an energy 0.8 kcal.mol-1 above **4TSnew-1**. The other two transition states have higher energies above 3.0 kcal.mol^{-1} as they do not have the furan interaction and longer contacts with hydroxybenzaldimine.

Selectivity with the Rueping catalyst is thus associated again to the attractive π–π interactions between substrate and catalyst.

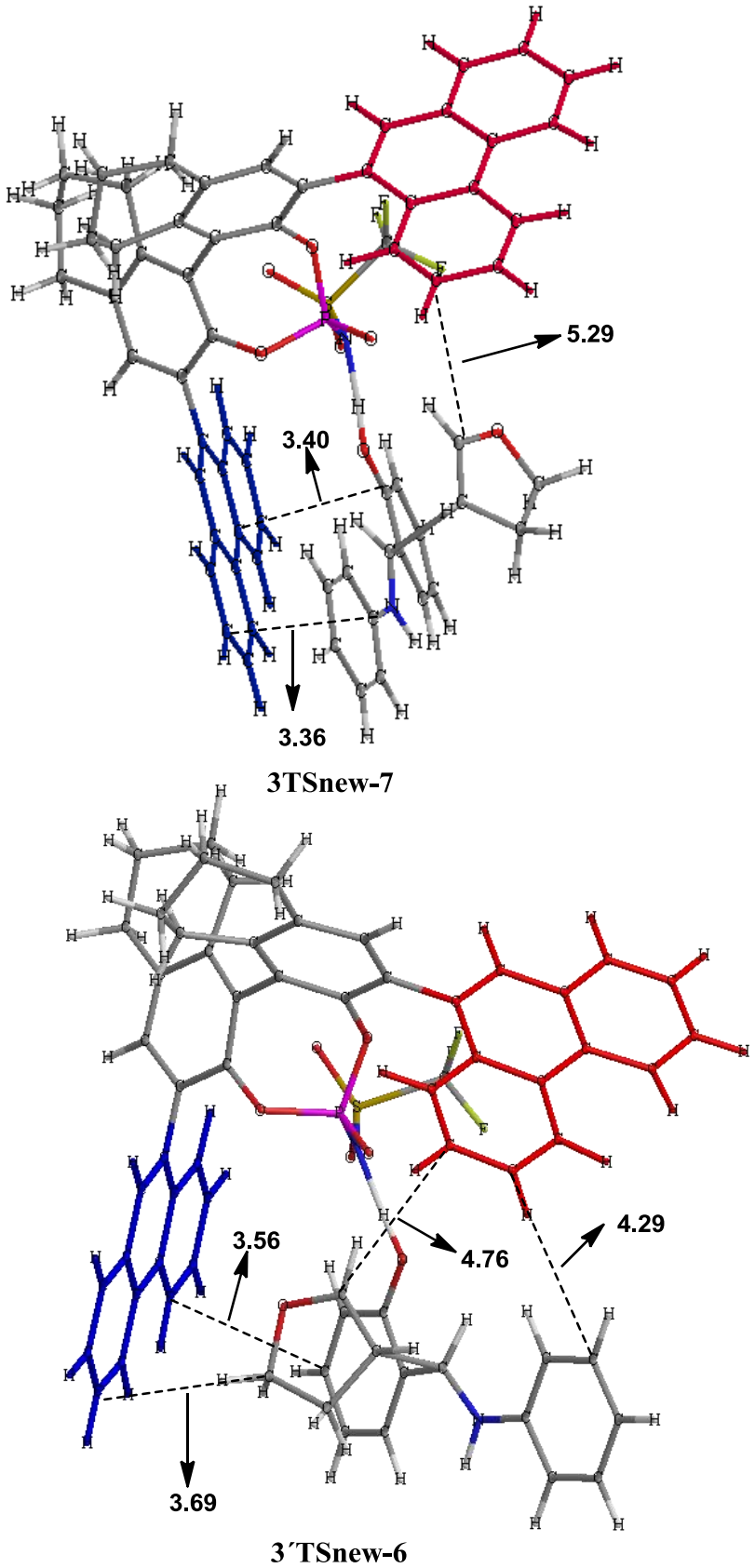

Figure 4.15 The views of **3TSnew-7** and **3´TSnew-6**. Selected distances are given in Å.

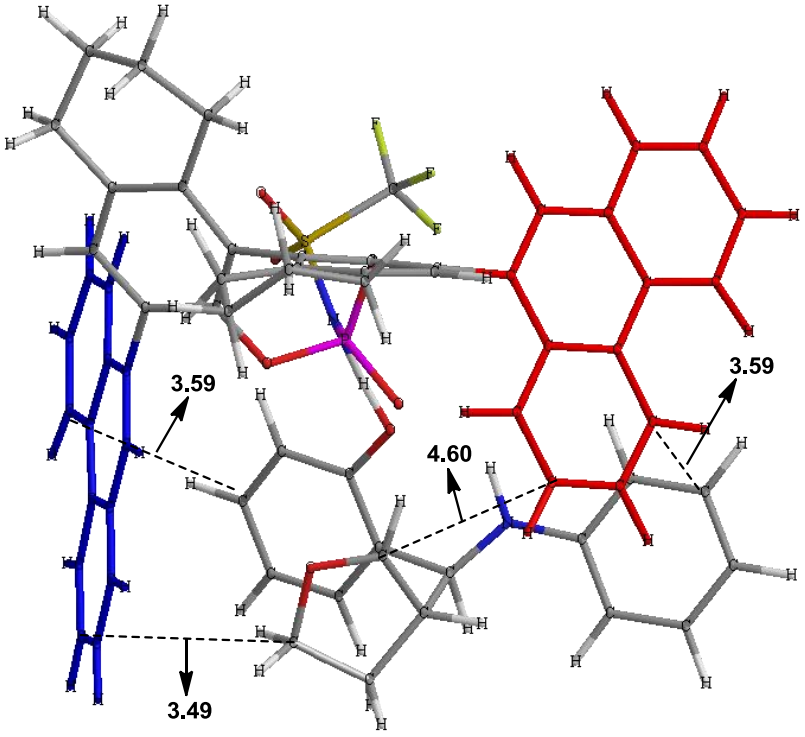

4´TSnew-3

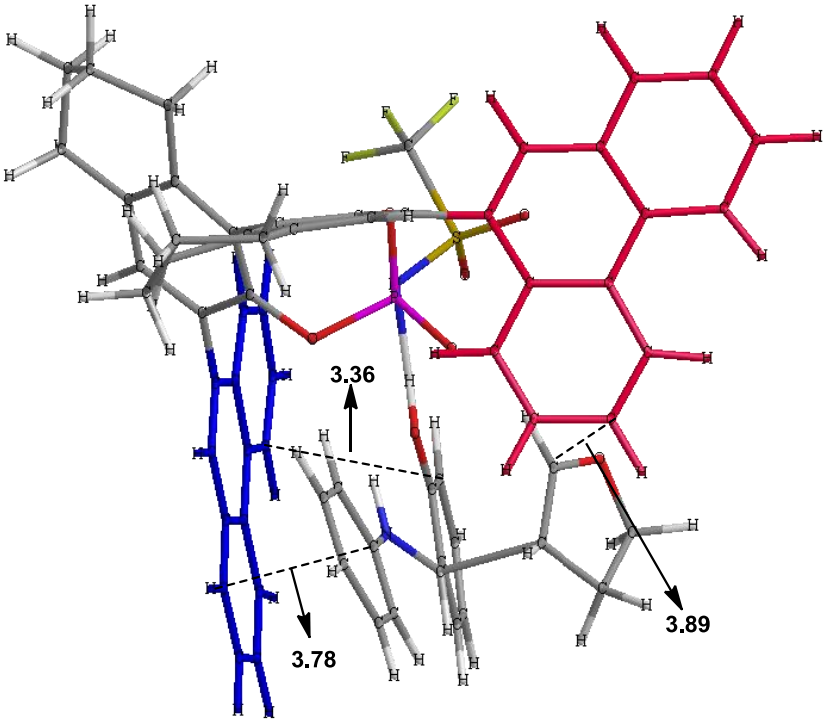

4TSnew-1

Figure 4.16 The views of **4TSnew-1** and **4´TSnew-3**. Selected distances are given in Å.

4.7 Comparison between the two catalysts

We have shown in the previous sections that we can reproduce the selectivity of the cycloaddition reaction under study for both catalysts, and explain the origin of this selectivity as a function of the π–π interactions between catalyst and substrates in the key transition state. We will analyze now the difference between the two systems. If the interactions ruling the selectivity are similar in both systems, why is **3** the preferred product with the Fochi catalyst, and **4** is the preferred product with the Rueping catalyst?

Table 4.3 Comparison between the key transition states for the Fochi and Rueping systems. Relative energies are in kcal.mol^{-1}. Shortest ring-ring distances in Å. Dihedral angle in degrees. Atomic labels for the definition of the dihedral angle taken from **Figures 4.17** and **4.18**. X is O_2 in Fochi system, N in Rueping system.

	3TS-8	**4TS-1**	**3TSnew-7**	**4TSnew-1**
ΔG	0.0	2.4	0.8	0.0
N-ring	3.44	3.44	3.36	3.78
O-ring	3.35	3.56	3.40	3.36
Furan	3.50	3.50	5.29	3.89
O_1-P-X-H	-36.5	12.7	54.1	43.8

The similarities and differences between the best transition states leading to product **3** and **4** with both catalysts are analyzed in this section. Their structures are presented in **Figure 4.17** and **4.18** and their structures are compared in **Table 4.3**. Most of the information in **Table 4.3** is a summary from what had been reported above in **Tables 4.1** and **4.2**. The differences in stability can be related to differences in the ring-ring distances, as discussed above. When comparing the ring-ring distances in both distances, the largest difference is in the distance involving the furan ring in **3TSnew-7**. This is the only case where this distance is above 4.0 Å, and it goes as far as 5.29 Å, clearly indicating the absence of this interaction. The distribution of distances involving N-ring and O-ring is similar in both cases. The different behavior between both catalysts can be thus traced down to the furan

ring-ring distance in **3TSnew-7**. The lack of this interaction destabilizes the formation of product **3** in the Rueping system that as a result gives **4** as the major product.

The reason why the furan interaction is absent in **3TSnew-7** is likely related to the values of the O_1-P-X-H dihedrals, also collected in **Table 4.3**, and explained in **Figures 4.17** and **4.18**. This dihedral angle is similar for the Rueping catalyst transition states **3TSnew-7** (54.1) and **4TSnew-1** (43.8). But the values are diverse for the Fochi catalysts **3TS-8** (-36.5) and **4TS-1**(12.7). If we inspect the structures in **Figure 4.17**, it becomes apparent that the dihedral of O_1-P-N-H cannot be changed freely because of Tf group. If we change the O_1-P-N-H dihedral from 54.1 to -36.5, the resulting structure will be sterically hindered as the Tf group would be too close to a phenanthryl group of the catalyst. Therefore, we cannot improve **3TSnew-7** geometry to become more similar to **3TS-8**. This is the reason why the Fochi system reaches product **3**, but the Rueping system does not, and yields instead product **4**.

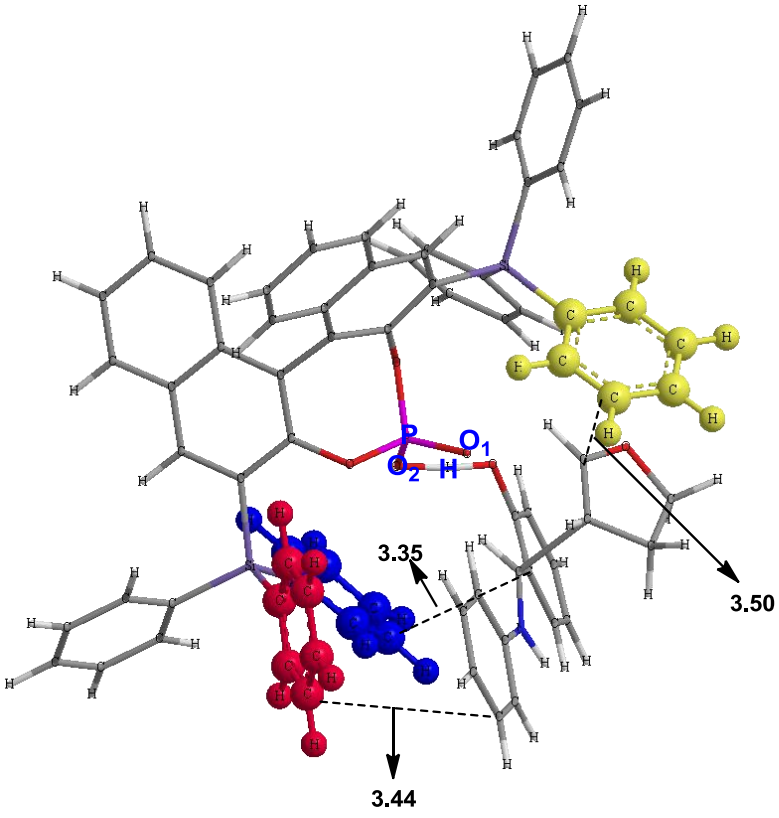

3TS-8(Fochi system)

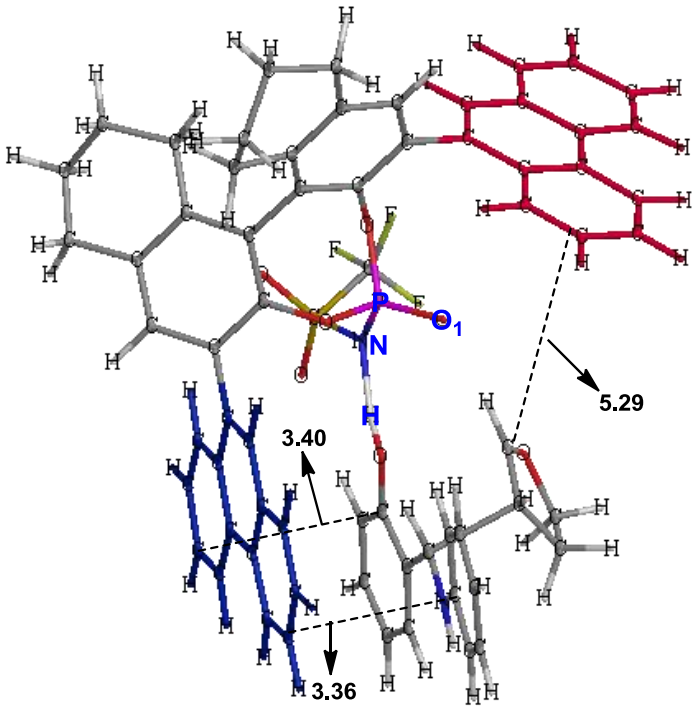

3TSnew-7(Rueping system)

Figure 4.17 Best transition states leading to product **3** in each of the systems. Selected distances are given in Å.

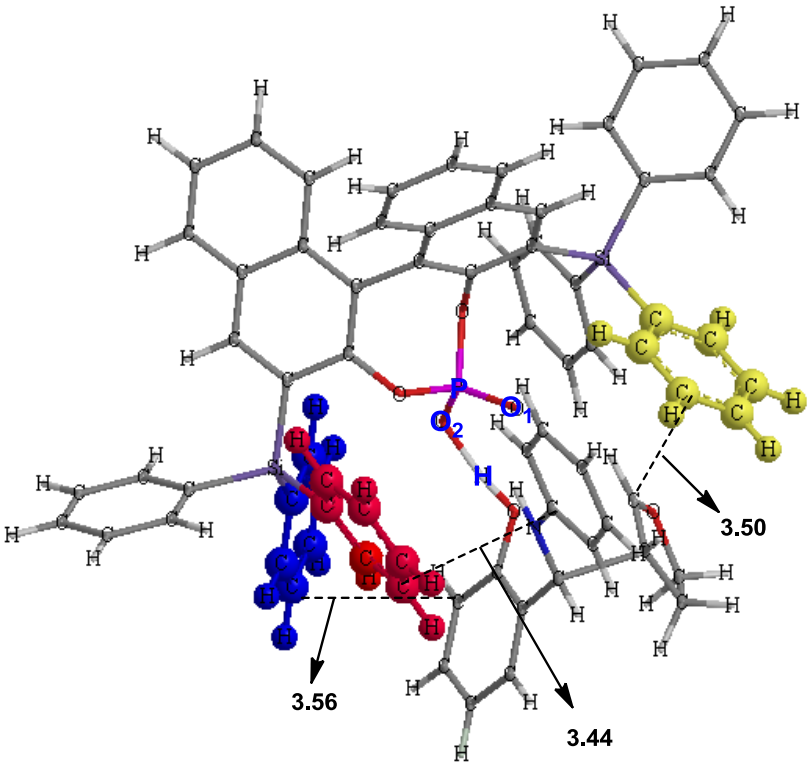

4TS-1(Fochi system)

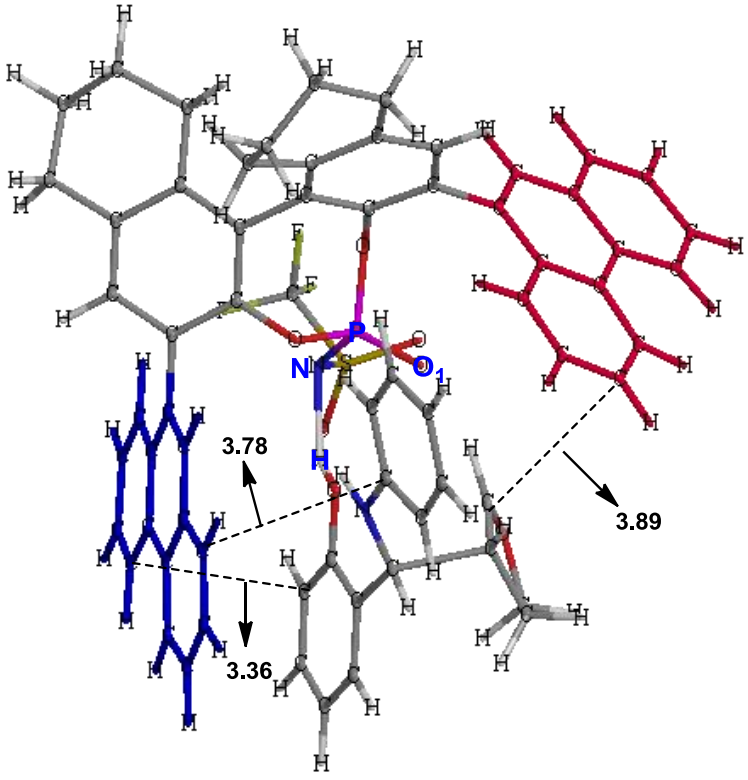

4TSnew-1(Rueping system)

Figure 4.18 Best transition states leading to product **4** in each of the systems. Selected distances are given in Å.

4.8 Conclusion

The pathways for the [4+2] cyclization reaction leading to furanobenzopyrans catalyzed by the two phosphoric acid derivatives considered are the same. First the initial imine is transformed into an amine through transfer of a hydrogen atom. After, the catalyst binds to the amine through a strong hydrogen bond, resulting in an adduct. In the next step, dehydrofuran (DHF) attacks this adduct to produce a transition state with low free energy barriers, where the new C-C and C-O bonds are made. The resulting adduct releases the product and the catalyst.

The transition state for the attack of DHF on the adduct controls the selectivity of the process. Hydrogen bonds play a critical role on the structure of the transition state, but their strength does not rule the selectivity. The lowest energy transition states have one hydrogen bond, while some higher energy transition states have two hydrogen bonds of similar strength. The selectivity is instead controlled by attractive ring-ring interactions between catalysts and substrates. The lower energy transition states have more interactions, or shorter (thus likely stronger) ones.

The difference between the (*S*)-BINOL-derived phosphoric acid (Fochi system), leading to a *cis*-fused furanobenzopyran, and the (*S*)-BINOL--derived N-triflylphosphoramide system (Rueping system), leading to a *trans*-fused furanobenzopyran, has been reproduced and explained. The presence of the triflyl substituent on the nitrogen atom of the Rueping system constrains the possible orientations of the hydrogen atom on this same atom, and as a result precludes the optimal orientation of the furan ring that led to the stabilization of the key transition state in the Fochi system leading to the *cis*-fused product. The *cis*-fused product being disfavored because of this constraint, the *trans*-fused product is formed with the Rueping catalyst.

4.9 References

[1]. (a) Simon L., Goodman J. M., *J. Org. Chem*, **2010**, 75, 589; (b) Simon L., Goodman J. M., *J. Am. Chem. Soc*, **2008**, 130, 8741; (c) Simon L., Goodman J. M., *J. Am. Chem. Soc*, **2009**, 131, 4070; (d) Grayson M. N., Pellegrinet S. C., Goodman J. M., *J. Am. Chem. Soc*, **2012**, 134, 2716; (e) Simon L., Goodman J. M., *J. Org. Chem*, **2011**, 76, 1775.

[2]. Zheng C., Sheng Y. F., Li Y. X., You S. L., *Tetrahedron*, **2010**, 66, 2875.

[3]. (a) Yamanaka M., Itoh J., Fuchibe K., Akiyama T., *J. Am. Chem. Soc*, **2007**, 129, 6756; (b) Yamanaka M., Hirata T., *J. Org. Chem*, **2009**, 74, 3266; (c) Akilyama T., Morita H., Bachu P., Mori K., Yamanaka M., Hirata T., *Tetrahedron*, **2009**, 65, 4950.

[4]. (a) Marcelli T., Hammar P., Himo F., *Adv. Synth. Catal*, **2009**, 351, 525; (b) Marcelli T., Hammar P., Himo F., *Chem. Eur. J*, **2008**, 14, 8562.

[5]. Shi F.Q., Song B. A., *Org. Biomol. Chem*, **2009**, 7, 1292.

[6]. (a) Nicolaou K. C., Pfefferkorn J. A., Roecker A. J., Cao G. Q., Barluenga S., Mitchell H. J., *J. Am. Chem. Soc*, **2000**, 122, 9939; (b) Bergmann R., Gericke R., *J. Med. Chem*, **1990**, 33, 492.

[7]. (a) Rovnyak G. C., Ahmed S. Z., Ding C. Z., Dzwonczyk S., Ferrara F. N., Humphreys W. G., Grover G. J., Santafianos D., Atwa K. S., Baird A. J., McLaughlin L. G., Normandin D. E., Sleph P. G., Traeger S. C., *J. Med. Chem*, **1997**, 40, 24; (b) Evans J. M., Fake C. S., Hamilton T. C., Poyser R. H., Watts E. A., *J. Med. Chem*, **1983**, 26, 1582.

[8]. (a) Miyazaki H., Honda K., Asami M., Inoue S., *J. Org. Chem*, **1999**, 64, 9507; (b) Kumar R. S., Nagarajan R., Vijay K., Perumal P. T., *Lett. Org. Chem*, **2005**, 2, 458; (c) Kumar R. S, Nagarajan R., Perumal P. T., *Synthesis*, **2004**, 949; (d) Yadav J. S., Reddy B. V. S., Madhuri C., Sabitha G., Jagannadh B., Kumar S. K., Kunwar A. C., *Tetrahedron. Lett*, **2001**, 42, 6381; (e) Anniyappan M., Muralidharan D., Perumal P. T., Tetrahedron, **2002**, 58, 10301; (f) Yadav J. S., Reddy B. V. S., Reddy P. N., *Chem. Lett*, **2004**, 1436; (g) Wang J., Xu F-X., Lin X-F., Wang Y-G., *Tetrahedron Lett*, **2008**, 49, 5208.

[9]. Rueping M., Lin M. Y., *Chem. Eur. J*, **2010**, 16, 4169.

[10]. Bernardi L., Comes-Franchini M., Fochi M., Leo V., Mazzanti A., Ricci A., *Adv. Synth. Catal*, **2010**, 352, 3399.

[11]. (a) Maseras F., Morokuma K., *J. Comp. Chem*, **1995**, 16, 1170; (b) Matsubara T., Sieber S., Morokuma K., *Int. J. Quantum Chem*, **1996**, 60, 1101; (c) Dapprich S., Komáromi I., Byun K. S., Morokuma K., Frisch M. J., *J. Mol. Struct (Theochem)*, **1999**, 462, 1.

[12]. Frisch M. J., Trucks G. W., Schlegel H. B., Scuseria G. E., Robb M. A., Cheeseman J. R., Montgomery J. A., Jr., Vreven T., Kudin K. N., Burant J. C., Millam J. M., Iyengar S. S., Tomasi J., Barone V., Mennucci B., Cossi M., Scalmani G., Rega N., Petersson G. A., Nakatsuji H., Hada M., Ehara M., Toyota K., Fukuda R., Hasegawa J., Ishida M., Nakajima Honda T., Y., Kitao O., Nakai H., Klene M., Li X., Knox J. E., Hratchian H. P., Cross J. B., Adamo C., Jaramillo J., Gomperts R., Stratmann R. E., Yazyev O., Austin A. J., Cammi R., Pomelli C., Ochterski J. W., Ayala P. Y., Morokuma K., Voth G. A., Salvador P., Dannenberg J. J., Zakrzewski V. G., Dapprich S., Daniels A. D., Strain M. C., Farkas O., Malick D. K., Rabuck A. D., Raghavachari K., Foresman J. B., Ortiz J. V., Cui Q., Baboul A. G., Clifford S., Cioslowski J., Stefanov B. B., Liu G., Liashenko A., Piskorz P., Komaromi I., Martin R. L., Fox D. J., Gaussian, Inc., Wallingford CT, **2009**. Gaussian09, Revision A.02.

[13]. Rappé A. K., Casewit C. J., Colwell K. S., Goddard III W. A., Skiff W. M., *J. Am. Chem. Soc*, **1992**, 114, 10024.

[14]. Zhao Y., Truhlar D. G., *Theor. Chem. Acc*, **2008**, 120, 215.

[15]. Marenich A. V., Cramer C. J., Truhlar D. G., *J. Phys. Chem. B*, **2009**, 113, 6378.

[16]. (a) Chang G., Guida W. C., Still W. C., *J. Am. Chem. Soc*, **1989**, 111, 4379; (b) Saunders M., Houk K. N., Wu Y. D., Still W. C., Lipton M., Chang G., Guida W. C., *J. Am. Chem. Soc*, **1990**, 112, 1419.

[17]. Mohamadi F., Richards N. G. J., Guida W. C., Liskamp R., Lipton M., Caufield C., Chang G., Hendrickson T., Still W. C., *J. Comp. Chem*, **1990**, 11, 440.

[18]. Allinger N. L., Yuh Y. H., Lii J. H., *J. Am. Chem. Soc*, **1989**, 111, 85.

[19]. Sinnokrot M. O., Sherrill. C. D., *J. Phys. Chem. A*, **2006**, 110, 10656.

[20]. Dahl T., *Acta Chem. Scand*, **1994**, 48, 95.

Chapter 5

Conclusions

We have studied three different organocatalytic processes leading to chiral products with density functional theory (DFT) and density functional theory / molecular mechanics (DFT/MM) methods and we have been able to obtain a reasonable agreement with experimental results, and to provide qualitative explanations for the origin of enantioselectivity in each of the cases.

The computational study of enantioselective organocatalysis closely resembles that of enantioselective transition metal catalysis, but there are some significant nuances. In first place, the electronic description of the organocatalytic system is in principle easier, although the introduction of dispersion corrections is mandatory, as in any process where steric interactions may play an important role. In second place, the problems related to isomeric and conformational complexity are much more critical in organocatalysis. The density of available isomers, conformational or not, available at low energy is much higher, and this poses a severe strain in the effort that has to be made to obtain quantitatively accurate energy barriers.

We have characterized the mechanism of the Friedel–Crafts (FC) reaction between ethyl 3,3,3-trifluoromethylpyruvate and indole catalyzed by water plus the iridium complex (η^5–C_5Me_5) Ir {(*R*)–Prophos} (Prophos = propane–1,2–diylbis(diphenylphosphane). The catalytic role of the metal complex is the modulation of the acid/base properties of the coordinated water, and the water molecule acts as a proton donor and acceptor. It is thus an organocatalytic process, as the transition metal complex is a spectator that never interacts directly with the substrate. We have been also able to explain the origin of the the enantioselectivity of the process, which is a result of a subtle combination of the non-

covalent interactions, both attractive and repulsive, between catalyst and substrate, that favor the transition state leading to the major product.

We have been able to clarify the mechanism of the intramolecular aldol reaction leading to Wieland-Miescher ketones catalyzed by N-Ts-(S_a)-binam-L-prolinamide in the presence of carboxylic acids. It follows the general trends of the mechanism with proline, with the important caveat that the presence of a carboxylic acid as co-catalyst is mandatory to increase the reaction rate, as it participates in the rate-determining initial steps; but has no effect on the enantioselectivity, which is decided afterward. The origin of the enantioselectivity of the reaction is based on the rigidity of the catalyst, which has two anchoring points for the substrate, the C=N double bond in the enamine intermediate, and the N-H...O hydrogen bonds between catalyst and substrate. The substrate has to distort to bind properly to these anchoring points, and this distortion is smaller for the transition state leading to the favored enantiomer**.**

The mechanism for the [4+2] cyclization reaction between *o*-hydroxybenzaldimine and 2,3-dihydro-2H-furan leading to furanobenzopyrans catalyzed by phosphoric acid derivatives has been clarified. The new C-C and C-O bonds are made in a single transition state, which is where the selectivity of the process is decided. Hydrogen bonds play a critical role on the structure of the transition state, but they do not rule the selectivity, which is instead controlled by attractive ring-ring interactions between catalysts and substrates. The experimental difference between the (*S*)-BINOL-derived phosphoric acid ester catalyst, leading to a *cis*-fused furanobenzopyran, and the N-triflylphosphoramide-derived system, leading to a *trans*-fused furanobenzopyran, has been reproduced and explained. The presence of the triflyl substituent on the nitrogen atom of the triflylphosphoramide-derived system constrains the possible orientations of the hydrogen on this same center, and as a result precludes the optimal orientation of the furan ring that led to the stabilization of the key transition state with the other catalyst.

The whole body of work in this thesis confirms the power of computational chemistry for the study of chiral organocatalysis. It also gives insight into the different mechanisms by which enantioselectivity can be transmitted in organocatalysis, from the usual steric interactions between catalyst and substrate to the less frequent key role of catalyst rigidity

observed in the prolinamide system. The field of computational enantioselective organocatalysis is just starting, and we can expect new exciting results in the foreseeable future.

Chapter 5